SPIM

Thèse de Doctorat

école doctorale **sciences pour l'ingénieur et microtechniques**

UFC UNIVERSITÉ DE FRANCHE-COMTÉ

Algorithmes et Méthodes pour le diagnostic ex-situ et in-situ de systèmes piles à combustible haute température de type oxyde solide

KUN WANG

SPIM

Thèse de Doctorat

école doctorale **sciences pour l'ingénieur et microtechniques**

UFC UNIVERSITÉ DE FRANCHE-COMTÉ

N° 2012107

THÈSE présentée par

KUN WANG

pour obtenir le

Grade de Docteur de
l'Université de Franche-Comté

Spécialité : **Sciences Pour l'Ingénieur**

Algorithmes et Méthodes pour le diagnostic ex-situ et in-situ de systèmes piles à combustible haute température de type oxyde solide

Soutenue le 21 Décembre 2012 devant le Jury :

M. OLIVIER JOUBERT	Président	Professeur Université de Nantes
M. BELKACEM OULD BOUAMAMA	Rapporteur	Professeur Ecole Polytechnique de Lille
Mme. LATIFA OUKHELLOU	Rapporteur	Directrice de Recherche IFSTTAR
M. ANDRE WEBER	Examinateur	Chercheur KIT (Allemagne)
M. DANIEL HISSEL	Directeur de thèse	Professeur UFC
Mme. MARIE-CÉCILE PÉRA	Co-directeur de thèse	Professeur UFC
Mme. NADIA YOUSFI STEINER	Co-encadrante	Ingénieur de Recherche EIFER
M. BORIS IWANSCHITZ	Examinateur Invité	Ingénieur de Recherche HEXIS (Suisse)

N° d'ordre : 2012107 Année 2012

THESE

Présentée pour obtenir le grade de

DOCTEUR DE L'UNIVERSITE DE FRANCHE-COMTE

Ecole Doctorale : Sciences Pour l'Ingénieur et Microtechniques
Spécialité : Sciences Pour l'Ingénieur

Kun WANG

Master Génie Electrique à l'Université de Lille

Algorithmes et Méthodes pour le diagnostic ex-situ et in-situ de systèmes piles à combustible haute température de type oxyde solide

Soutenue le 21 Décembre 2012 devant le jury composé de :

M. Olivier Joubert	Professeur Université de Nantes	Président
M. Belkacem Ould Bouamama	Professeur Ecole Polytechnique de Lille	Rapporteur
Mme. Latifa Oukhellou	Directrice de Recherche IFSTTAR	Rapporteur
M. Andre Weber	Chercheur KIT (Allemagne)	Examinateur
M. Daniel Hissel	Professeur UFC	Directeur de thèse
Mme. Marie-Cécile Péra	Professeur UFC	Co-directeur de thèse
Mme. Nadia Yousfi Steiner	Ingénieur de Recherche EIFER	Co-encadrante
M. Boris Iwanschitz	Ingénieur de Recherche HEXIS (Suisse)	Examinateur Invité

Thèse préparée au Département Energie de l'Institut FEMTO-ST (UMR CNRS 6174)
dans le cadre de la Fédération de Recherche FCLAB (FR CNRS 3539)

Ex-situ and In-situ Diagnostic Algorithms and Methods for Solid Oxide Fuel Cell Systems

Kun Wang

Ph.D dissertation

ENERGIE department of FEMTO-ST institute
University of Franche-Comté

Ph.D dissertation prepared in Department Energie of Institute FEMTO-ST (UMR CNRS 6174)
in the framework of the Fédération de Recherche FCLAB (FR CNRS 3539)

Abstract

The EU-project “GENIUS” is targeted at the investigation of *generic* diagnosis methodologies for different Solid Oxide Fuel Cell (SOFC) systems. The Ph.D study presented in this thesis was integrated into this project; it aims to develop a diagnostic tool for SOFC system fault detection and identification based on validated diagnostic algorithms, through applying the SOFC stack as a sensor.

In this context, three algorithms, based on the k-means clustering technique, the wavelet transform and the Bayesian method, respectively, have been developed. The first algorithm serves for ex-situ diagnosis. It works on the classification of the polarization measurements of the stack, aiming to figure out the significant response variables that are able to indicate the state of health of the stack. The parameter “Silhouette” has been used to evaluate the classification solutions in order to determine the optimal number of classes/patterns to retain from the studied database.

The second algorithm allows the on-line fault detection. The wavelet transform has been used to decompose the SOFC’s voltage signals for the purpose of finding out the effective feature variables that are discriminative for distinguishing the normal and abnormal operating conditions of the system. Considering the SOFC as a sensor, its reliability must be verified beforehand. Thus, the feature variables are also required to be indicative to the state of health of the stack.

When the stack is found being operated improperly, the actual operating parameters should be estimated so as to identify the system fault. To achieve this goal, a Bayesian network has been proposed serving as a meta-model of the stack to accomplish the estimation.

At the end, the databases originated from different SOFC systems have been used to validate these three algorithms and assess their generalizability.

Key words:

- Fuel cell
- *K*-means clustering
- Non-intrusive diagnosis
- Artificial intelligence
- SOFC
- Wavelet transform
- Bayesian network
- State of health

Résumé

Le projet Européen « GENIUS » ambitionne de développer les méthodologies génériques pour le diagnostic de systèmes piles à combustible à haute température de type oxyde solide (SOFC). Le travail de cette thèse s'intègre dans ce projet ; il a pour objectif la mise en œuvre d'un outil de diagnostic en utilisant le stack comme capteur spécial pour détecter et identifier les défaillances dans les sous-systèmes du stack SOFC.

Trois algorithmes de diagnostic ont été développés, se basant respectivement sur la méthode de classification k-means, la technique de décomposition du signal en ondelettes ainsi que la modélisation par réseau Bayésien. Le premier algorithme sert au diagnostic ex-situ et est appliqué pour traiter les donnés issues des essais de polarisation. Il permet de déterminer les variables de réponse significatives qui indiquent l'état de santé du stack. L'indice Silhouette a été calculé comme mesure de qualité de classification afin de trouver le nombre optimal de classes dans la base de données.

La détection de défaut en temps réel peut se réaliser par le deuxième algorithme. Puisque le stack est employé en tant que capteur, son état de santé doit être vérifié préalablement. La transformée des ondelettes a été utilisée pour décomposer les signaux de tension de la pile SOFC dans le but de chercher les variables caractéristiques permettant d'indiquer l'état de santé de la pile et également assez discriminatives pour différentier les conditions d'opération normales et anormales.

Afin d'identifier le défaut du système lorsqu'une condition d'opération anormale s'est détectée, les paramètres opérationnelles réelles du stack doivent être estimés. Un réseau Bayésien a donc été développé pour accomplir ce travail.

Enfin, tous les algorithmes ont été validés avec les bases de données expérimentales provenant de systèmes SOFC variés, afin de tester leur généricité.

Mots clés :

- Pile à combustible
- Classification *k*-means
- Diagnostic non-intrusif
- Intelligence artificielle
- SOFC
- Transformé en ondelettes
- Réseau Bayésien
- Etat de santé

Preface

The work, which is presented in this PhD thesis, has been done at FCLAB and FEMTO-ST, from October 2009 to October 2012. It has been carried out in the framework of a collaborative European project “GENIUS” with the support of the Fuel Cell and Hydrogen Joint Technology Initiative of the FP7 energy program of the European Commission.

Acknowledgements

This dissertation is not only a result of my own dedication but a credit to the patient and helpful people that I have worked with over these past three years. I would like to take this opportunity to express my deepest appreciation to everyone who contributed or supported to my work.

My first thank goes to Prof. Hissel and Prof. Péra who offered me the possibility to join FCLAB and the group ENERGIE at FEMTO-ST and the opportunity to take part in a European project and to work in a multicultural environment with talent engineers and researchers from different countries. I really appreciated the freedom I had in my work, the working conditions and the atmosphere.

Many thanks go also to Dr. Nadia Steiner, my co-advisor, for her confidence and encouragement to me and for her valuable guidance during the study.

My sincere thanks to Prof. Olivier Joubert for agreeing to act as the president of the jury. I also warmly thank to members of the jury and rapporteur of this thesis. I sincerely thank them for reading and evaluating this thesis critically. This thesis has been carefully studied by the examiners who had a large number of interesting questions. Their comments have been instrumental in making this thesis more effective and I'm grateful for their valuable suggestion and information they have shared with me.

I am most thankful to Prof. Cesare Pianese and Prof. Fabio Postiglione for their gracious reception and helps when I worked in University of Salerno, Italy. Working with them has been a very enriching experience. I wish also to express sincere gratitude to all my Italian friends (Gina Scorziello, Raffaele Petrone, Dario Marra, Luigi Bruno, Paolo Braca and Fabio Mazzarella) for their cares and concerns during that period.

I would like to thank all colleagues and partners in the GENIUS project for their infinite friendship and encouraging supports. This work was in joined collaboration with Hexis in Switzerland and VTT in Finland, which are thanked for providing experimental data and information on the studied SOFC systems.

During my stay at FCLAB, I shared my office with Serge Agbli, Mona Ibrahim and Zhixue Zheng. I’d like to thank them for the good times spent in and outside the office.

Finally, I would like to acknowledge my family, especially my fiance Huaqiang Shu for his support and cares during this thesis.

Nomenclature

Abbreviation

AC	**A**lternating **C**urrent
AI	**A**rtificial **I**ntelligence
AIC	**A**kaike's **I**nformation **C**riterion
ANN	**A**rtificial **N**eural **N**etwork
APU	**A**uxiliary **P**ower **U**nit
ASE	**A**node **S**upported **E**lectrolyte
ASR	**A**rea **S**pecific **R**esistance
AU	**A**ir **U**tilization
BIC	**B**ayesian **I**nformation **C**riterion
BN	**B**ayesian **N**etwork
BoP	**B**alance **o**f **P**lant
BP	**B**ack**P**ropagation
CBM	**C**ondition **B**ased **M**aintenance
CHP	**C**ombined **H**eat and **P**ower
CO	**C**arbone **M**onoxide
CPD	**C**onditional **P**robability **D**istributions
CPO	**C**atalytic **P**artial **O**xidation
CPT	**C**onditional **P**robability **T**able
DAG	**D**irected **A**cyclic **G**raph
DESIGN	Degradation Signatures Identification for Stack Operation Diagnostics
DIR	**D**irect **I**nternal **R**eforming
ECM	**E**quivalent **C**ircuit **M**odel
ECM	**E**quivalent **C**ircuit **M**odel
EIS	**E**lectrochemical **I**mpedance **S**pectroscopy
F	**F**ault
FC	**F**uel **C**ell
FFT	**F**ast **F**ourier **T**ransformation
FU	**F**uel **U**tilisation

GENIUS	**GE**neric diag**N**osis **I**nstr**U**ment for SOFC **S**ystem
IE	**I**nference **E**ngine
IIR	**I**ndirect **I**nternal **R**eforming
ITSOFC	**I**ntermediate **T**emperature **S**olid **O**xide **F**uel **C**ell
JPD	**J**oint **P**robability **D**istribution
KBES	**K**nowledge-**B**ased **E**xpert **S**ystem
LSM	**LaSrMn**O_3
MCMC	**M**arkov **C**hain **M**onte **C**arlo
MEA	**M**embrane-**E**lectrode-**A**ssembly
ML	**M**aximum **L**ikelihood
MPD	**M**arginal **P**robability **D**istribution
NG	**N**atural **G**as
OC	**O**perating **C**ondition
OCV	**O**pen **C**ircuit **V**oltage
PEMFC	**P**roton **E**xchange **M**embrane **F**uel **C**ell
PID	**P**roportional–**I**ntegral–**D**erivative
PM	**P**reventive **M**aintenance
RBFNN	**R**adial **B**asis **F**unction **N**eural **N**etwork
RWE	**R**elative **W**avelet **E**ntropy
RWP	**R**elative **W**avelet entro**P**y
S	**S**ymptom
SOFC	**S**olid **O**xide **F**uel **C**ell
SoH	**S**tate of **H**ealth
SR	**S**atisfaction **R**ate
STFT	**S**hort **T**ime **F**ourier **T**ransform
TPB	**T**riple-**P**hase-**B**oundary
TWP	**T**otal **W**avelet entro**P**y
WP	**W**avelet **P**acket
WT	**W**avelet **T**ransform
YSZ	**Y**ttria-**S**tabilized **Z**irconia

Symbols

<s(x)>	Average silhouette of the cluster *x*
C(u,s)	Wavelet coefficient
cA_j	Approximation subsignal obtained in the j^{th} level of decomposition
cD_j	Detail subsignal obtained in the j^{th} level of decomposition
d(.)	Distance between two points
e^-	Electron
E_j^d	Wavelet energy of a detail subsignal obtained in the j^{th} level of decomposition
F_{air}	Flow rate of air
F_{H2}	Flow rate of hydrogen
f_s	Sampling frequency of signal
I	Fuel cell or stack current
J	Current density
j	Level of decomposition
K2	Bayesian score algorithm
N	Length of signal
O^{2-}	Oxygen ion
p_j^d	Percentage ratio of wavelet energy of a detail subsignal obtained in the j^{th} level of decomposition
Pr(.) or *p*(.)	Probability
Pr(.| .)	Conditional probability
s	Scale parameter of wavelet
S	Symptom
s(*x*)	Silhouette of the cluster *x*
S_{WT}	Total wavelet entropy
$S_{WT}(.|.)$	Relative wavelet entropy
T_f	Furnace temperature
T_s	Stack temperature
U	Fuel cell or stack voltage
u	Translation parameter of wavelet
μ	Mean value of a set of data
σ	Standard deviation

Table of Contents

General introduction

The gradual maturation of fuel cell technologies presents an opportunity to achieve significant improvements in electric power generation efficiencies and reduce greenhouse gases emissions. Among various types of fuel cells, Solid Oxide Fuel Cells (SOFCs) have attracted increasing attentions, owing to their fuel flexibility and the suitability for natural gas internal reforming. Moreover, due to the high operating temperature, this type of fuel cells enables Combined Heat and Power (CHP) generation for attaining higher system efficiency (up to 90%). These features make them a promising technology for energy conversion. However, to bring out the advantages of this technology, system-level reliability and cost reduction issues regarding its application must be addressed. A European project, titled "**GE**neric diag**N**osis **I**nstr**U**ment for SOFC **S**ystems (GENIUS)"[*], was therefore carried out with the aim of developing generic diagnosis methodology to ensure the required stability level for SOFC systems so that the lifetime of the fuel cell stack could be extended.

In this project, an entire SOFC system is separated into two parts: 1) the SOFC stack; 2) the rest of the system, known as Balance of Plant (BoP). It is believed that the severe degradation in the stack can be often attributed to improper operating conditions resulted from the faults in the BoP part, such as gas leakage in the joint point between the pipe and the manifold of the stack, temperature control failure, air blower failure and so on. The ultimate aim of the GENIUS project is hence to diagnose the BoP faults. Nevertheless, in order to avoid complicating the supervised system and increasing the diagnostic cost, no additional sensors are permitted to be superimposed on the system. To meet this requirement, an innovative idea is given in the GENIUS project, that is, to treat the SOFC stack as a specific sensor to support for the diagnosis.

Under this context, FCLAB, as one of the participant organization in the GENIUS project, proposed 3 steps to complete the on-line diagnosis for the BoP part. Firstly, the specific sensor, i.e. the SOFC stack, must be confirmed a priori being in a good state of health. Then, the fault detection is performed to see whether or not the stack is operated in normal condition. If not, a meta-model is activated to estimate the actual operating parameters, aiming at BoP fault identification. The implementation of all these 3 steps is demanded only based on the stack's voltage and/or current density measurements. In addition, for off-line diagnosis, FCLAB suggested to work on the fuel cell's polarization test data, applying classification technique to implement data analysis and fault indicator research.

Based on these concepts, 3 algorithms are developed to achieve SOFC systems' off-line and on-line (or on-board) diagnosis. The first algorithm, pointing to the off-line diagnosis, is based on the *k*-means clustering technique for data analysis and knowledge extraction. The second algorithm works for the confirmation of the state of health of SOFC and the ascertainment of the occurrence of BoP fault. It resorts to wavelet transform technique to realize SOFC voltage signal processing and fault indicators extraction. The third algorithm

[*] Refer to the web page: https://genius.eifer.uni-karlsruhe.de/

relies on a Bayesian network model used to estimate the stack's actual operating parameters. These parameters could help identify or position the fault.

All these algorithms are asked to be validated by experimental data. 5 datasets obtained from different SOFC system tests are thus prepared. The first dataset includes the historical polarization measurements originated from a series of SOFC stacks' tests on a Hexis system. These tests were devoted to a previous European project which aimed to increase understanding in SOFC degradation mechanisms. This dataset will be used for the off-line diagnosis algorithm validation. The second and the third datasets issue from two rounds experiments carried out on an SOFC test bench in VTT laboratory for the GENIUS project. The fourth and the fifth datasets are from FCLAB's historical experimental database. These four datasets serve for the validation of the on-line diagnosis algorithms. Since they are obtained from different SOFC test benches, the generalizability of the algorithms could be tested, as well.

This thesis presents our works in the framework of the GENIUS project. It is composed of 5 chapters:

- *The 1st chapter* firstly presents the state of the art about the SOFC technologies in terms of stack configurations and cell materials. Then, the durability issues of SOFC system are overviewed. They are summarized into two types: the SOFC stack failure and the BoP fault. The SOFC failure can be in depth divided into two categories: soft and hard failures. The soft failures are reversible while the hard failures are irreversible. SOFC degradation mechanisms related to these failures are introduced. The causal relationships between some of these failures and the relevant BoP faults are also mentioned. The diagnosis methodology developed in the framework of GENIUS project aims principally at detecting abnormal operating conditions caused by the BoP faults so as to avoid consequent SOFC failures.
- *The 2nd chapter* is focused on the introduction of three basic diagnosis approaches, i.e. the model-based, the signal-based and the knowledge-based approaches. A literature research on the applications of these approaches in the field of fuel cell diagnosis is presented. This work has been published in [Wang'11a] and [Wang'11b]. In the GENIUS project, FCLAB is in charge of developing the non-model based approaches in the application of SOFC system diagnosis. The signal-based approach is selected for the fault detection while the knowledge-based approach for the fault identification. In order to realize the usage of these approaches in the on-line diagnosis, the wavelet transform and the Bayesian network-based inference are used. The data clustering method is considered for the implementation of the off-line diagnosis. The databases originated from 5 tests on the different SOFC systems are prepared for the algorithms' validation. The descriptions about these tests are given in the end of this chapter.
  The following 3 chapters are the main part of this thesis. Each of them is dedicated to one of the developed diagnosis algorithms (the data clustering based algorithm, the wavelet transform based algorithm and the Bayesian network based algorithm), introducing its principles, clarifying its application in SOFC system diagnosis, and presenting the validation results.

- *The 3rd chapter* reviews two clustering techniques: the *k*-means and the fuzzy *k*-means clustering. The former belongs to hard data classification. The later is one of the soft data classification methods. It has already been applied in FCLAB to analyze electrochemical impendence measurements for Proton Exchange Membrane Fuel Cells (PEMFCs) diagnosis. In this work, the *k*-means clustering is exploited for off-line SOFC stack and system diagnosis, working on the analysis of the polarization measurement data of the stacks. The application of this algorithm starts by the classification of the operating variables' data, in order to discriminate the different operating conditions of interest. Then, it is used to classify the stacks' response variables data to see if the result is in accordance with that of the previous classification. The objective is to find out the significant response variable(s) able to indicate the actual operating condition and the state of health of the SOFC stacks.
- *The 4th chapter* presents the wavelet-transform based algorithm. This algorithm is an extension on the work of Nadia Steiner [Steiner'09] (performed between FCLAB and EIFER) who developed a wavelet-packet-transform based method for PEMFC diagnosis. Wavelet transform is a technique for signal decomposition, which allows analyzing signals in time-scale domain. We use this technique to study the fluctuations present in the SOFC's voltage signals. These fluctuations are considered able to indicate the operating condition of the system as well as the state of health of the fuel cell. Their indicative capability is validated with 4 groups of data.
- *The 5th chapter* clarifies how to employ Bayesian network to achieve SOFC system diagnosis. Firstly, the principles of Bayesian network are introduced. Then, a Bayesian network model is proposed for the estimation of SOFC operating parameters based on its electrical output measurements (the stack voltage and current), with the aim of fault identification. This model is parameterized and validated by the experimental data from two different SOFC test benches. A part of this work has been published in [Wang'12].

Chapter I Introduction

According to the 2007 report of the U.S. Department of Energy on greenhouse gases, the combustion of fossil fuels gives per year a net increase of around 10.65 billon tones of atmospheric carbon dioxide [Akorede'12], which will in turn have adverse effects on the environment for human survival. In order to slow down the increasing trend of CO_2 emissions, the European Union (EU) has in accordance with the Kyoto Protocol committed itself to reducing its greenhouse gas emissions by 8% during the period 2008–2012 compared to its levels in 1990. In January 2007, new emission-reduction target was established by European leaders for the post-2012 period in the Commission's Communication, which increased the reduction goal to 20% by 2020. To meet these goals, a series of mitigation measures have been proposed such as carbon sequestration, clean development mechanism and most importantly use of non-polluting sources of renewable energies like solar, wind, geothermal energy sources [VijayaVenkataRaman'12] as well as fuel cells. The later can generate clean, highly efficient power onsite from a wide variety of fuel sources. Fuel cell is a device able to directly convert chemical energy of fuel gases into electrical work without the requirement of combustion. It is much more efficient than conventional power generation and thus considered as an alternative to the medium- and large-scale heat engines and the batteries.

Different fuel cell types have been tried and developed in the decades to solve the fundamental problems regarding reaction rate and hydrogen availability [Larminie'03]. Among, the Proton Exchange Membrane Fuel Cells (PEMFCs) and the Solid Oxide Fuel Cells (SOFCs) have both attracted the most attentions. The formers operate at low temperatures (around 80°C) with a polymer electrolyte. Their electrical efficiency is about 40% to 50% and adaptable for mobile applications. In contrast, the SOFC, operating at high temperatures (700°C–900°C) to reach the electrolytes ionic conductivity requirement, can achieve a slight higher electrical efficiency up to 60%. The high operating temperature makes it suitable for added-value utilization by heat recovery for cogeneration in the case of which the overall efficiency can reach close to 90%. Apart from the higher energy conversion efficiency, high operating temperature also enables internal fuel reforming inside SOFCs. Owing to the tolerance to impurities in the fuel, SOFCs can be used with a number of hydrocarbons as fuel. The solid electrolyte avoids any corrosion and electrolyte management problems encountered in liquid electrolyte [Nesaraj'10]. The flooding phenomenon occurred

on the membrane of PEMFC is not present in SOFC either, because the produced water is in gaseous form under high operating temperature and thus can be easily moved out with the fuel flow. However, the high-temperature environment also imposes some challenges on SOFC fabrication (e.g. stability of materials and sealing under high temperature) and application (e.g. thermal management issues). For the reason that the time required to reach the operating temperature is significant, and due to the limits on start-up/shut-down cycles, SOFCs are more suited to stationary power supply applications. They are also applied as auxiliary power units (APUs) for vehicles.

This chapter gives an introduction to SOFCs as well as to the major challenges and problems in their practical applications.

I.1. The solid oxide fuel cell

I.1.1. Basic principles

The development of SOFC can be traced back to the 1890s when Nernst firstly found that stabilized zirconia (ZrO_2) was ion-conductive in red hot conditions, between 600°C and 1000°C. In the late 1930s, this discovery regained attentions of researchers after Baur and Preis using it in a fuel cell concept. Until today, the most favoured electrolyte for SOFCs is the fluorite-structured electrolytes, especially the Yttria-Stabilized Zirconia (YSZ, a zirconium-oxide based ceramic) which can become a conductor of oxygen ions above 800°C. Other fluorite-structured oxide ion conductors, such as doped ceria, have also been proposed as the electrolyte materials for SOFCs, especially for a reduced temperature operation at temperatures between 600 °C and 800°C [Singhal'03].

In an SOFC, the solid electrolyte is sandwiched around by two electrodes: the anode and the cathode. During operation, hydrogen is fed into the anode and oxygen/air is carried to the cathode where oxygen atoms are electrochemically reduced into oxygen ions (O^{2-}) by consuming the electrons transported through the external circuit. Then, the oxygen ions flow through the electrolyte towards the anode side and react with hydrogen. Electrons (e^-) are released from this reaction and flow to the cathode through the external electrical connection (see Figure 1-1). In this way, as long as the supply of fuel and oxygen/air is not cut off, oxygen ions can be continuously yielded and transported from the cathode to the anode, which maintains overall electrical charge balance and ensures the electric power generation.

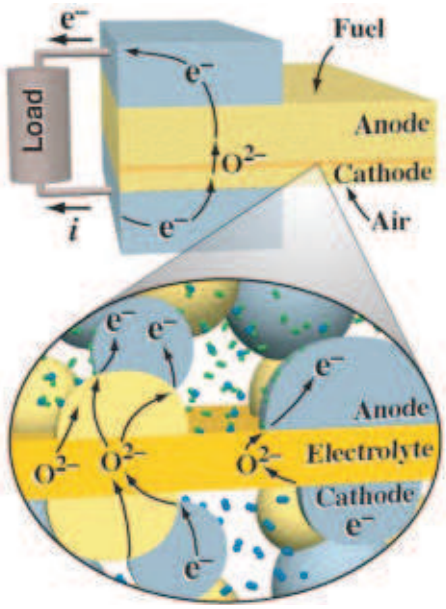

Figure 1-1 Charge flow in a SOFC*

The allowance of internal reforming is one of the attractive features of SOFC. Due to this capability, it can also use, apart from hydrogen, other fuels such as gaseous hydrocarbons (e.g. methane) and carbon monoxide (CO). These fuels can directly react with steam on the anode in the presence of required catalysts at reaction sites. For example, fuel reforming can take place on Ni/YSZ anode. Ni/YSZ is a cost-effective material and can provide catalytic reforming activity for the reaction between methane and steam to produce CO and H_2. CO then continues to react with the steam, releasing more hydrogen. In this shift reaction, CO_2 is the other product and will be transferred out of the fuel cell together with the produced steam (H_2O) and the unused fuel. The chemical equations of the steam reforming and shift reactions are given below:

Steam Reforming: $CH_4 + H_2O \rightarrow CO + 3H_2$ Eq. 1-1

Water-gas Shift Reaction: $CO + H_2O \rightarrow CO_2 + H_2$ Eq. 1-2

Additionally, methane may be reformed with CO_2:

Dry Reforming: $CH_4 + CO_2 \rightarrow 2CO + 2H_2$ Eq. 1-3

The reforming procedure discribed above is called Direct Internal Reforming (DIR), in which the reforming reaction occurred simultaneously with electrochemical reaction at the anode side of SOFC and thus a high heat transfer rate can be achieved. Nevertheless, the anode material for DIR-SOFC must be optimized for both reactions as it is susceptible to deactivation and poor durability due to carbon deposition. Moreover, direct internal reforming gives rise to a sharp endothermic cooling effect at the cell inlet, generating inhomogeneous temperature distributions and a steep temperature gradient along the length of the anode,

* Source: Robert J.K. & Zhu H., Oral presentation: Solid-oxide fuel cells (SOFC) with hydrocarbon and hydrocarbon-derived fuels, International Symposium on Combustion, USA, 29 July, 2004

which is very difficult to control and can result in cracking of the anode and electrolyte materials [Singhal'03].

There is another approach known as Indirect Internal Reforming (IIR), in which a reformer is integrated in close thermal contact with the anode side of SOFC so that the catalyst for reforming reaction at the reformer part and the material for electrochemical reactions at the anode side can be optimized individually, which prevents the anode from the possible degradation caused by carbon deposition [Laosiripojana'07]. Another advantage of indirect over direct reforming is that, from a thermodynamic standpoint, it is much easier to control [Singhal'03]. However, for most SOFC systems, the gas reforming is often performed outside the stack.

For the conventional concept of the electrochemical reaction in SOFCs, the substance reacting finally with oxygen is always H_2, no matter what kind of fuel is used as the inlet gas [Tu'04]. The electrochemical reaction and the oxygen reduction reaction taking place on the electrodes are formulated as follow:

$$\text{At the anode:} \quad H_2 + O^{2-} \rightarrow H_2O + 2e^- \qquad \text{Eq. 1-4}$$

$$\text{At the cathode:} \quad O_2 + 4e^- \rightarrow 2O^{2-} \qquad \text{Eq. 1-5}$$

The steam as a product of the hydrogen oxidation can be directly re-circulated for the internal reforming such that less steam must be pre-produced in comparison with external reforming, improving the system efficiency. The steam reforming (endothermic) and the water-gas shift (exothermic) reactions can be combined to be an auto-thermal process in which the partial combustion of a portion of the hydrocarbon provides the heat required by the endothermic reforming reactions to proceed. This process is known as autothermal reforming.

I.1.2. SOFC components and materials

A SOFC is mainly composed of 4 elements: the anode, the cathode, the electrolyte and the interconnector, as shown in Figure 1-2. Each of them serves several functions and has to fulfill different requirements. For instance, electrolyte and interconnector have to be gas tight and purely ion-conducting membranes whereas the electrodes must allow the transport of electrons, gaseous reactants and products [Ivers-Tiffée'01]. However, they also have certain common requirements to meet, such as [Stambouli'02]:

- Proper stability (chemical, phase, morphological and dimensional);
- Proper conductivity;
- Chemical compatibility with other components;
- Similar thermal expansion to avoid cracking during the high-temperature operation;
- High strength and toughness properties;
- Fabricability;

- Low cost.

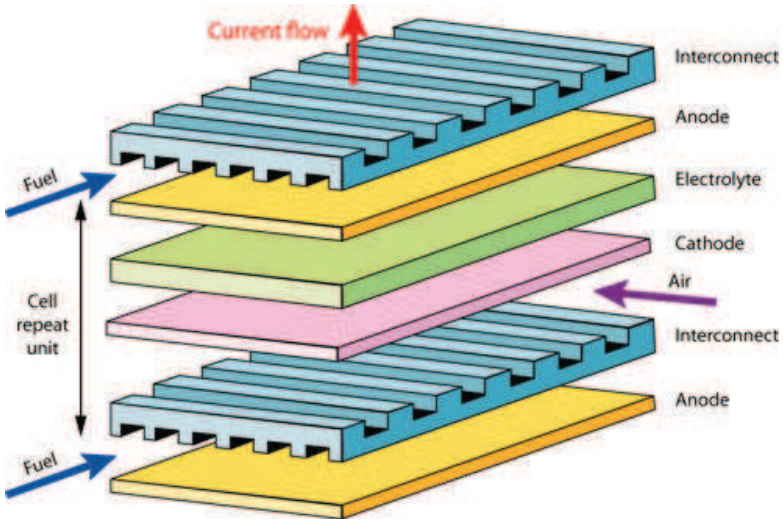

Figure 1-2 Cross-flow planar SOFC*

I.1.2.1. Anode

The anode is the part of SOFC where the electrochemical reaction takes place and the electrons are released. It is thus very crucial with respect to the FC performance. The material of the anode not only requires having the catalytic capability to promote fuel oxidation but also should be of high electrical conductivity to convey the liberated electrons to the current collector. In addition, the anode needs to provide a large number of active reaction sites for the fuel to react with the oxygen ions. Therefore, the structural concept for the anode (also for the cathode) always involves the creation of a porous system, which aims to increase the reactive surface and additionally ensures that the gaseous reactants can easily penetrate from the electrode surface at the side of gas supply channels to the electrochemical reaction zone.

Until now, a lot of investigations have focused on these requirements in order to develop an anode of high performance; and researches on this topic are still continuing. Early in the 20th century, many candidate anode materials were tested, including precious metals like platinum and gold, and transition metals such as iron and nickel [Singhal'03]. At last, the nickel was selected for the anode as the best suitable material in terms of both the catalytic and cost efficiencies. However, the nickel-based anode did not success until the 1970s when Spacil solved the nickel aggregation problem by combining it with YSZ electrolyte particles.

While the nickel (Ni) plays the role to meet the main requirements for the anode regarding electrical performance and conversion kinetics, the YSZ is added into the anode in order to support the Ni particles, to maintain the stability of their electronically conductivity, and to

*Source: University of Cambridge, DoITPoMS > TLP Library > Fuel cells > Solid oxide fuel cells, http://www.doitpoms.ac.uk/tlplib/fuel-cells/high_temp_sofc.php

provide an anode thermal expansion coefficient close to the one of the zirconia based electrolyte. Currently, such a cermet (a combination of ceramic and metal) anode has been widely used in SOFC technology. It is commonly made from YSZ and NiO powders. This NiO powders can be reduced in situ to nickel metal when exposed to the reductive environment as the fuel is continuously fed over the anode; as a result a porous Ni–YSZ composite will be formed. This composite has a homogeneous or graded structure consisting of three phases, Ni, YSZ and gases. The line where these three phases meet is referred to as the triple-phase-boundary (TPB) and is considered to be electrochemically active. The length of TPB has been found correlated with the rate of the electrochemical reaction on the anode and is thus significant to the fuel cell performance.

One significant disadvantage of Ni-based anode is that it is not suitable for operation with hydrocarbon fuels, due to carbon deposition that we will introduce in detail in the Section I.2.1.1.2. Addressing to this problem, some strategies have been proposed. One of the solutions is to add other metals such as Cu. Cu is an excellent electronic conductor but a poor catalyst for C-C bond formation (a reaction related to carbon formation). The addition of Cu in the Ni-YSZ anode can inhibit Ni's catalysis on coke formation. In [Park'09], the experimental result showed that in the same operating time (5 hours), the amount of carbon deposited on the Cu–Ni–YSZ anode was from 30% to 50% less than that on the Ni-YSZ anode. However, on the other hand, Cu is also a very poor catalyst for activation of hydrocarbons [Gorte'03], which will reduce the reaction rate of fuel reforming. Accordingly, a compromise must be reached between the positive and negative effects of Cu when it is considered as a component part of SOFC anode. In the recent decade, new materials such as Cu–CeO_2–YSZ composite [Lu'04, Park'09] have emerged to deal with carbon formation problem of the Ni-based the anode.

I.1.2.2. Cathode

On the SOFC cathode, the oxygen is reduced into oxygen ions which then migrate through the electrolyte to the anode. Similar to the anode, it is also made from porous ceramic materials. Perovskite materials such as $LaSrMnO_3$ (LSM) are the most commonly used SOFC cathode material. They can offer excellent thermal expansion match with zirconia electrolytes and provide good performance at operating temperatures above 800°C [Stambouli'02]. In order to obtain better performance, SOFC manufacturers explored a composite cathode by mixing the electrolyte materials (YSZ) with LSM. This incorporation increases the ionic conductivity of the LSM-based cathode and the volume of active sites available for the full electrochemical reduction of oxygen. Furthermore, the obtained LSM–YSZ cathode exhibits an improvement of performance at lower temperatures [Gong'11]. Like in the anode, three-phase (LSM, YSZ and air/oxygen) sites also exist in the cathode. Due to the low ionic conductivity in the bulk LSM, the active sites for the full electrochemical reduction of oxygen are largely confined to the length of this TPB at the cathode side [Liu'09, Mizusaki'91].

I.1.2.3. Electrolyte

For optimal cell performance, SOFC electrolyte should have the conductivity value for oxygen ions close to 1 while for electrons close to 0 as possible. It also must be free of porosity so as not to allow gases to permeate from one side of the electrolyte to the other [Singhal'00]. Using YSZ as the electrolyte, SOFC is restricted to operate in high temperatures (around 1000°C) because of the thermal activation requirement for the oxide ion conductivity of YSZ. A 10% decrease in temperature will result in about 12% drop in cell performance, due to the increase of the internal resistance to the oxygen ions transport [Stambouli'02]. While the high temperature requirement enables internal reforming and co-generation application of SOFCs, it equally brings challenges and problems to SOFCs manufacturing and commercialization. Materials problems associated with this high operating temperature include electrode sintering, interfacial diffusion between electrolyte and electrode and mechanical stress due to different thermal expansion coefficients [Souza'97]. In addition, expensive high temperature alloys and ceramics are required respectively to house the cell and to serve as interconnection materials, increasing the cost of fuel cell substantially [Stambouli'02]. In applications, a long-term heat-up process is necessitated by SOFC systems so that quick start-up/shut-down cycling is likely impossible to be achieved. SOFCs also suffer from the thermal cycling issue and the temperature gradient problem in operating conditions.

On the other hand, decreasing the operating temperature of SOFCs can lower the ion conductivity of the electrolyte and result in large internal resistance. For instance, a SOFC with YSZ as the electrolyte, Ni–YSZ cermet as the anode and a LSM–YSZ composite as the cathode is able to operate in a temperature range from 1000°C to 850°C whereas at lower temperatures, the polarization resistances are too large such that the efficiency or power density is not satisfying [Ivers-Tiffée'01]. Furthermore, the reactions at the electrodes will become less active when the operating temperature is reduced. Additionally, natural gas reforming necessities an undermost operating temperature of about 650°C, which leads to a very limited room for operating temperature reduction [Ivers-Tiffée'01]. These limitations promoted researchers to seek the substitutes for YSZ electrolyte which are expected to have high ion conductivity in medium operating temperatures (600°C–800°C).

Doped-ceria based electrolytes have been studied as alternative for oxygen ion conductors for Intermediate Temperature SOFC (ITSOFC) [Badwal'00, Zhu'01]. This kind of materials has a high concentration of oxygen-ion vacancies, exhibiting high ionic conductivity. For example, the conductivity of Gd–doped ceria at 800°C is about 0.1 S/cm and is approximately one order of magnitude higher than that of YSZ [Joshi'04]. However, their electronic conductivity can increase with the increasing degree of non-stoichiometry (increasing temperature and decreasing oxygen partial pressure) [Badwal'00], resulting in an internal short circuit in the cell. Lanthanum gallate (Sr and Mg doped $LaGaO_3$, LSGM) based electrolyte has been also found to have relatively high ionic conductivity at 800°C in both oxidizing and reducing atmospheres [Feng'94, Ishihara'94,, Huang'98 Joshi'04]. However, the use of LSGM–based electrolyte can also provoke problems in the aspects of durability and cost, due to the low mechanical stability of LSGM and the high costs of Gallium [Ivers-Tiffée'01]. Currently, the

oxygen ion conducting electrolyte materials for intermediate temperature are still on research stage, being accompanied by the development of suited electrode and interconnector materials.

Another approach to counteract the increase of the electrolyte ohmic resistance at lower temperature is to decrease the electrolyte thickness [Souza'97, Charpentier'98, Will'00, Gannon'09]. For example, for an area-specific resistance (ASR) of 0.15 $\Omega.cm^2$, the decrease in thickness of a 10 mol% YSZ electrolyte from 15 μm to 500 nm allows a decrease of operating temperature from 700°C to approximately 525°C [Steele'01, Litzelman'08]. The thickness-reduced electrolyte looks like a thin film supported by one of the electrodes. Since the electrolyte resistance accounts for a large proportion of SOFC internal resistance, the usage of thin-film electrolyte contributes to a significant reduction of the ohmic resistance of the cell. This effect offsets the negative influence caused by the lowering of the operating temperature of SOFCs. With such thin electrolytes, ohmic losses are no longer rate-controlling, thereby making polarization losses the dominant loss mechanism for fuel cell performance [Chao'11].

I.1.2.4. Interconnector

The interconnector is an important component for a fuel cell stack. Thanks to it, the individual fuel cells can be electrically connected in series to form a stack in order to meet higher voltage requirement in practical applications. The interconnector physically connects the anode of a fuel cell to the cathode of the adjacent fuel cell in the stack, serving as an electrical connection and acting as a physical barrier to segregate the air electrode side and the fuel electrode side. Since the interconnector is simultaneously exposed to an oxidizing atmosphere and to a reducing environment during the fuel cell operation, it must be made of chemically stable materials with high oxidation resistance. In addition, it should have a high electrical conductivity to allow the transport of the electronic current between the individual cells and towards the external circuit [Cabouro'06]. The interconnector also serves as a transport channel to provide the reactants to both the anode and the cathode side, and to allow the reaction products flowing out of the cell so that electrochemical reaction can proceed [Zhu'03].

Two main types of material, i.e. ceramic or metallic, are commonly used for the interconnection of SOFCs. The doped lanthanum and yttrium chromites ($LaCrO_3$) based compounds with the perovskite structure are the most promising ceramic material for SOFC interconnectors, owing to their high electrical conductivity and high corrosion resistance under both oxidizing and reducing atmospheres in high temperature (around 1000°C). Nevertheless, certain weaknesses of $LaCrO_3$ are obvious [Wu'10]: (i) $LaCrO_3$ is a p-type semiconductor, and its conductivity decreases with decreasing oxygen partial pressure as lanthanum chromite becomes oxygen deficient; (ii) compared with typical engineering materials, lanthanum, being a rare-earth element, is more expensive; (iii) $LaCrO_3$ is difficult to sinter to a high relative density so the processing of a hermetic $LaCrO_3$ layer is quite difficult. By contrast, metallic materials show many advantages such as low cost, easy manufacture and good workability. Furthermore, they also have higher electronic and thermal conductivities. The crucial barrier for the metallic interconnectors to be used in SOFC is their high temperature corrosion in long-term operation. Fortunately, recent researches succeeded

in lowering operating temperature of SOFCs have relieved this concern and favoured the use of metal interconnectors in planar-type SOFC.

For the ITSOFCs operated in the range of 600–800°C, ceramic interconnectors are not applicable because their electrical conductivity will greatly decline when the operating temperature is reduced to below 800 °C [Piccardo'09]. In this case, low cost metallic alloys are proposed as interconnectors [Huang'00, Zhu'03, Cabouro'06]. To have high corrosion resistance, a protective layer is needed on the surface of the metallic interconnector. Alumina, silica and chromium can all provide excellent protective surface scales by means of the oxidization to form Al_2O_3, SiO_2, Cr_2O_3, respectively. Nevertheless, the former two oxides have much lower electrical conductivity than the third one, leading to unacceptably high electrical resistances at the current-connector/interconnect interface [Fergus'05]. Hence, only chromia-forming alloys were explored in the last decade as the best candidate of metallic interconnectors. Using this kind of alloys can bring considerable cost reduction in the fabrication of SOFCs without sacrificing the cell performance. However, many issues concerning the chemical stability of these alloys in the real operating condition of SOFCs must be primarily handled [Sakai'06].

The chromia-forming alloys mainly involve three categories: the chromium Cr-based, the iron Fe-based and the Ni–based alloys. Among, the Cr–based alloys are developed for electrolyte-support planar SOFC that typically operate around 1000°C because their thermal expansion behaviours in the temperature range of 25°C–1000°C exhibit considerable similarity to that of the other ceramic components [Piccardo'09]. But for the ITSOFCs operating around 800°C, Fe– or Ni–based alloys are more favoured owing to the reduced cost and improved ductility [Zhu'03]. Moreover, the Fe–based alloys, i.e. stainless steels, also have the advantage on the thermal expansion coefficient which is preferably matched with those of other ITSOFC components.

In spite of using different metal as the base, all the alloys mentioned above contain chromium for forming corrosion-resistant Cr_2O_3 scale in the presence of oxidant. However, due to the high oxidation rate of chromium, this scale is instable in oxidizing environment (locating not only at the higher oxygen pressure end of the cathode but also at one end of the anode side where the hydrogen has been diluted by produced water gas) and can be further oxidized, forming volatile gaseous Cr species such as CrO_3 or $CrO_2(OH)_2$ which leads to higher oxidation rates [Fergus'05] and fuel cell poisoning [Fontana'09, Piccardo'06] . One solution is to add into the alloys other chemical elements such as Mn and Ti, or reactive elements such as La, Nd, Y, etc. Another solution is to coat these alloys with a protective oxide layer to suppress the volatilization of chromium.

In a planar-type SOFC stack, the interconnector is repeatedly deposited between the individual cells. Using metallic interconnectors will obviously increase the overall weight of the stack. According to [Cable'07], the metallic interconnectors can account for up to 75% of the stack weight. Furthermore, the formation of oxide scales on the surface of such repeated element leads to significant ohmic losses. In addition, the contact resistance between the interconnector and the adjacent ceramic-contained components is also important. Serving as

an electrical conduction between the cells and the external circuit, the interconnector plays a crucial role in the stack. The failure of one interconnector means the failure of the whole stack.

I.1.3. SOFC geometries and stack configuration

SOFCs come in several different designs, including tubular and planar geometries and other novel designs.

I.1.3.1. Tubular SOFC

The tubular SOFC was pioneered by the US Siemens-Westinghouse Power Corporation in the late 1970s [Larminie'03] and has been greatly developed. It is in configurationally a long tube with the electrolyte and the anode built up in layers on the air electrode, as shown in Figure 1-3. The fuel flows on the external surface of the tube while the air is fed into the cell through a thin delivery tube. An axial interconnector is deposited on the cathode for conducting the electrons to the external circuit and allowing cells to be connected in series. In tubular SOFC stack, the outer anode layer of one tubular cell is connected to the inner cathode layer of the next tube by the interconnector. With the tubular design, the input air can be directly heated up to the operating temperature by the heat released from the cell internal reactions. Moreover, the dimension of the interconnector is much smaller when compared to the planar SOFC so that the high cost ceramic interconnectors still play a dominant role in tubular design SOFCs where only small amounts of interconnects are required [Tietz'02]. However, this design results in a long current path inside the cell (see Figure 1-4), leading to large Joule heats production.

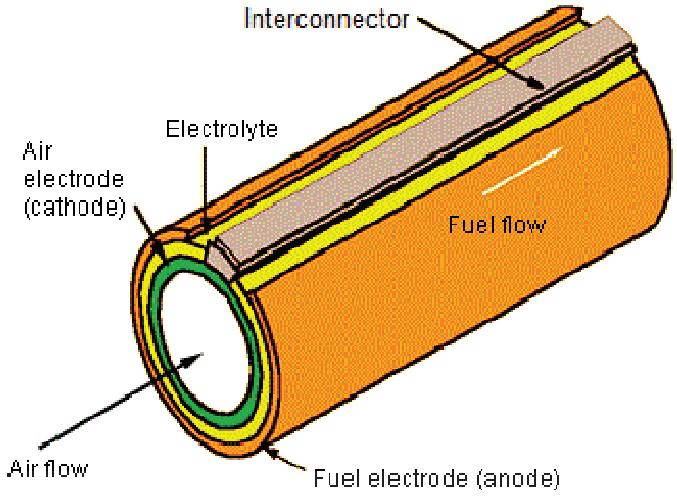

Figure 1-3 Siemens-Westinghouse single tubular SOFC*

*Source : http://www.stubhollow.com/Transportation/Electric/boats/fuelcellboats.htm

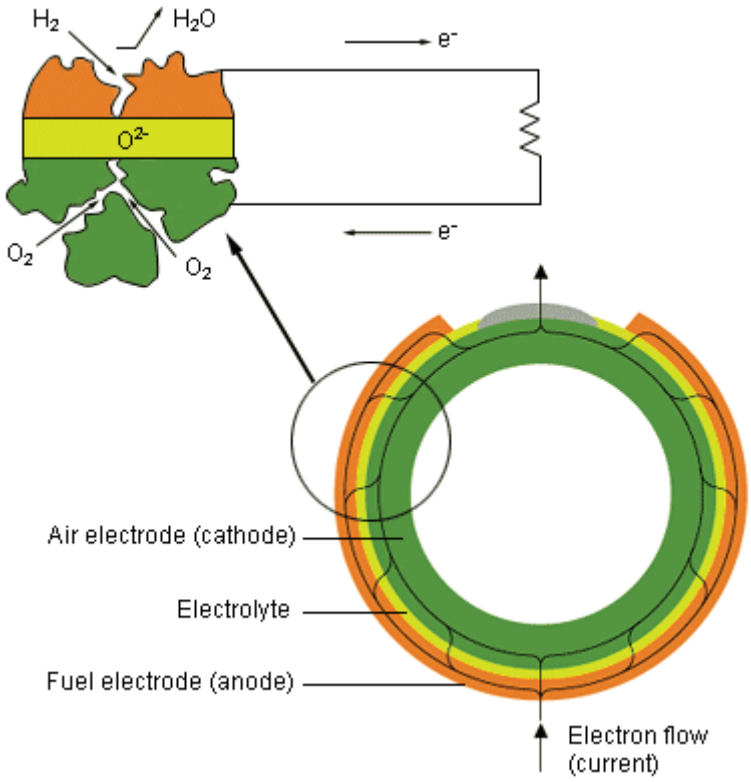

Figure 1-4 Single tubular SOFC operation and current path*

I.1.3.2. Planar SOFC

The development of planar SOFCs started later than that of tubular SOFCs. They are built analogously to other types of fuel cells, such as PEMFCs [Bagotsky'09]. The planar SOFC displays much higher power density (which can reach about 2 W/cm^2 at 1000°C) than that of the tubular SOFCs (about 0.25–0.30 W/cm^2 at 1000°C) [Mench'08]. This design enables the simple cells connection with shorter current path and favours the application of low-cost stack fabrication methods such as screen printing and tape casting [Larminie'03]. Unlike the tubular SOFC in which the reactant gases flow in an open passage along the electrode surface, in the planar SOFC the fuel and the air flow down along the parallel channels located on the two sides of the bipolar plate interconnector (see Figure 1-2). According to the flow directions of the fuel and the air, planar SOFCs can be further divided into 3 types: co-flow, cross-flow and counter-flow. The parts sandwiched by two bipolar interconnectors are the core of the fuel cell. They are always assembled together and known as membrane-electrode-assembly (MEA) which can also appear in various configurations such as anode-support, electrolyte-support, and cathode-support. From the point of view of manufacturing, a key issue in planar SOFC design is the difficulty of sealing the flow fields at the edges of the fuel cell, due to non-matched thermal expansion properties of materials over the large temperature variation.

I.1.3.3. Hexis SOFC

There is another attractive SOFC design developed by Sulzer Hexis Ltd. who targets to the application in small-scale combined heat and power (CHP) system. In this design, the stack is cylindrical, composed by a series of repeated units in planar design and with a round hole in the center. Each unit contains a disk-shaped electrolyte supported cell and a metallic interconnector in the same form (see Figure 1-5). The active area per cell is roughly 100 cm^2. During operation, the fuel (reformed natural gas) is fed along the centre axis of the cylindrical stack and radially diffuses into the fuel channels of each unit's bipolar interconnector while the air is directly blown into the air channels. The excess fuel will mix with the air around the cylinder surface and then be burnt off surrounding the stack to maintain the operating temperature (850°C–900°C). Such design minimizes demands on seals and simplifies the thermal management of the system [Mai'11]. Based on such SOFC stack, Hexis has developed a micro-CHP unit known as Galileo 1000 N system which covers both the entire heat requirements and the basic requirements for electrical power of a single-family home. This system can supply an electrical power of 1 kW and a thermal capacity of 2kW with an overall efficiency of more than 90% [Nerlich'10].

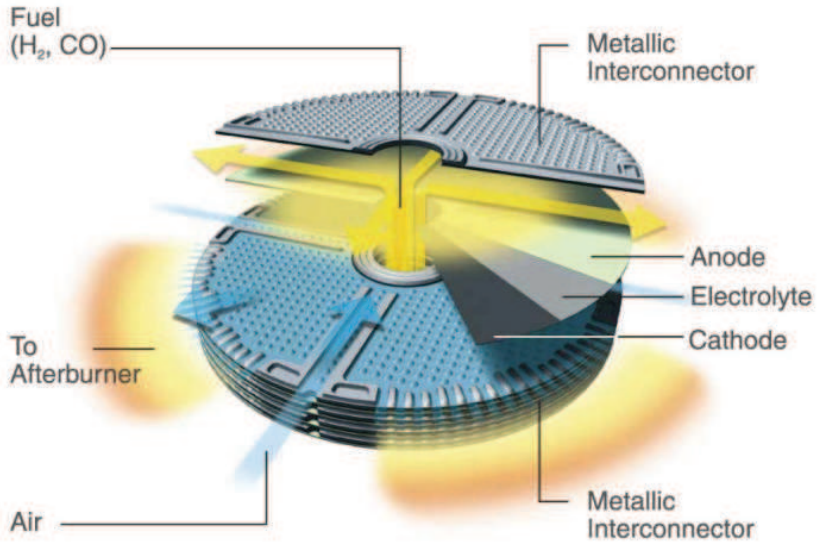

Figure 1-5 Hexis SOFC stack*

I.1.4. Summary of the advantages and disadvantages of SOFC

Compared to other fuel cell systems, the SOFC has many advantages:

1. High operating temperature increases the reaction rate and eliminates the need for expensive catalysts. It also enables internal reforming of complex fuels.

2. SOFCs can operate with various types of fuels such as methanol and hydrocarbons and is tolerant to carbon monoxide which is a major poison to PEMFC.

*Source : http://www.hexis.com/en/graphical-material

3. They produce high quality heat by-product which can be used for CHP applications so as to attain higher overall efficiencies.

4. They have a potential long life expectancy of 40000–80000 hours [Stambouli'02, Tu'04].

However, SOFC is not a perfect fit for all applications and has some technical challenges to overcome. Although the high-operating-temperature nature brings many benefits, it is the principle origin of most problems encountered in the SOFC application, such as the following issues:

1. A significant start-up time is required for the system to elevate the stack temperature to the operating value.

2. High operating temperature increases the difficulty of temperature control and is related to the SOFC degradation in various cycling conditions such as thermal cycle, redox cycle and load cycle.

3. It causes thermal stresses and microstructural changes on the fuel cell components in long-term operation, resulting in irreversible damages to SOFC.

Although the operating temperature of SOFC has been decreased with the development of new electrolyte materials in recent years, these issues still remain and limit the reliability and lifetime of SOFC stacks. Moreover, the usage of metallic interconnector in ITSOFC stacks, in spite of the attractive benefit on cost reduction, also evokes new problems such as cathode catalysis degradation [Matsuzaki'01]. Accordingly, durability extension is a continual improvement process for SOFC system, as for any other ones.

I.2. Durability and reliability issues of SOFC system

For the purpose of commercialization, SOFCs are asked to have a small degradation rate during a cell and/or stack lifetime more than 40000 hours for stationary application and up to 20000 hours as auxiliary power units (APU) for transportation. Although this type of fuel cells themselves has a potentially long life in the order of 40000–80000 hours, rare SOFC systems to date can satisfy this demand.

The degradation/failure of SOFCs can be generally attributed to two aspects: either to the material selection mistakes as well as the defective design on the fuel cell/stack itself, or being caused by the improper system operations. In the past decades, great investigative efforts, including the improvement on the compatibility of materials for SOFC repeat unit and the optimisation for the stack configuration, have been contributed to solve the problems in the first aspect in order to achieve higher cell performance and reliability, whereas the later aspect had been ignored. It was until the recent years that the researchers began to attach the importance to the effect of system failures upon the SOFCs' durability. It is worth noting that the system failure mentioned in here is referring to the malfunction that occurs in the sub-

systems and components other than the fuel cell stack itself. This part is the so-called balance of plant (BoP) which, together with the stack (s), forms the fuel cell system [Larminie'03].

A BoP failure, being either a control mistake or an equipment fault, can lead to accelerated aging/ degradation of fuel cells. This kind of failures often takes place incidentally and is difficult to perceive in the early stage of occurrence when their effect upon the fuel cell performance is not significant. However, at the end, they always result in catastrophic damage to the fuel cells.

Normally, the BoP failure does not have direct impact on the SOFC but induces a progressive deviation of operating condition from the rated one. Since the cell performance and its state of health are both sensitive to the operating condition, the later is a key issue in the investigation of fuel cell systems' reliability and durability.

Improper operating conditions can lead to a variety of degradation mechanisms in SOFCs [Yokokawa'08]. For the stationary applications, the chemical instability at the interfaces of FC's components is a key issue. In the transportation applications where frequent thermal cycles are required, the thermo-mechanical instability of FC materials is a crucial problem [Yokokawa'03].

In a SOFC stack, degradation is inhomogeneous on the whole active cell surfaces. Moreover, different degradation phenomena could occur simultaneously, interacting and being cumulated [Larrain'06]. In such a case, the degradation behaviour observed in stacks is difficult to interpret. It is therefore essential to increase the understanding in SOFC degradation mechanisms. Such investigation is also helpful for differentiating the abnormal operating conditions from the normal and tolerant ones.

This section gives a literature overview on fundamental mechanisms of the aging and degradation in SOFCs as well as on different types of BoP failures.

I.2.1. SOFC degradation mechanisms

SOFC failures can be divided into two types: (i) hard failures caused by the mechanical damages such as physical breaking and delamination of layers; and (ii) soft failures due to the chemical instability of materials and the consequent microstructural changes. The hard failures are inherently irreversible whereas the soft ones could be recovered in specific environments. Though, the later can eventually lead to hard failures if none of corrective actions is taken.

I.2.1.1. Soft failures

I.2.1.1.1 Ni–based anode reoxidation

One of the challenges related to Ni-based anode is the problem of redox instability. The anode in a factory-fresh anode supported electrolyte (ASE) SOFC is commonly a combination of NiO and YSZ powders. On the first operation of the cell, the NiO is reduced in situ to metallic nickel when exposed to the heated fuel stream and a porosity structure is obtained. When the metal content of the composite is sufficiently increased, the randomly packed well conductive metal particles start to connect with each other and form percolating networks with the insulating ceramic matrix [Pihlatie'10]. The connected nickel-nickel particles, on the one hand, serve as an electronic conductor and as a catalyst for the electrochemical reaction; on the other hand, they cause several undesirable characteristics. A crucial one is their chemical instability under high temperature conditions. This drawback leads to the risk of Ni reoxidation, that is, the so-called 'redox' phenomenon.

As the anode is maintained in a reduced state (through continuously providing fuel to the anode), the anode redox does not happen. However, once the fuel supply is interrupted (either intentionally or as the result of a fault), the oxygen ions that have passed through the electrolyte will cumulate on the anode side, resulting in an oxidizing atmosphere in which Ni will be re-oxidised into NiO.

Because the solid NiO is larger (about +70%) than the Ni particles in the volume [Sarantaridis'07], its expansion will block up the pores in the composite, obstructing the penetration of reactants and decreasing the TPB, and finally impacting the electrochemical reaction rate. In more serious cases, this will give rise to internal stress in the composite when the accommodation of the porosity is not sufficient and thereby alter the microstructure of the anode [Pihlatie'10]. As a consequence, cracks and fractures in the NiO scale will take place and open up pathways for inward oxygen diffusion, aggravating the anode reoxidation [Pihlatie'09]. Furthermore, the expansion of NiO can bring about shear forces at the electrode-electrolyte interfaces [Tu'04] which lead to the delamination between the anode and the electrolyte layers. Even if subsequent restoration of the fuel can convert the NiO back to Ni, the original state of the anode is not very likely to be recovered after such kind of mechanical damage. In practice, the SOFC stack is combined with a nitrogen supply sub-system which reacts for start-up, shut-down and emergency cases where it provides nitrogen gas to flush the anode so as to protect it from air inflow and consequently oxidation.

Besides, local anode reoxidation can also occur in long-term operation [Ma'10]. It is related to high vapour content in the situation of fuel starvation. The later is usually attributed to the high fuel utilisation which is applied in order to attain high system efficiency. In addition, the fuel supply state could be another factor causing high local vapour content if the flow rate is too low to effectively move away the oxidation products from the reactive sites. Due to the low electrical conductivity of the NiO, a significant decline on cell performance can happen. However, differing from the mechanical damage, this kind of alteration (on the electrical property) is reversible at a lower degree of oxidation. The process of Ni oxidation in the temperature range of 600°C–1000°C begins with the adsorption of the oxygen atoms on the surface of the metal [Pihlatie'10]. After the initial oxide, a thin film is established on the metal surface and will thicken logarithmically. Thus, as long as the reductive atmosphere can be regained over the anode during the initial oxide, the oxidation of Ni can be effectively

inhibited and reverted. The reduction of NiO particles occurs at the interface between NiO and previously reduced porous Ni at an approximately linear rate [Sarantaridis'07].

Although the anode reoxidation is reversible at the primary stage, the irreversible microstructural changes in the anode are inevitable in the reduction and reoxidation cycles. According to [Cassidy'96], the initial reduction of NiO in anode cermet does not affect electrode structure and performance but the reoxidation has indeed a negative effect. In order to extend the lifetime of the SOFC, it is preferable to control the kinetics of the anode degradation. The later, according to the investigations on this topic [Fouquet'03, Hagen'06, Iwata'96], is mainly related to the operating parameters such as temperature, gas composition, especially the partial pressure of water and the current density when the SOFC is operated in steady mode [Yokokawa'08]. However, for transportation applications where the SOFC is expected to sustain as many as possible redox cycles, material solutions to enhance redox reliability of the Ni-based anode are still important [Yokokawa'08].

I.2.1.1.2 Carbon deposition

Another undesirable characteristic of the Ni-based anode is the problem of carbon deposition (coking). It is encountered in the direct internal reforming (DIR) SOFCs operated with carbon-contained fuels such as the methane. In an environment full of hydrocarbons, Ni has the propensity to catalyse carbon formation especially under high temperature environment [Baker'75, Keep'77]. The formed carbon will deposit on the surface of Ni, blocking up the anode pores, hindering the fuel transport and decreasing the electrical conductivity of the anode, and as a consequence reduces the electrical efficiency as well as the durability of the fuel cell [Park'09, Lorente'12].

In order to avoid this drawback without sacrificing the advantage of SOFCs in fuel flexibility, a number of investigations had been conducted attempting to replace the Ni in the anode cermet with other metals. However, because of its high catalytic activity for both electrochemical and reforming reactions, Ni remains the most promising anode material for SOFCs. In this context, some researchers have turned efforts on suppressing the carbon forming reaction on the anode. With this view, the understanding in carbon formation mechanism as well as in the reactions kinetics is essential.

Take the methane-fuelled SOFC as an example. When the mixture of CH_4 and vapour is feed, steam reforming and shift reaction can occur at the anode catalyst (i.e. on the surface of Ni) to generate H_2, CO and CO_2. Simultaneously, decomposition of CH_4 and Boudouard reaction take place and the carbon is formed. The relative chemical equations are:

$$\text{Methane Cracking:} \quad CH_4 \leftrightarrow C + 2H_2 \qquad \text{Eq. 1-6}$$

$$\text{Boudouard Reaction:} \quad 2CO \leftrightarrow C + CO_2 \qquad \text{Eq. 1-7}$$

In high temperature, these two reactions are the major pathways for carbon formation [Laosiripojana'07]. The high temperature will then dissolve the carbon and precipitate it into

the bulk of the metal nickel, forming a graphite fibre [Kim'06]. Moreover, it was reported that the amount of carbon adsorbed on the anode could increase progressively and become more strongly bound with the rise of reaction temperature [Finnerty'98].

The double headed arrows in the above chemical equations imply the recoverability of the anode coking. From the point of view of chemical kinetics, the risk of carbon formation could be reduced by moving the reaction equilibrium point towards the left side. In this regard, the literature suggests several methods to change the concentration of reactants, such as increasing the Steam-to-Carbon (S/C) ratio of input fuel or the current density. Note that although temperature has a major effect on the rate of chemical reaction, it is not recommended to deal with the carbon deposition problem in a DIR SOFC by changing operating temperature because its variation can incur permanent mechanical degradation inside the fuel cell.

The addition of excess steam into the fuel is an effective method to not only inhibit carbon formation but also for the removal of pre-formed carbon deposits. The principle is to promote the water gas shift reaction so as to reduce the amount of CO produced from the reforming reaction whilst increasing those of CO_2 and H_2 on parallel such that Boudouard and methane cracking reactions could be reversed. Besides, high steam content is favourable to carbon gasification process that occurs via the following reaction:

$$\text{Carbon Gasification: } C + H_2O \rightarrow CO + H_2 \qquad \text{Eq. 1-8}$$

He et al. (2007) [He'07] reported that the addition of excess steam to the methane could decrease the carbon amount by about 20%. Usually, carbon deposition problems for SOFCs running on hydrocarbons can be avoided when an appropriate S/C ratio of more than 2 : 1 is applied [Novosel'08].

On the other hand, however, the addition of excess steam can cause a huge energy waste for extra steam generation and lead to a drop of open circuit voltage of the fuel cell at high steam contents, resulting in a significant reduction of the overall efficiency of the system. Furthermore, this method risks of deactivating the metal catalyst by oxidation. Accordingly, in practice, the adequate S/C ratio for internal reforming must be carefully determined to restrict the carbon formation in a safety range. In fact, the addition of only a small quantity of steam to the methane can lead to a significant lowering of the rate of carbon formation on the Ni-YSZ anode [Finnerty'98].

Apart from S/C ratio, current density also has a significant impact on carbon deposition [Mermelstein'10]. As the current density increases, the concentration of oxygen ions at the anode side rises simultaneously, promoting the methane partial oxidation reaction (as represented in Eq. 1-9).

$$\text{Methane Partial Oxidation: } CH_4 + 4O^{2-} \rightarrow 2H_2O + CO_2 + 8e^- \qquad \text{Eq. 1-9}$$

Alzate-Restrepo et al. (2008) [Alzate-Restrepo'08] found that the carbon formed under working condition was more weakly bound to the Ni–YSZ than that formed at open circuit condition.

In addition, the quantity of the carbon formed in a certain amount of time may be related to the fuel flow rate. Under a homogeneous formation rate, more carbon deposits with longer residence times, corresponding to lower flow rates [Kim'06].

In summary, carbon deposition on the anode is relevant to a series of operating parameters (temperature, S/C ratio, current density and fuel flow rate). Proper selection and optimisation of the operating condition is hence significant for the durability of stationarily operated SOFC stacks.

I.2.1.1.3 Sulphur Poisoning on the anode

Anode poisoning is one of the degradation mechanisms in the practical application of the DIR SOFCs, due to their limited tolerance to the impurities contained in the natural gas or coal syngas. These commercial fuels can contain tens to thousands parts per million (ppm) of H_2S which is known to have detrimental effects on SOFC performance [Lussier'08]. Although a desulphurizer unit is always available for SOFC to clean up the fuel before being entered, minor content of sulphur (around 0.1–10ppm) still exists in the post-processed gas and can degrade the fuel cell during long-term operation. For example, Sasaki et al. (2011) [Sasaki'11] observed in an SOFC a slightly higher cell degradation rate of 0.68%/1000hours with 5ppm H_2S compared to the value of 0.3%/1000hours without H_2S. In addition, breakthrough of sulphur impurity can be encountered when accidental desulphurizer failure happens. Fortunately, it has been found in many investigative experiments that cell degradation caused by low content sulphur poisoning could be recovered after the removal of H_2S. The degree of remedy (fully or partially) was found dependent on the operating conditions and the concentration of H_2S in the fuel. Li et al. (2010) [Li'10] had investigated the effects of operating current density and temperature upon the sulphur poisoning deterioration and upon the recovery degree. They concluded that a relatively high current density could not only reduce the H_2S poisoning effect but also help with cell performance recovery. In addition, they reported that the temperature was not an independent factor influencing H_2S behaviour although the increase in it could be favourable for the recovery process.

Typical Ni-based anode poisoning by H_2S is a stepwise degradation procedure. When H_2S is present at the anode side, it can react with the oxide ions and form sulphur on the surface of Ni. A wide range of sulphur adsorption is energetically favoured under SOFC operating conditions. It is considered as the predominant mechanism for the sulphur-induced performance degradation, especially at low temperatures where the adsorpted sulphur is more stable on the Ni surface [Gong'07] so that the sulphur poisoning becomes irreversible. In contrast, at high temperatures, low concentrations of sulphur in the feed gas can be tolerated. Additionally, at high current density, a large amount of O^{2-} is transported to TPBs and can oxidize the excess H_2S and the pre-formed S into SO_2 [Li'10]. Since the sulphur dioxide is considered less adverse for SOFC, sulphur poisoning can be mitigated in this condition. The corresponding chemical reactions are given in the following:

$$H_2S + O^{2-} \rightarrow S + H_2O + 2e^- \quad \text{Eq. 1-10}$$

$$H_2S + 3O^{2-} \rightarrow SO_2 + H_2O + 6e^- \quad \text{Eq. 1-11}$$

$$S + 2O^{2-} \rightarrow SO_2 + 4e^- \quad \text{Eq. 1-12}$$

H_2S can also sulfurize Ni in a H_2S-rich fuel environment, due to the high vulnerability of Ni to sulfur poisoning. The formula of the possible sulfurization reactions can be generalized as follow:

$$3Ni + xH_2S \rightarrow Ni_3S_x + xH_2 \quad \text{Eq. 1-13}$$

The nickel sulfide formation influences the electrical conductivity of the anode. It can thus be regarded as a key contribution for the sharp cell current/voltage drop encountered in the beginning of introduction of the rich-H_2S-contained fuel.

In sum, the performance loss of SOFC anode due to sulphur poisoning can be related to 3 major factors which are respectively influenced by 3 different physicochemical degradation mechanisms [Cayan'08]:

1. Decrease in the mass transport of fuel gas molecules due to physical adsorption of the sulphur on the anode surface and consequent blockage of gas diffusion channels;
2. Decrease in the catalysis of Ni toward chemical and electrochemical reactions because the sulphur atoms from H_2S deactivate the active sites (due to dissociative adsorption mechanism);
3. Decrease in the electrical conductivity of Ni due to compound formation.

I.2.1.1.4 Effect of air humidity on cathode performance degradation

In fuel cell operation, considerable heat is set free from the electrochemical reaction and produced due to the Joule losses. Part of them is absorbed by the endothermic internal reforming reactions while the rest must be eliminated in order to avoid high thermal stresses inside the fuel cell. In power plants with SOFCs, it is often required to blow the air of the amount much larger than that needed for the reaction so as to take off the excess heat. This measure may provoke a relatively high concentration of the impurities (contained in ambient air) at the cathode side and induce cathode degradation in long-term operation.

The water gas existing in ambient air, in spite of accounting for only several percentages in volume, has considerable effects on the performance of SOFC cathode in operating condition. This effect had been proven irrelevant with the gas composition but related to cathode polarisation [Nielsen'10]. Hagen et al. (2009) [Hagen'09] had tested a series of SOFCs firstly with dry air and then with the air of ~4% humidity (air was humidified by leading it through a water flask at room temperature, giving a humidity of ~4%). In the former case, no cell voltage degradation was observed whereas in the later case, the cell voltage degraded

progressively. The impedance spectrum given in Figure 1-6 reveals this degradation. Moreover, after shifting the cathode gas to dry air, the voltage was found being partially regained. They concluded that there were two mechanisms of humidity-induced cathode degradation: one was reversible, the other was irreversible. The former was explained by the promoted mobility of impurities in steam and polarization condition which makes them concentrate around the TPB points and thereby leads to performance degradation. When the humidity is removed, these impurities could return to their original locations and the TPB is re-freed for electrochemical reaction so the performance is recovered. The irreversible degradation mechanism could be explained by the catalysis of water vapour to the decomposition of perovskite LSM cathode [Liu'11]. In high steam concentration, LSM may decompose to LaO_3 and Mn_2O_3, leading to fatal degradation of the cathode.

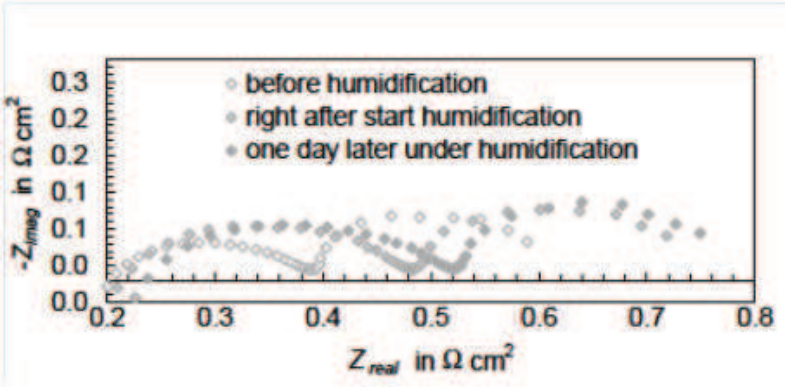

Figure 1-6 Impedance spectra recorded under current density at 750°C and 0.75A/cm^2 just before starting the 4% humidification of air, right after start and after one day in humid air [Hagen'09].

I.2.1.2. Hard failures

Hard failures in SOFC mainly mean structural failure that is usually irrecoverable. General structural failures in SOFCs can be categorized into cohesive and adhesive failure. Cohesive failure refers to the fracture (cracking) of individual materials or components. These cracks may be pre-existing defects formed during the production or be initiated during operation due to inadequate material selection. Adhesive failure refers to delamination that often occurs at the interfaces formed by dissimilar materials or components in the cell or the stack. It can be encountered during the operation of the cell/stack in which high temperature gradient appears, leading to thermal stress generation due to the mismatch of cell materials in thermal expansion coefficients. A splitting force consequently arises from this stress and can detach the assembled cell components when it increases to a certain degree. At the place where the delamination is present in the SOFC, both the current path and the reactive sites are destroyed. In galvanostatic mode, the cell will deliver a constant current while the voltage declines. Since no electron can flow in the degraded interface, the remaining intact areas have to supply extra current paths to sustain the current density. Due to the non-negligible ohmic resistance, considerable Joule heat may be locally produced and bring about high temperature gradient

over the cell unit, which risks provoking one and another delamination event as a domino effect. Such kind of delamination often extends between interconnector and electrode or between interconnector and current connector, being reflected by a progressive increase in contact resistance. It would finally result in individual cell failure and can even spread to adjacent cells in the same stack. In case of low current delivery, however, owing to the high electronic conductivity of the metallic material in the interconnector, the extension of delamination is not very likely to occur.

In addition to the area on the interconnector, the delamination can take place at the interface between electrode and electrolyte as well. The electrode/electrolyte detachment is usually a consequence of thermal cycling or rapid heating [Gazzarri'08]. Its impact upon the cell performance is higher than that of interconnector detachment because this phenomenon can not only impede the ionic transport but also irrecoverably reduce the length of TPB, thereby directly leading to partial or complete cell deactivation. The open gap arising from the delamination contributes to a large resistance to the oxide ions transport. This will build up a cumulated internal pressure at the cathode/electrolyte interfaces and cause total cathode cracking. Once the cathode has delaminated, subsequent degradation will continue to occur and at an accelerated pace [Virkar'10]. When the cell sealing is destroyed, leakage of oxygen toward the anode side may occur, leading to anode destruction by re-oxidation. Generally, gas leakage increases with the increasing of the stack temperature. It can cause direct combustion of gases inside the fuel cell, leading to local heating [Yokokawa'12]. In the extreme case, a negative voltage could exhibit at the troubled cell. It has been demonstrated that one of the cells operating under negative voltage would be prone to the stack degradation, especially for planar type stacks [Virkar'10]. It is thus suggested to measure the voltage across each cell during real operation so as to prevent catastrophic failure of the whole stack. More than that, monitoring and ensuring every cell operated above 0.5 V is recommended, because anode oxidation of nickel catalysts can be accelerated if the SOFC is operated below 0.5V. The event that individual cell’s voltage decreases to less than 0.5V is easy to happen, due to flow misdistribution, degradation, cold temperature, or other influences [Mench'08].

I.2.2. BoP failures

The Balance of Plant (BoP) is the sum of all equipments for safe operation and the technical coordination of all concerned parts of an energy system. It consists of the remaining systems, components, and structures that are not included in the prime energy generation unit (fuel cell stack in this case). In an SOFC system, BoP equipment can include reformer, ejector, burner, air blower, pipe and other ancillary components to support safe operation of the fuel cell. It can account for around 75% of the volume of the entire FC system. To operate effectively and efficiently, fuel cell systems must have a reliable BoP, which is yet very difficult to achieve. In real applications, poor durability of FCs is often attributed to BoP failures. According to the research of Ramesohl et al. (2011) on several different SOFC CHP systems [Ramesohl'11], 49%–56% of the system failures or accidental shut-down are caused by the faults in the BoP part. .

For a SOFC system, the common and frequent-occurred BoP failures include stack temperature control failure, mistakes in fuel supply control, air blower failure, no water supply, gas leakage due to untight pipes, load failure (too high current or load rejection), desulphurizer failure and so on. Their occurrence frequencies vary for different system designs and are strongly related to how the component or the sub-system is being used. These failures take place suddenly or progressively and would not be easily detected by the sensors. Furthermore, sensor failure is also a usual and crucial event during long-term high temperature operations, leading to fatal mistake in controlling and thereby catastrophic system failure. Hence, supervision relying on single sensor monitoring is not an effective way to ensure the reliability of SOFC systems.

In this context, a number of mathematical and statistical methods have been developed to quantify the frequency of BoP component failures, serving for preventive/scheduled maintenance purpose. It must be emphasized that it is not necessary to consider all BoP failures for the reliability estimation of the system. Generally, the supervision tool is developed based on a graphical fault tree that is afore-constructed with the expert knowledge to portray logical occurrence of undesired faults. Relying on it, not only the detection mechanism of a given fault can be determined but also the consequences of the fault could be deduced. Arsie et al. (2010) [Arsie'10] had set up such fault trees for the failures regarding air supply and temperature control in the SOFC system. In each fault tree, the analysed failure was linked to the possible mechanisms or consequent events and the associations were extended to the operating variables that may be influenced by the fault. In the study of Åström et al. (2007) [Åström'07], a fault tree had also been established for a 20kW SOFC system for the purpose of developing a simulation algorithm serving for system reliability analysis.

I.3. Solutions to ensure SOFC system durability and reliability

The issues of materials degradation and the problems in the BoP equipment have great negative impacts on the reliability, durability and cost of SOFC system. That is the barrier which prevents SOFC from a successful replacement of the traditional fuel-combustion system for power generation. With the development of manufacturing techniques and emergence of new materials, lowering the operating temperature is widely believed being a solution able to extend SOFC's durability and cut down its cost. However, it does not allow solving the problem of system reliability.

SOFC system is usually combined with other sub-system or auxiliary components for cogeneration in order to gain higher efficiency. Such a complicated system is more vulnerable to faults, malfunctions and unexpected operating modes. Hence, a reliable and universal monitoring tool is particularly necessary and important in the application of this kind of complex system.

Classical methods for system monitoring are mainly based on specific sensors to check if the characteristic parameters of an individual component are within acceptable bounds. For a

SOFC system with a large number of components and combined with various sub-systems, this kind of method is obviously not applicable because:

1. Install additional sensors on each component to monitor will further increase the complexity of the entire system, and can lower the system reliability instead of being favourable to;

2. The addition of specific sensors and extra equipments for signal transfers will result in higher cost for system supervision, not meeting to the requirement of commercialisation;

3. Some measurements may become unavailable or have low precision in the situation where the process does not stay in steady-state and the monitored variables change dynamically following different operating points, which could lead to diagnostic mistake or failure;

4. At last, measuring a great number of variables by sensors can result in a large dimensional database which complicates the reliability analysis, increasing the difficulty of information extraction from the measurement data, and diminishing the real-time applicability of the algorithm.

Nowadays, a supervision tool allowing to prevent catastrophic failure is popularly required for large-scale power system. This implies that the tool must be capable of detecting the failure at the early stage of its occurrence. To achieve this goal, the fault diagnosis procedure should be implementable in real time.

For the case of SOFC system where many components are present in a high temperature condition, the diagnosis work is even more complex and difficult. As introduced in the last section, not only the SOFC stack but also its sub-systems can have a failure or degradation in long-term operations, leading to breakdown of the system. Furthermore, a single fault may have a chain of influences on the fuel cell, giving rise to more severe problems. For instance, a fuel leakage event at the outside of the stack (classified to the BoP failure) can cause partially anode reoxidation due to local fuel starvation. The anode reoxidation can influence the anode microstructure and may provoke severe electrode degradation. Since the limitation on the number of actual monitoring sensors restricts the achievability of fault allocation, the original cause of the system failure may fail to be recognized, resulting in misdiagnosing. Under this background, innovative diagnosis concepts should be developed for SOFC systems.

To meet this requirement, an R&D European project program, titled as "**GEneric diagNosis InstrUment for SOFC Systems (GENIUS)"**, was proposed aiming to develop universal diagnosis methodologies applicable for different SOFC systems. Its interest and innovative part is that it proposes to use the SOFC/stack as a "sensor" for diagnosing the failures in the BoP by using only the existing sensors in the system whereas the addition of extra sensors is not allowed. Artificial intelligence, data mining and signal processing techniques are recommended to apply in this project to accomplish intelligent analytic algorithms for both

off-line and on-board diagnosis applications. More details about the GENIUS as well as our tasks in this project will be introduced in the next chapter.

Chapter II GENIUS project & Diagnosis approaches for FC systems

II.1. Introduction to the GENIUS project

The GENIUS project* is a response to the call for proposals from the Fuel Cell and Hydrogen Joint Undertaking APPLICATION AREA SP1-JTI-FCH.3: *STATIONARY POWER GENERATION & CHP topic Operation diagnostics and control for stationary applications*. It was developed in coordination with the "ASSENT" and the "EuroFC-life" proposals that aim to address system efficiency optimization and improve the understanding about FC degradation mechanisms.

II.1.1. Concept and objectives

The GENIUS project targets to the development of GENERIC methodologies applicable for diagnosing different SOFC systems. The final outcome of this project is a device integrated with generic diagnostic algorithms. This device is permitted to apply only the existing sensors on the supervised system. Under this limitation, an innovative idea is proposed, that is, to use the FC stack as a special sensor for system monitoring. All available measurements on the FC can be regarded as the outputs of this "sensor", serving for the system diagnosis. The developed algorithms should enable either on-board or off-line diagnosis. Once a fault is detected and identified, counter-measures, such as the optimisation of operating parameters, could be carried out by the control system in order to maintain the system reliability or at least mitigate the influence of the fault upon the state of health of the fuel cell.

II.1.2. Consortium members and their roles

GENIUS is a collaborative project. It consists of 4 academia (EIFER, UNIGE, UNISA, FCLAB) and 7 industrial partners (CFCL, EBZ, Hexis, HTceramix, Topso Fuel cell, Wärtsilä, VTT), as shown in Figure 2-1. The 3 academia (UNIGE, UNISA, EIFER and FCLAB) are in

* Refer to the web page: https://genius.eifer.uni-karlsruhe.de/

charge of diagnosis algorithm development. EIFER and the industrial partners are mainly in charge of systems testing to generate and collect experimental data as well as validation tests of the developed algorithms. They choose themselves the appropriate operation level for their own stack/system, defining the range of the operating parameters.

Figure 2-1 Map of the consortium of GENIUS

The development of diagnosis methodologies is preceded in 3 different directions, based on 3 approaches of fault diagnosis, respectively, i.e. model-based, signal-based and knowledge-based approaches. UNIGE and UNISA focus their efforts on the first approach, trying to establish models (grey-box and black-box) to simulate the FC performance at the normal state and in abnormal operating conditions. FCLAB mainly applies the later two approaches to achieve the SOFC systems' fault diagnosis in real-time. It is worth noting that the modern diagnosis system is usually required to not only realize the fault detection and identification/isolation but also able to estimate the fault magnitude. In our case, however, the developed diagnostic tool is only asked to implement the former task. .

II.1.3. Potential contribution to condition-based maintenance

Development of real-time fault detection and identification technologies will allow a migration from expensive scheduled maintenance (also known as preventive maintenance) to the more efficient, less costly alternative of condition-based maintenance (CBM) [Chebil'09]. The basic principle of CBM is to continuously monitor the considered system, based on the sensors data, so as to prevent the system from a possible malfunction or damage before it happens [Abdelghani'00]. It extends the concepts of preventive maintenance (PM) which is currently the most widely accepted approach applied to maintain electrical equipment and

power supply system [Dileo'99]. In these years, the interest in CBM has greatly increased in industrial applications [Cadick. PE'99].

For a SOFC system, due to the relatively high failure risk caused by its operating condition and the high cost of fuel cell materials and fabrication, “run it until it breaks” is obviously not a reasonable and wise strategy for its application; neither is the predictive maintenance strategy which only serves to exploit SOFC benefits throughout its lifetime instead of ensuring the system reliability cannot be guaranteed; nor is the PM that intends to replace the SOFC/stack before the end of their useful life. In contrast, the CBM displays potential benefits in ensuring the reliability of such kind of “costly” systems in long-term operation without the need of interruption. Its primary advantage is the capability of performing maintenance only when it is needed and at the most opportune times, through actively managing the health condition of the core or the ensemble of the system. Such concept allows thus an attractive reduction in the maintenance cost and exploiting the lifetime of the supervised component/system.

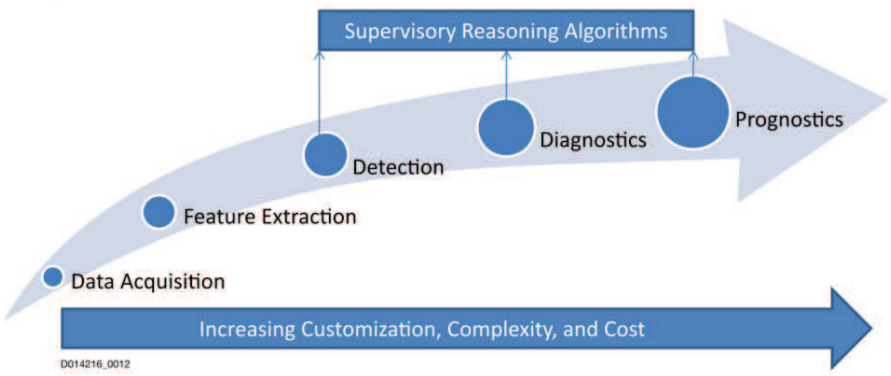

Figure 2-2 The complete process of condition-based maintenance [SRI'09]

To carry out an effective CBM, 5 sequential stages can be followed before performing maintenance activities, i.e.: data acquisition, feature extraction, fault detection, fault diagnosis/identification and prognosis at the end (see Figure 2-2). The difficulty and complexity of the implementation will increase along the steps. Diagnosis and prognosis are two important procedures in the CBM program. Most difficulties in the realization of the CBM lie in these two phases. According to [Lewis'97, Jeong'06], diagnosis is the process of finding the source of a failure (that is, a fault) while prognosis is the process of estimating/predicting a coming failure. The main aim of diagnosis is to provide early warning signs to engineers when the monitored equipment/system is operating in abnormal conditions. Although the equipment/system is running in abnormal/deterioration state, this does not mean that it has failed but just signs that a failure would be caused by the fault after a certain amount of time [Ahmad'12]. Concerning when this failure will take place, it is the prognosis that addresses this issue.

The GENIUS project is planned for the implementation of the diagnosis for SOFC system, thereby only covering the first 4 stages of the CBM program. It is expected that the diagnosis

results can provide information on the actual operating condition of the stack, supporting for the prognosis for the state of the system.

II.2. Diagnosis methodologies for FC system

In the field of system maintenance, fault diagnosis has become an issue of primary importance in modern process automation as it provides the prerequisites for the purpose of system failure prevention. When a physical parameter change due to the fault has occurred in a system, the fault effect will hardly be visible in the output performance [Athamena'03]. The classic fault diagnosis methods mainly rely on a set of different sensors integrated into the system, intending to capture the variation of eventually impacted variables that could indicate occurrence of the fault. This kind of methods can lead to great maintenance cost as well as poor system reliability, because a complicated system is often more subject to malfunction. Furthermore, noise-corrupted measurements and unreliable sensors can also influence the reliability of the diagnostic result.

In order to go beyond the restriction in the number of sensors and the limitation of the capacity of the sensors themselves, process modelling was introduced into the concept of fault diagnosis. The fundamental idea is to generate signals that reflect inconsistencies between nominal and faulty system operating conditions. Owing to the analytic models, the values of significant characteristic variables could be easily estimated without relying on the specific, costly sensors. However, the processes of the complex systems are often difficult to model with physical equations; and even if it could be, the modelling procedure would be very complicated, usually necessitating a set of auxiliary parameters which, however, is usually unavailable or incomplete. Furthermore, the higher accuracy is demanded, the more complicated the model will become and thus more time will be required for the simulation, which is not permitted in real-time diagnostics. To overcome these problems, new diagnostic methodologies have to be developed.

A number of researchers work on developing intelligent fault diagnosis methods by using the artificial intelligence technologies arisen with the application of mathematical and computer sciences. These technologies, such as data mining and pattern recognition, had been successfully applied in the field of business and finance (ex: customer relationship management, risk management, market forecasting where studying on large volumes of data is always involved) and demonstrated good practicability. During the recent decade, their application has extended to various domains and disciplines (ex: machinery, medicines, aerospace, communication industry, engineering etc.), helping realize the automatization of the data analysis as well as the procedure of decision-making. Likewise, the development of fault diagnosis techniques has also benefited from these technologies for achieving real-time system supervision and maintenance.

To date, different methods are available for carrying out fault diagnosis. They can be classified into three categories: 1) model-based approach; 2) signal-based approach; and 3) knowledge-based approach in which category the methods can be further divided into two types: pattern-

based and rule-based. In this section, these approaches are outlined, respectively. The corresponding techniques that have been applied for FC system diagnosis are overviewed.

II.2.1. Model-based approach

The design of a diagnostic tool begins usually by mathematically modelling the process of the considered entity so as to simulate its behaviours mostly without faults. Then, through a comparison between the measured parameters and the simulated ones without the presence of fault, a residual vector can be generated and evaluated to determine if a fault has happened. The residuals should be ideally close to zero under fault-free conditions, minimally sensitive to noises and disturbances, and maximally sensitive to the studied faults [Athamena'03]. Once the fault is confirmed being present, a decision-making process will be performed to identify its type based on a pre-constructed fault signature matrix. Sometimes, models for specific faults can also be set up to support for fault identification. Such a model-based diagnosis procedure is illustrated in Figure 2-3.

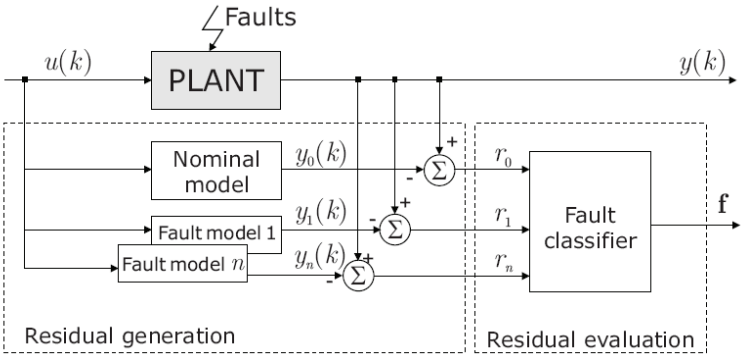

Figure 2-3 Schema of process model-based fault diagnosis [Isermann'06]

In fuel cell engineering, the application of the model-based approach has been investigated for fuel cell and/or system diagnosis. Escobet et al. (2009) [Escobet'09] used it to diagnose six faults of interest in the PEMFC systems: 1) increase of the friction in the compressor motor and 2) its overheating, 3) blocking of the channels in the diffusion layer of the fuel cell, 4) leakage in the air supply manifold, 5) the compressor motor control failure and 6) the stack temperature control failure. Four fault feature variables, i.e. the oxygen excess ratio, the compressor's current density and its speed as well as the stack voltage, were used to characterize these faults. The sensitivity of the residual to a fault was studied in order to differentiate the faults. A theoretical relative fault sensitivity matrix with the residual sensitivity in the row and the faults in columns was derived as a reference to support for fault identification. In the research of Steiner et al. (2010) [Steiner'10], a model was built and used to estimate the cathode pressure drop based on the stack current, the dew point temperature, the stack temperature and the air inlet flow rate, with the aim of diagnosing flooding phenomenon in a PEMFC stack. Then, they developed the model to estimate another feature variable, i.e. the stack output voltage, for diagnosing both the flooding and the drying failures in the PEMFC [Steiner'11b].

A fundamental difficulty related to the model based diagnosis approach is the fact that there are always modelling uncertainties due to unmodelled disturbances, simplifications, idealizations, linearization, model parameter inaccuracies and so on, which restrict the generalizability of the model. Another difficulty concerns the intrinsic non-linear characteristic of most engineering systems [Patan'08] because conventional analytical models can only be applied to linear systems. In this context, the black-box modelling method based on artificial neural networks is considered as a solution.

II.2.1.1. Black-box model

The black-box model is used to predict the response of a device, a system or an object without any knowledge on their internal working behaviours. It can be derived from a data set based on a neural network. With artificial intelligence techniques, the network is capable of learning and generalizing non-linear functional relationships between input and output that are described by the data.

II.2.1.1.1 Artificial neural network

These years, some researchers [Arriagada'02, Milewski'09] have successfully applied artificial neural network (ANN) to model the operating behaviour of SOFC stacks and evaluate their performance. These models belong to the class of feed-forward network that is constructed with a certain number of single processing units which are analogous to the brain neurons of human. These “neurons” are associated and grouped into several layers. Similar to the cerebral behaviour, in a neural network, information (vector input) is delivered to the neurons in which it is weighted, synthesized (summed up), shifted by a bias to form a net input which is then treated by a transfer function; the processed information is passed on to the next layer (called hidden layer) for further treatment; at the end, the response to the input can be estimated in the last layer of neurons (called output layer). The weight and bias for every neuron are adjustable scalar parameters. For a neural network with more than one output variables (as shown in Figure 2-4), each layer of neurons is characterized by a weight matrix and a bias vector (denoted by “W” and “b”, respectively) as well as the selected transfer function. In the learning stage, the elements in the weight matrix and in the bias vector are repeatedly adjusted by the back-propagation (BP)-type learning algorithm, based on the input-output pair data, until that the network model attains the desired simulation accuracy. Such parameterization procedure is also known as data-driven training/learning. Note that instead of “the higher the better” approach, the fitness of the model to the training data must be restricted at a reasonable level in order to avoid overfitting.

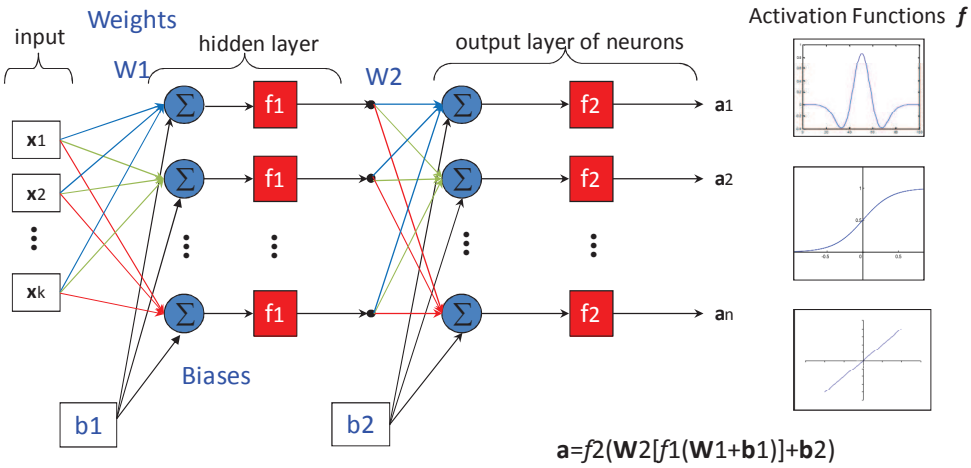

Figure 2-4 A feed-forward 2-layer neural network [Wang'11b]

The main difficulty to establish an ANN based model is the selection of the number of hidden layers and neurons. Until now, there are no effective tools or methods to automatically find out optimal network structure. Generally, modellers must try and train several networks of different structures with the same training algorithm and data, and then select the pertinent one according to the model's performance in specified aspects such as accuracy and computing time.

II.2.1.1.2 Radial basis function neural network

There is another feed-forward neural network structure known as radial basis function neural network (RBFNN) which has also demonstrated good performance in SOFC modelling [Wu'07, Huo'08,]. Its structure is much simpler than that of the multiple-layers ANN, only including an input layer, a non-linear hidden layer and a linear output layer. Differing form the ANN in which the transfer functions are selectable, RBFNN uses only Gaussian function which is parameterized by the centre and the width of symmetric Gauss curve. As illustrated in the Figure 2-5, the inputs are respectively assigned to the nodes in the input layer of the RBFNN and then delivered to the neurons in the next layer without being weighted. In the hidden layer, non-linear responses are calculated as a function of the Gauss curve width as well as the Euclidean distances between the centres and the input vector. These responses will be finally weighted and summed up in the last layer to produce an output. To accomplish a model with multiple outputs, individual RBFNNs should be established for estimating each output variable. They are then connected in parallel to compose a large neural network.

Like the ANN, the training for the RBFNN is also based on the data. The parameters in the Gaussian function (the centre and the width of the Gauss curve) and the weights are the network model parameters. They are adjustable during the learning procedure. The learning algorithm involves data mining techniques such as clustering methods used for determining the centres. It can also automatically try and compare different network structures so as to determine the optimal number of neurons in the hidden layer. However, this automated

network structure discovery procedure will take a lot of time if the optimal number of neurons is very large.

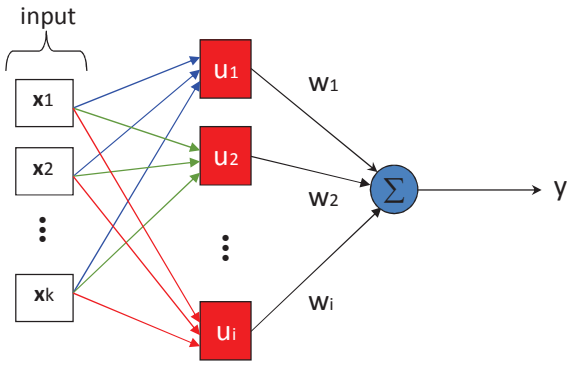

Figure 2-5 A simple radial basis function neural network [Wang'11b]

II.2.1.2. Equivalent circuit model based on electrochemical impedance spectroscopy technique

Another interesting model for the fuel cell is the equivalent circuit model (ECM), an interpretation of the AC impendence spectroscopy of the fuel cell/stack. It is often constructed with electrical elements such as parallel R-C circuit and electrical resistance (take Figure 2-6 as an example) which represent the resistances to the individual processes (such as mass transfer, chemical and electrochemical reactions) at different FC components. These resistances are often demonstrated in sum as a total internal resistance of the fuel cell in the time domain but are differentiable in the frequency domain. They are thus usually represented in the form of impedances. With the help of electrochemical impedance spectroscopy (EIS), different types of polarisations present on the fuel cells or batteries can be separated. EIS measurement is carried out by exciting the fuel cell with small voltage/current sinusoidal signals of various frequencies so as to obtain current/voltage AC responses in the same frequency bands. The divisions between the excitations and the corresponding responses yield a group of electrochemical impedances over a wide range of frequencies. Through fitting the equivalent circuit model to these impedance data, the parameters of the electrical elements in the model could be empirically determined. In the diagnosis application, these parameters are employed as indicators to reflect the actual state of health of the fuel cell/stack, such as in [Fouquet'06].

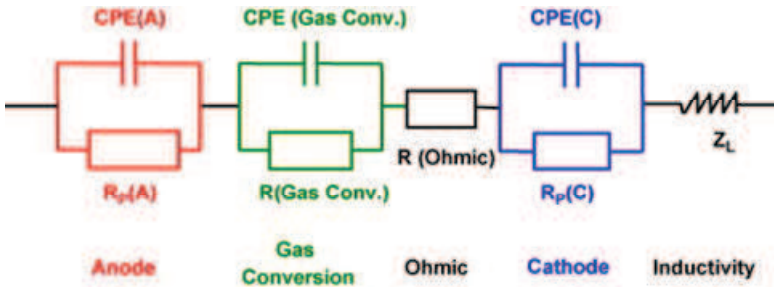

Figure 2-6 An equivalent circuit model for SOFC stack established by [Lang'08]

However, the EIS measurement is often time-consuming, especially for the measurement of impedances at low frequency band. During the measurement, the operating condition may slightly vary so that the state of the system reflected by the subsequently measured impedances is not in accordance with that reflected by the previously measurements. Such a set of impedance data cannot be used for the ECM parameterization or else misunderstanding may occur in the diagnosis phase. In addition, the EIS measurement is subject to noises. This issue can have negative effects upon the reliability of the ECM-based diagnosis and thus requires special attention.

Besides the ECM, other models have also been developed to represent the electrochemical impedance spectrum of a FC/stack in operation, for the purpose of stack diagnosis. For example, Onanena et al. approximated the real part of a PEMFC's impedance with a model of four parameters related to a "logsig" function [Onanena'10, Onanena'11]. In this study, the four parameters in the model were treated as the feature variables for the state of health of FC.

II.2.2. Signal-based approach

Diagnosis by signal analysis arises from the fact that many processes, whether being normal or faulty, can be characterized by their oscillating, fluctuating or cyclic time behaviour. This fact inspired some researchers applying simple and effective transform to the original signals, in order to discover the important information contained in these signals and extract the dominant fault features for the diagnosis use. Since the frequency composition of the response signal contains information on the state of the system, analysing frequency characteristics of the signals plays a significant role in the signal-based diagnosis method.

II.2.2.1. Frequency analysis

There are many transformation techniques available for analysing signals in the frequency domain. Among, Fast Fourier Transformation (FFT) is the most commonly used, which is particularly suitable for analysing stationary signals whose frequency components are supposed to be invariant from the beginning of the signal to the end. However, in the field of diagnosis, since the time when the fault happens is usually unknown, the measured signals can cover both the normal and the faulty mode periods. This means that the studied signals are non-stationary, that is, its frequency composition is varied over the time. For this case, both FFT and other frequency domain techniques are not adaptable any more. To extract information from this kind of signals, especially for the implementation of CBM in which early fault diagnosis is demanded, not only the frequency domain but also the time domain must be taken into account in the signal analysis.

II.2.2.2. Time-frequency analysis

II.2.2.2.1 Short time Fourier transform & Wavelet transform

Hitherto, a number of time-frequency domain signal analysis techniques have been proposed, including the Short Time Fourier Transform (STFT) and the recently developed Wavelet Transform (WT). These methods consist in mapping a one-dimensional signal to a two-dimensional function of time and frequency/scale. Both the STFT and the WT recur to a window function sliding on the time axis to scan and transform the signal segment by segment. However, the STFT uses a constant frequency resolution for the time-evolving window function, which means that if we use wide window to obtain a good frequency resolution for the analysis of low-frequency components, we would not be able to obtain good time resolution (narrow window) for analysing high-frequency components [Peng'04]. To address this problem, the usage of flexible window function with varied frequency appears in the WT method.

In the WT, the flexible windows are in fact referring to a group of wavelets that evolved from a basic wavelet function, known as “mother wavelet”. These wavelets represent different time-scale resolutions. Based on them, the WT possesses the ability of adaptive time-frequency analysis.

II.2.2.2.2 Application of wavelet transform in fault diagnosis

The WT, as other kinds of transformation, is merely a method of signal decomposition which yields a new representation for the signals that are initially shown by the time series. After the transformation, a matrix of wavelet coefficients is obtained to re-depict the studied signal in the time-frequency domain. This feature provides a breakthrough for the detection and timing location of the fault. From the wavelet coefficient matrix, different parameters could be extracted to reproduce the information hidden in the signal. If the signal involves the occurring period of a fault, these parameters could be treated as fault features for diagnosis use. According to Peng et al. (2004) [Peng'04], such fault features could be roughly classified into 4 categories: the wavelet coefficients based, the wavelet energy based, the singularity based and the wavelet function based features. The last category is often used for image processing. Here, we only introduce the first three categories.

- In the **wavelet coefficients based** method, the wavelet coefficients that are greater than the threshold value are kept to be fault features while other smaller ones are discarded. The retained coefficients are then analysed by a classification machine in order to identify the type of the fault.
- In the **wavelet energy based** method, the wavelet energy is calculated for each component of the signal such that the energy distribution over the different frequency bands could be studied. This distribution can be treated as a representation of the information on the system process described by the studied signal. It can be quantified with the Shannon entropy proposed in information theory [Shannon'48] and be compared to a reference in order to determine if a fault has happened.

- The **singularity based** diagnosis method is developed aiming to find out the singularity points that indicate the fault, such as the peaks, the discontinuities and the jumps points present in the signals. Since the local weak singularities could be masked by the polynomial trends in the signals [Peng'04], they are often invisible and thus not easy to capture. Owing to the WT, the polynomial trend can be removed from the original signal so as to uncover the high frequency sub-signals on which the singularity points could be clearly shown up. Based on wavelet modulus maxima method, the modulus lines can be drawn to go through these points in the time-scale (or time-frequency) plane in order to stick out the singularities. In the review paper of Peng et al. (2004) [Peng'04], a figure of the wavelet modulus maxima lines of a vibration signal sampled from a defect rotor (see Figure 2-7) is given as an example to demonstrate this method in the use of machinery diagnosis.

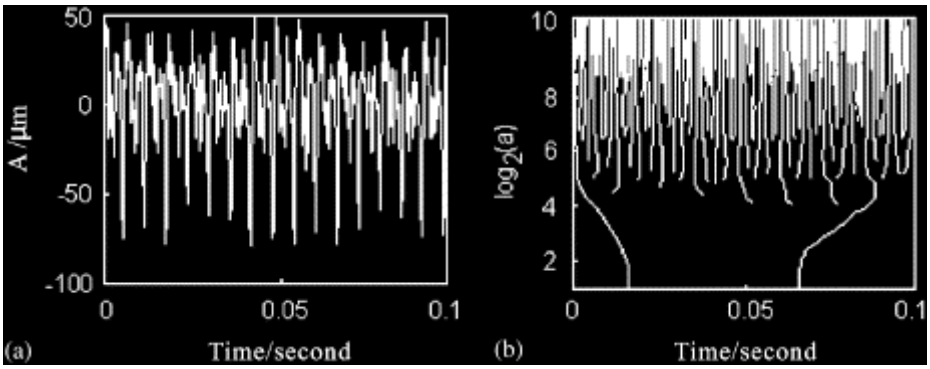

Figure 2-7 (a) the vibration signal; (b) its wavelet modulus maxima [Peng'04].

In the fuel cell diagnosis domain, the WT method has been successfully used for PEMFC diagnosis by Steiner et al. (2011) [Steiner'11a] to detect the flooding phenomenon in a PEMFC. In their investigation, the wavelet energy was applied to select the significant component of the signal and treated as the basis of the fault feature. Yet, the potential of this method for high temperature fuel cells or their systems diagnosis has not been explored.

II.2.3. Knowledge-based approach

In the afore-introduced approaches, fault features, being produced either by residual generation or relying on signal decomposition, play an important role in the fault diagnostic task that generally involves two sequential procedures: fault detection and fault identification. Differing from such diagnostic concept, in knowledge-based approach, these procedures are merged into a single diagnostic step by means of simulating human reasoning activities. Such one-step diagnosis usually refers to a decision-making process that can be automated by an expert system based on artificial intelligence technology. This knowledge-based expert system (KBES) is expected to be able to not only interpret real-time signals but also to deliver the required control action, to conduct test and to recommend diagnostic procedures [Angeli'10]. The reasoning performed by such a system is actually an inference process that

aims to determine the possible fault based on the existing knowledge about the system as well as the observations [Sajja'10].

A KBES consists of a knowledge base and an inference engine (IE). The knowledge base is a repository of expert knowledge. The IE is an algorithm which analyses the available information and performs reasoning based on the knowledge base. Constructing the knowledge base for the KBES involves two key issues: knowledge acquisition and knowledge representation.

- *Knowledge acquisition*

Fault diagnosis for technical systems and processes requires both empirical knowledge and scientific knowledge [Angeli'10]. According to Sajja et al. (2010) [Sajja'10], database is a form of information; empirical knowledge is a result of processing such information by means of synthesis, filtration, comparison and analysis. In the situation where the scientific knowledge that involves physical concepts is not available, data collection and information extraction become significant for knowledge acquisition. In fact, in fault diagnosis domain, empirical knowledge is more useful than scientific knowledge, since the target in the diagnostic phase is to find the specific faulty element instead of representing the system behaviour. On the contrary, scientific knowledge plays the dominant role in the prognostic phase in which the prediction of eventual failure or consequent system activity is considered as an essential objective.

To obtain empirical knowledge of the domain of interest, data collection is usually implemented by performing groups of goal-oriented experiments and measurements. Then, knowledge extraction can be carried out either by using statistical data mining techniques to analyse and model the probability distribution of the data, or by applying computational data mining techniques such as clustering methods which aim to retain patterns from the data. The applications of these two categorical methods in the field of fuel cell diagnosis have been exploited by Hernandez et al. (2006) [Hernandez'06] and Hissel et al. (2007) [Hissel'07].

The statistical data mining and the computational data mining can be separately used to solve a single problem from two different points of view, or applied together to solve a series of problems. Hernandez et al. (2006) [Hernandez'06] intelligently used their combination to settle the fault diagnosis problem in PEMFC. They employed the stochastic distribution of cell voltage measurements to characterize various FC working conditions (including several faulty operating modes). Then, clustering approach was applied to define, in the space of the characteristic variables, the zones representing the normal operation and the failures.

- *Knowledge representation*

No matter which data mining approach is used, a model should be yielded after the data analysis to synthetically organise and represent the obtained knowledge in a numerical

formation. This model, as an extensible knowledge base, can interact with the information coming from on-board sensor measurements (signals) in order to identify the state of the monitored system. The system state identification is actually a decision-making process that is automated by algorithmic reasoning technique, allowing the on-line diagnosis. An appropriate knowledge representation is favourable to the diagnostic reasoning. It has dominant effect upon the diagnosis performance.

Two different methods can be considered to represent the knowledge obtained from the data mining:

1) **Categorization & Instantiation**. Knowledge is possible to be categorized and then interpreted with the typical instances that are well known by experts. Based on this form of knowledge, pattern matching can be performed to relate the observed phenomenon to the similar instance and interpret it. This method is known as pattern-based method. It is often carried out after the data classification phase, taking each class of data as a paradigm to describe a category of knowledge. Owing to clustering techniques, the dataset that constructs a paradigm can be modelled to a cluster characterized by several geometrical parameters. Any observation that falls in this cluster is considered having the same meaning/label with the paradigm.

2) **Describe the knowledge by a collection of if-then rules**. It is analogous to that one or several human experts make reasoning with propositional logics created according to their own area of expertise, in order to solve a problem or give advice. Within this approach, the knowledge is represented declaratively instead of explicitly. For example, we can declare that smoking causes the lung cancer even if we do not understand how it causes the cancer. However, we cannot be sure that lung cancer must be caused by smoking unless having relevant evidences. This example involves two types of rules of encoding the necessary domain knowledge: i) causal rules and 2) diagnostic rules. Causal rules describe the relationship between the causes and their results in a direct way. Diagnostic rules work in the opposite way, allowing the reasoner to infer possible causes from observed events/symptoms [Rodionov'96]. Generally, a causal rule is easier to establish and has higher reliability than a diagnostic rule, because the former can be easily acknowledged and confirmed through experiments, whereas the later can only be ensured by empirical knowledge.

   In order to increase the credibility of inference, the idea to capture the inherent degree of uncertainty in the expert knowledge has been popularly considered in the concept of modern KBESs. Under this idea, a certainty factor is usually integrated into each of rules so as to declare the *degrees of belief* in that the rule is true. Bayesian theory is a typical technique concerned with this method, which performs the effect-to-cause inference based on the probabilistic logic. Another uncertainty design is the fuzzy logic. It is mathematically similar to the probabilistic logic but declares the *degrees of truth*.

   The problems of rule extraction and construction can be solved by machine learning. The later is a branch of AI technology, serving for finding relations and regularities

present in the data. Machine learning is capable of relieving data analysts from the dull and complex work in information collection and synthesis. With this technique, the database relevant to the studied problem will be the only material required for building a knowledge base.

The following paragraphs will be focused on introducing the application of these two kinds of knowledge representation in online FC system diagnosis. The AI techniques serving for knowledge learning will be mentioned.

II.2.3.1. Pattern-based method

The pattern-based knowledge representation that relies on classification techniques aims to regroup the information present in the data into several classes such that each class represents a single pattern of interest. Since the computational classification is always based on data spatial distribution, this kind of knowledge representation is very sensitive to the data structure. According to the classification expectation, the number of classes can be determined beforehand. After being classified, the data attributed to a class should be carefully studied in order to confirm the information covered by the data is in accordance with the expected class definition. It is important that the class labelling process should be objectively performed based on the data information, since the target is to represent the knowledge rather than to create it. Any subjective assuming for class labellization will impact the quality of the knowledge base.

There are various methods available for implementing the classification. Among, clustering method has been tried in FC durability analysis. It is able to find the centre point for each class so that the data in the class could be represented in geometrical way by its distance to the centres. Hissel et al. (2007) [Hissel'07] used fuzzy k-means clustering to classify the data of two hyperparameters extracted from EI measurements, in order to set up patterns to represent the states of a PEMFC system. As a result, the classification results corresponded with the expectation—three distinguishable clusters which are labelled with the “young”, the “old-ageing condition 1” and the “old-ageing condition 2” stage during the FC lifetime, respectively.

After the clustering, a set of centre points and a distance threshold can be yielded to position the clusters and limit their dimension so as to avoid overlapping region. These geometrical parameters and the labels of the clusters constitute the knowledge base. Relying on it, a geometric classifier could be set up to implement the recognition for the state of the studied system.

II.2.3.2. Rule-based methods

As afore-mentioned, domain knowledge can be represented into two kinds of rules, causal rules or diagnostic rules. To predict the failure eventually occurring in the future time when a

fault has happened (prognosis), the propagation of observed symptoms to the eventual failure can be declared with causal rules, by following cause-effect relationships, whereas to infer the fault which results in these symptoms (diagnosis), a backward reasoning following effect-cause chains is needed. In CBM maintenance (see Figure 2-8), the symptoms are regarded as intermediate events that causally associate the upstream faults (cause) to the downstream failures (result). No matter for the fault diagnosis or for the failure prognosis, the inference starts always from the same point, i.e. the observed symptoms/events. Merely, the directions of inference are opposite—one toward the reason whereas the other pointing to the ultimate effect. Here, we only talk about the diagnostic inference (i.e. event-to-fault reasoning).

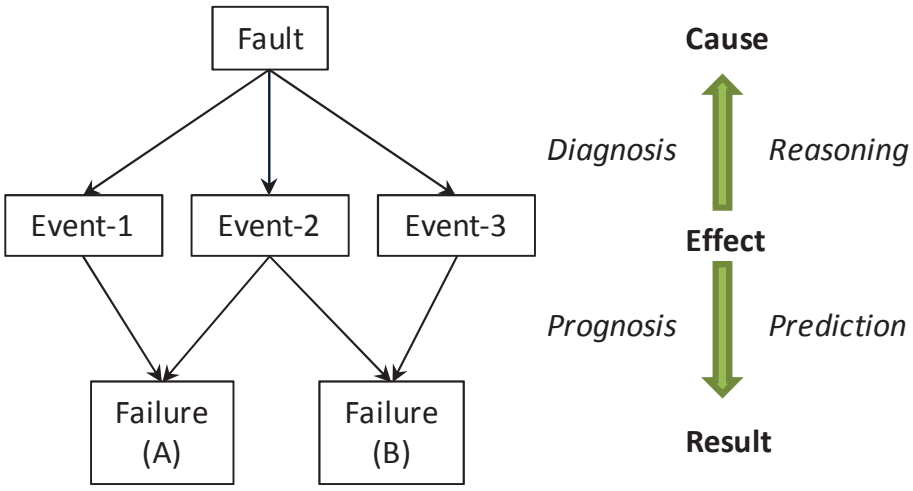

Figure 2-8 Diagnosis and prognosis procedures in CBM maintenance

II.2.3.2.1 Neuro-fuzzy system

To declaratively represent event-to-cause relationships, a semantic network that consists of a series of if-then (or if-then-thus) statements could be established. These reasoning statements can be converted to fuzzy logic that involves linguistic variables. A linguistic variable is allowed to have qualitative values such as “low” or “high”, or “very high”. Using this kind of interpretable variables can facilitate the expression of rules and facts. For instance, a rule could be described as follow:

***If** the variable A is very low and the variable B is high, **then** the fault is critical.*

This description captures the imprecise modes of reasoning that play an essential role in the human ability to make decisions in an environment of uncertainty and imprecision [Jang'93].

In general, a basic fuzzy logic system is composed of a set of membership functions, a linguistic rule base and a defuzzification unit. The membership functions firstly transform a number of variables into a fuzzy result, producing membership degrees to measure the belongingness of the inputted numerical value to each linguistic value. This procedure is known as fuzzification. Then, the linguistic rule base maps this fuzzy result to a qualified

consequent (linguistic). In the defuzzification process, the linguistic result is reconverted to a quantitative result by another set of membership functions (see Figure 2-9).

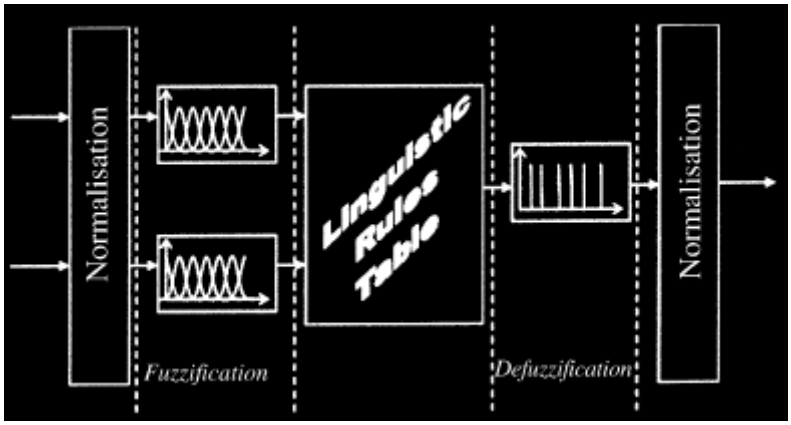

Figure 2-9 A Sugeno-type fuzzy model [Hissel'04]

The parameters in membership functions and the rule base are two key factors which determine the quality of a fuzzy logic system. Owing to the development of AI techniques, both of them can be solved by data learning. In practical applications, this work is usually taken by neural network which is combined with the fuzzy system to form a hybrid neuro-fuzzy system. The basic idea behind this combination is to use a fuzzy system to represent knowledge in an interpretable manner and apply the learning ability of the neural network for parameter optimisation and rule learning. On-line parameter tuning is also possible to be achieved by using adaptive neuro-fuzzy system [Jang'93].

Hissel et al. (2004) [Hissel'04] had applied a Sugeno-type fuzzy model to produce a so-called satisfaction rate parameter for diagnosing a PEMFC stack, based on the actual stack voltage and current. Figure 2-10 and Figure 2-11 demonstrate the indicative capability of the yielded SR for detecting the drying and the flooding phenomenon in the studied PEMFC.

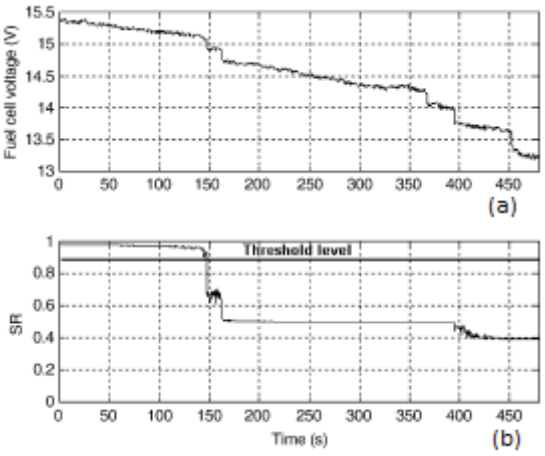

Figure 2-10 Evolution of voltage and SR when the flooding phenomenon occurs; (a) FC voltage and (b) SR value [Hissel'04].

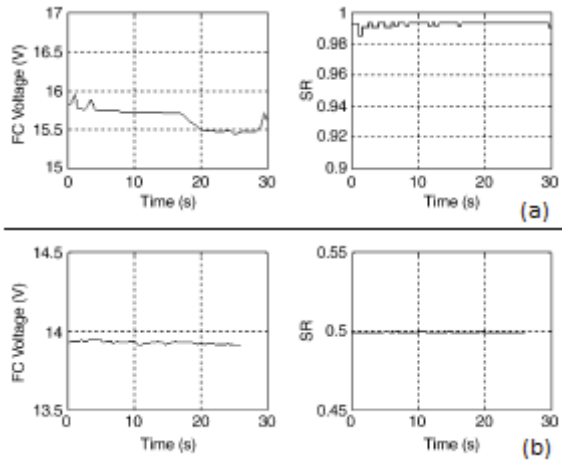

Figure 2-11 Evolution of voltage and SR for different operating temperatures. (a) At 18°C; (b) at 50°C (drying) [Hissel'04]

II.2.3.2.2 Bayesian method

Fuzzy logic offers a way to quantify the uncertainty of our expression. However, it doesn't permit to revise this uncertainty when new evidence appears, due to the parallelization of the fuzzy if-then rules. To address this problem, Bayesian probability could be considered. The use of probability to quantify the uncertainty in diagnostic rules is similar with the use of membership degrees in fuzzy logic reasoning system. It is not an ad-doc choice but is inevitable if we have to respect common sense while making rational coherent inferences [Bishop'06].

Probabilities are generally viewed in term of frequencies of random, repeatable events. For example, in a system where there are 3 possible faults to happen, the probabilities of occurrence for each fault are 20%, 50% and 30%, respectively, according to the expertise. In Bayesian view, these probabilities are *prior probabilities* purely determined by subjective assessment of experienced expert. If now a symptom (S) (or an evidence) to one of the faults is observed, our belief in the occurrence of this fault (F) will increase. In this case, the probability of occurrence for this fault should be revised. In Bayesian statistics, the updated probability is called *posterior probability*, denoted by $p(F|S)$. Bayes' theorem provides an equation to calculate it from the prior probability, by incorporating the evidence from the observed data. In this equation, the conditional probability, $p(S|F)$, (referring to the occurring probability of the observed symptom given the fault, which can be evaluated from data) and the prior probability of the symptom, $p(S)$, are assumed being known. Details about this equation are given in Chapter 5.

From the causality point of view, the fault (F) is the cause and the observed symptom (S) is the effect. Hence, $p(S|F)$ captures the uncertainty of the causal rule that:

If *F* has happened, **then** *S* will be observed,

Whereas $p(F|S)$ represents the uncertainty of the diagnostic rule that:

If *S* is observed, **then** the fault is *F*.

If a second symptom (*S'*) is sequentially observed, the equation can continue to be used to update the probability of the assumed diagnostic result to $p(F|S,S')$, which declares the uncertainty of the interpolated diagnostic rule that:

If *S* is observed **and** *S'* is also observed, **then** the fault is *F*.

Evidently, the rule expression manner in the Bayesian method is more flexible than that in the fuzzy logic. The feature of Bayes' theorem is that, on the one hand, it differentiates the effect-cause fashion from the cause-effect relationship and on the other hand it mathematically associates them together from the probabilistic viewpoint.

In the Bayesian method, the causal rules are graphically represented by a network structure. It employs nodes to represent variables and arrows to imply the cause-effect relationship between them. In a simple Bayesian network, one node is defined either as the cause or as the

effect. This kind of network is called naïve Bayesian classifier (see Figure 2-12). In a complex Bayesian network where intermediate events are present to relate the initial cause to the final result, the node is allowed to play the cause and the effect roles in parallel. When the node locates at the beginning of the arrow, it is the factor that has an effect upon the state of the node located at the end of this arrow. The conditional probabilities that encode the uncertainty of causal rules are registered in the nodes (since prior knowledge often comes in causal form). They will serve for the calculation of posterior probabilities that quantify the uncertainty of diagnostic rules in the effect-to-cause reasoning process.

- *Naïve Bayesian classifier*

Naïve Bayesian classifier applies the class specific density to characterize the relation between an observation and a certain class. In diagnosis application, the class specific density measures how likely this observation can be obtained if the assumed fault (correspondent to the class label) happens. Naïve Bayesian network has a very simple structure, consisting of only two layers, one is the cause layer (with only one node) and the other is the symptom layer (including more than one characteristic node/variable). All arrows start from the cause and point to the symptoms. In diagnosis application, the cause node represents a discrete variable that has qualitative values which express the faults; the symptom nodes represent feature variables that commonly characterise each fault. Inputting the values of symptom variables into the network, the classifier will work to calculate probabilities of the cause variable at each of its value. It is worth noting that in a naïve Bayesian classifier, arrows only serve to indicate the cause towards the effect rather than to represent causal relationships. Similar to fuzzy logic, Naïve Bayesian network only declares cause-observation relationships rather than explicates.

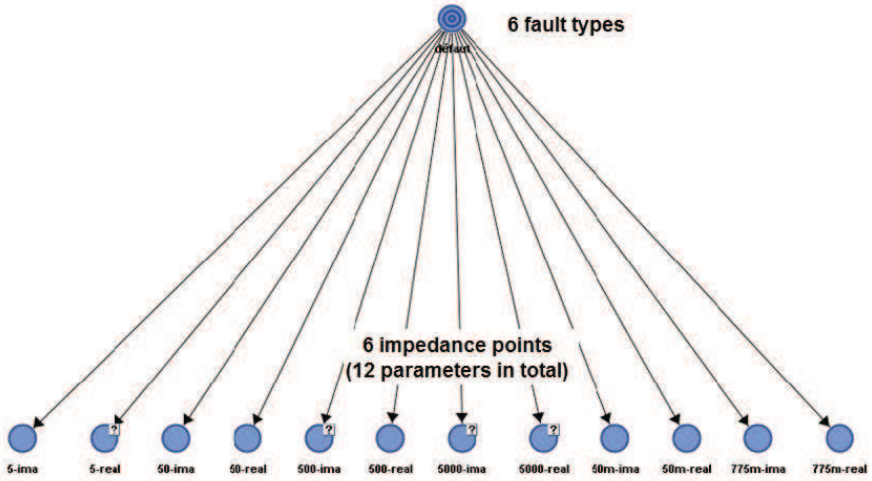

Figure 2-12 A Naïve Bayesian classifier for PEMFC fault diagnosis [Wasterlain'10]

Wasterlain et al. (2010) [Wasterlain'10] had tried to use Naïve Bayesian classifier to identify the faults in their PEMFC stack. The classifier structure is shown in Figure 2-12. In their research, six fault types were pre-determined, including the normal operating mode and 5

failure modes, i.e. minor membrane drying, moderate drying, slight flooding, minor flooding and moderate flooding. Six impedance points (that is, 6 real parts and 6 imaginary parts) were selected to characterise the state of the studied PEMFC stack. In the validation phase, they obtained a high rate of good classification up to 91.2%.

- *Bayesian network*

Comparing with Naïve Bayesian classifier, Bayesian network gives us a much better intuitive grasp of the causal relationships. It allows incorporating individual cause-effect relationships, aiming to show up complex relationships among a large number of variables. The causal relationships in a Bayesian network can be determined either by expert knowledge or be learnt from data with the aid of AI based machine learning techniques. In practice, the prior knowledge is used in conjunction with the data-based knowledge so as to determine reasonable causal rules. Since Bayesian network has both causal and probabilistic semantics, it is an ideal representation for combining prior knowledge and data [Heckerman'96].

Riascos et al. (2007) [Riascos'07] proposed a Bayesian network expert system to diagnose four types of faults in the PEMFC's BoP system: 1) faults in the air fan (**aF**); 2) faults in the refrigeration system (**rF**); 3) faults of the fuel crossover ($\mathbf{J_n}$); and 4) faults in the hydrogen pressure ($\mathbf{H_2}$). These faults were characterized by 5 symptoms: the change of ourput power (**Pow**), the stack's current ($\mathbf{I_{FC}}$) and voltage (**V**), the temperature (**T**) and the pressure of input hydrogen ($\mathbf{pH_2}$). The cause-effect (or fault-symptom) relationships were pre-determined by the expert knowledge. Then, they were optimised according to the data-based knowledge learnt from a database which was generated by a PEMFC physical model. As shown in Figure 2-13, this Bayesian network has a 3-layer structure. The nodes related to the studied faults are organised in the upper layer; the middle layer involves the nodes for the intermediate events—the faults that may occur in the fuel cell due to the BoP faults; passing through them, the ones of the measurable variables can be found in the bottom layer. All of these nodes represent Boolean variables which have only two qualitative values: normal (0) and abnormal (1). In the on-line diagnosis application, this diagnostic tool is designed to be activated only when the sensors capture abnormal variations during the FC operation. According to the authors, in all validation tests, this Bayesian network could always indicate the actual cause as the most probable fault cause.

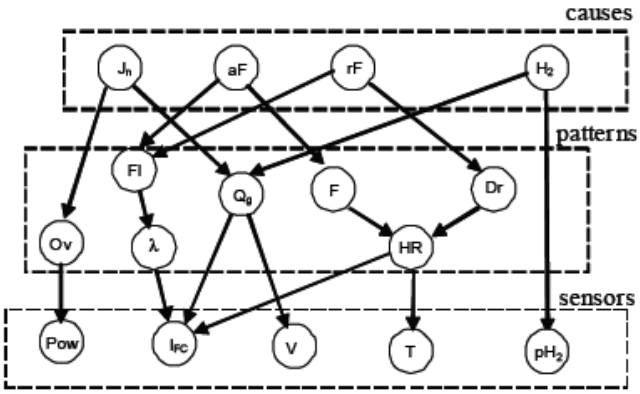

O_v: Overload; **Fl**: Volume of air flow; **λ**: Stoichiometrical air relationship;
Q_g: Generated heat; **F**: Flooding at electrodes; **HR**: Relative humidity;
D_r: Membrane Drying; **Pow**: Power difference; **I_{FC}**: Electric current;
V: Output voltage; **T**: Temperature; **pH_2**: H_2 pressure.

Figure 2-13 A Bayesian Network Structure for PEMFC's BoP system Fault Diagnosis

II.2.4. Summary

Figure 2-14 shows a summary of the methods that have been used for fuel cell system diagnosis to date. Except for the analytical model, all the others are based on data analysis and learning (the signals are time-series data). Since the experiments on a FC system are complex and time-consuming, having considerable uncertainties and are not possible to cover all operating points, analytical models can be applied for data generation.

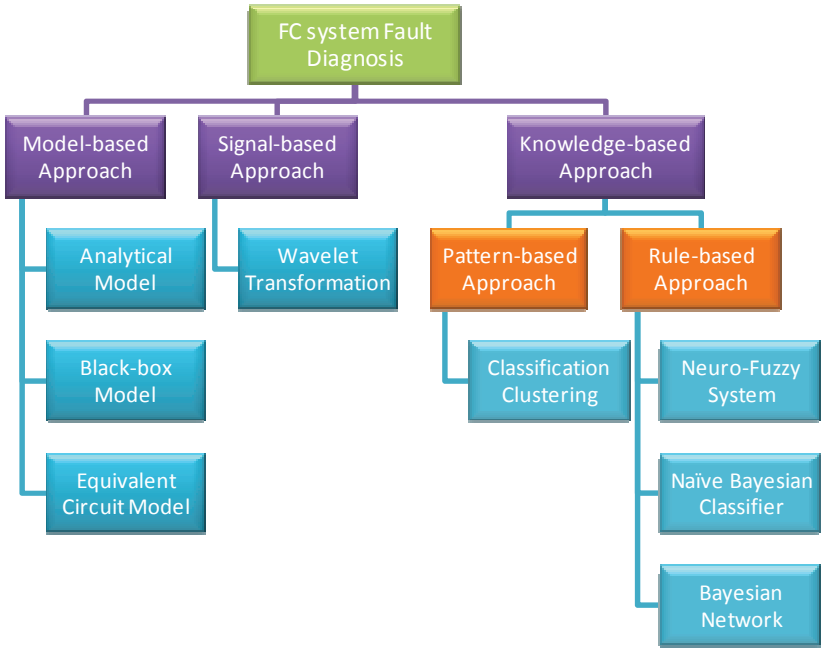

Figure 2-14 Classification of the considered diagnosis methods for FC system

II.3. About this work

The majority of the above-classified methods have been successfully applied in PEMFC system diagnosis. However, their application for SOFC system diagnosis has not been explored. In the framework of GENIUS, only data-based methods are considered for the development of SOFC system diagnosis methodology. The available data in this project are all collected from the real experiments. Since these experiments are performed on different SOFC systems, the measurement conditions are not identical and restricted by the concept of the tested system and the corresponding experimental design. Because of this, the selection of an appropriate data mining method should take into account the features of datasets (such as structure, sampling rate, etc) and be based on the available information on the experiments for data generation.

II.3.1. Our diagnostic strategy

As mentioned in the first section, in GENIUS project, FCLAB is mainly in charge of exploring the signal-based and the knowledge-based approaches in the application of SOFC system diagnosis. According to our experiences in PEMFC diagnosis, applying a single approach to independently realise the diagnostic process is very difficult and restricted. Moreover, the assertion of treating FC stack as a sensor for system fault detection evokes the concerns on the reliability of such special "sensor". Since degradations and failures can take place in the FC stack as well as in the BoP part, the state of health (SoH) of the FC must be confirmed before diagnosing BoP faults.

In this context, an integrated strategy for the diagnosis of SOFC systems is established. It is composed by three sequential stages, including

a) off-line diagnosis and knowledge acquisition,

b) FC SoH monitoring and on-line BoP fault detection, and

c) SOFC operating state estimation.

Three different data/signal-based algorithms are selected, respectively orienting to the implementation of one of the stages. They are the clustering algorithm, the WT-based algorithm and the Bayesian network algorithm. These algorithms have been proven able to solve the diagnosis problem independently. However, their applications are often circumscribed in certain operating conditions. In our diagnostic strategy, the selection of data analysis algorithm depends greatly on the organisation of the database, the way the data is generated and the aims of the analysis.

II.3.2. Data generation

In this work, there are several databases available for validating our diagnostic strategy as well as the algorithms. They were collected in the experiments on different SOFC test benches, i.e. the Hexis 5-cells system, the VTT system and the FCLAB's test bench with a HTceramix SOFC stack. In this sub-section, the experiments for the data generation are outlined.

II.3.2.1. Hexis system tests

The Hexis system database is originated from the experiments in the framework of RealSOFC project*. This European project aimed to gaining knowledge on the effects of the operating conditions upon the degradation of planar SOFCs' components, in order to find solutions to reduce ageing rate to below 0.5%/1000hours and to improve fuel cell materials. The experiments were performed on the same test rig, with the stacks of the same design but under different operating conditions. All of the tested stacks consisted of 5 cells and had been kept working stationarily in long term until severe degradation was observed. Since thermal cycling tolerance is one of the important requirements for SOFC commercialisation, a certain amount of thermal cycles were arranged into these experiments. In addition, redox cycling was also performed in some experiments. In order to follow the evolution of the SoH of the stacks, the experiments were designed to be discontinuous so that polarisation tests could be carried out during the out-of-service intervals. Each SOFC stack was supplied with reformed natural gas (NG) (4g of NG per hour and per cell) resulting from the Catalytic Partial Oxidation (CPO) and operated at full load conditions with constant current density. Air was introduced to the stack via an air pre-heater. A simplified flow chart of the test rig is given in Figure 2-15. Under different temperatures, the composition of the gases yielded from the CPO reformer is different. This gaseous mixture is mainly composed by H_2, CO, H_2O, CO_2, nitrogen from the air and a small quantity of unreacted CH_4. Their concentration percentage in a mol unite of CPO gas is a function of the reforming temperature, as shown in Figure 2-16.

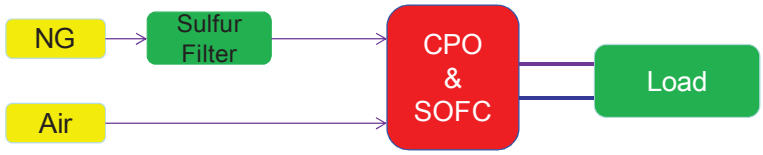

Figure 2-15 Simplified flow chart of the Hexis SOFC system

* Refer to the web page: http://www.real-sofc.org/

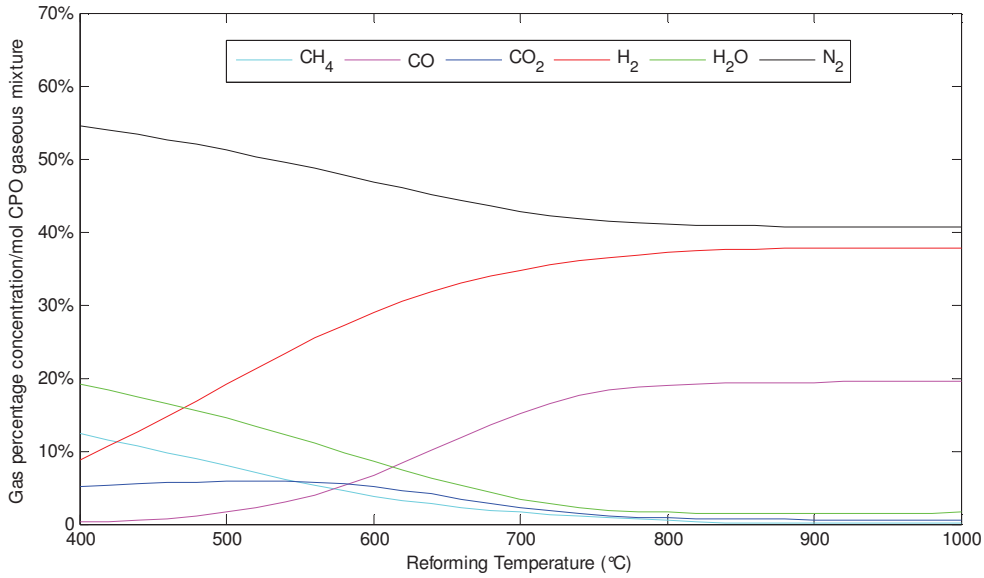

Figure 2-16 Effect of CPO temperature on reformed gas composition

The database includes two kinds of data matrix. One contains the time-series measurements in every hour during the stationary operation; the other is the polarisation measurement data matrix. The time points where the thermal or redox cycle took place are also known. After a polarisation test, the operating condition might be slightly varied. In every time-series data matrix, there are more than 15 variables and 20 to 2000 samples.

II.3.2.2. VTT system tests

Two rounds of tests were performed on the VTT's SOFC system in the framework of GENIUS project. A 6-cell S-design SOFC stack fabricated by HTCeramix was used for each test. A furnace was present in the system in order to keep the stack in desired temperatures. In the 1st round the pure humidified hydrogen was fed into the stack, while in the 2nd round the directly supplied fuel was a gaseous mixture composed of CH_4, CO_2, H_2, H_2O and N_2. The composition of such fuel is equivalent to the water reforming result of S/C ratio equal to 2 constant throughout the test. Both the tests were carried out following a full factorial test matrix according to the design of experiments (DoE) methodology. The effect of fuel utilization (FU), air utilisation (AU), current density (J) and furnace temperature (T_s) were determined by operating the stack in a total of 16 different operating conditions symmetrically around a nominal operating point. These 16 non-rated operating points demarcate a bounded area for tolerant/safety operating conditions in which the fuel cell is permitted to work.

These tested points in the 1st and the 2nd round tests were listed in Table 2-1 and Table 2-2, respectively. Steady state values were measured by allowing the stack to stabilize for 3 to 5 hours between every experiment point. All operating point transitions were done gradually, by "small" step-wise changes. The stack was galvanostatically controlled therefore the average current density was set directly. Similarly, the stack fuel utilization was also set directly by adjusting the fuel components' mass flow accordingly. The furnace temperature was regulated

at the given set-point by a PID controller. The stack I-U characteristic curve in nominal conditions was measured repeatedly, after different operating hours, in order to examine the SoH of the stack.

Table 2-1 The DoE of 1st round test

Point No.	Furnace Temp. (°C)	J (A/cm2)	FU	AU
0	760	0.3	0.5	0.4
1	700	0.1	0.4	0.3
2	700	0.1	0.4	0.5
3	700	0.1	0.6	0.3
4	700	0.1	0.6	0.5
5	700	0.5	0.4	0.3
6	700	0.5	0.4	0.5
7	700	0.5	0.6	0.3
8	700	0.5	0.6	0.5
9	820	0.1	0.4	0.3
10	820	0.1	0.4	0.5
11	820	0.1	0.6	0.3
12	820	0.1	0.6	0.5
13	820	0.5	0.4	0.3
14	820	0.5	0.4	0.5
15	820	0.5	0.6	0.3
16	820	0.5	0.6	0.5
Tested stack	HT Ceramix, S-design short stack with 6 cells, 50 cm2 active area/cell			
Fuel	H2/N2/H2O mixture			

Table 2-2 The DoE of 2nd round test

Point No.	Furnace Temp. (°C)	J (A/cm2)	FU	AU
0	760	0.3	0.5	0.235
1	730	0.2	0.4	0.17
2	730	0.2	0.4	0.3
3	730	0.2	0.6	0.17
4	730	0.2	0.6	0.3
5	730	0.4	0.4	0.17
6	730	0.4	0.4	0.3
7	730	0.4	0.6	0.17
8	730	0.4	0.6	0.3
9	790	0.2	0.4	0.17
10	790	0.2	0.4	0.3
11	790	0.2	0.6	0.17
12	790	0.2	0.6	0.3
13	790	0.4	0.4	0.17
14	790	0.4	0.4	0.3
15	790	0.4	0.6	0.17
16	790	0.4	0.6	0.3
Tested stack	HT Ceramix, S-design short stack with 6 cells, 50 cm2 active area/cell			
Fuel	CH4/CO_2/H2/N2/H2O mixture			

II.3.2.3. FCLAB's SOFC stacks tests

On the FCLAB's SOFC test bench, two tests were performed during former Ph.D thesis [Chnani'08] & [Gay'12]. One test used a stack with three S-design SOFCs; the other used a 6-cell stack with the same design. They were both fabricated by HTCeramix. The stacks were operated in galvanostatic mode.

1) The 3-cell stack was fed with $H_2/N_2/CO/CO_2/H_2O$ gaseous mixture which aimed to simulate the output gases from a reforming unit at the upstream of the stack. During the experiment, the stack temperature and the current density were variable while the other operating parameters (such as the flow rate of the fuel and the air, the anode and the cathode stoichiometry) were all kept constant. At the end of the experiment, the performance of the stack was found greatly degraded. From the measurement data, the voltage signals where the stack was stationarily operated under the temperature of 770°C and the current density of 10A were picked up. These signals were measured at different times of the operation and could reflect the evolution of the state of health of the stack. (Refer to [Chnani'08] for more details about the experiment.)

2) The 6-cell stack was fed with pure hydrogen and air. The stack was operated under a variety of temperatures from 700°C to 805°C and different current densities between 0–30A. Other operating parameters were constant. According to the I-U characteristic curves measured at different times of the operation, the stack did not have severe degradation. The data measured when the stack was operated under different temperatures were picked up and grouped into a database. (Refer to [Gay'12] for more details about the experiment).

II.3.3. Utilization of the databases for the algorithms' validation

II.3.3.1. For the clustering algorithm

The advantage of clustering algorithm consists in its capability of classifying large volume data into groups so that the information is homogeneous in each group and heterogeneous among groups. With this algorithm, the information is just re-categorized, neither changed on the representation nor reduced on the content. This algorithm is very useful in case where the individual datasets have been merged together into a large-size database such that the phenomena/events described by these datasets could not be differentiated. The clustering aims at decomposing such database so as to implement information re-separation.

The historical database from the RealSOFC project[*] is similar to this kind of database. It was cumulated from the different experiments, each of which was designed orienting to a specific objective and had produced a data set. The datasets from some experiments may contain the same information and be different from others. In this work, these datasets are firstly merged into a single data matrix which is then re-organized by the clustering algorithm. The classification results are examined with the real information obtained from the experimenters as well as other relevant data, in order to evaluate the performance of the clustering in the differentiation of the states of health of SOFC stack. Details about this validation work are given in Chapter 3.

II.3.3.2. For the wavelet-based algorithm

The wavelet transform mainly serves for signal processing. The fluctuating behaviors of signals are supposed to be related with the operating condition of the fuel cell stack that could reflect the state of health of both the system and the fuel cell. In this work, wavelet energy-based variables are extracted to quantify the signal fluctuation and used to characterize the operating condition as well as the state of health of SOFCs. The voltage signals from the VTT system tests and from the 3-cell stack test (in which the stack was degraded) performed in FCLAB are used to validate the indicative capacity of these feature variables. Chapter 4 is focused on this algorithm's introduction and validation.

[*] Refer to the web page: http://www.real-sofc.org/

II.3.3.3. For the Bayesian network model

The Bayesian network model is used to estimate the actual SOFC operating parameters for the purpose of providing analysable information on the actual state of the system. The data from the 1st round test on the VTT system and from the test of the 6-cell SOFC stack performed in FCLAB are used for the Bayesian network structure optimisation, parametrization and validation. This work is introduced in detail in Chapter 5.

II.3.3.4. Summary

The algorithms and the corresponding validation-oriented datasets are summed up in Table 2-3.

Table 2-3 The experimental datasets used for the algorithms validation

Algorithms	Hexis System Data	VTT System Data		FCLAB's Data	
		1st round	2nd round	3-cell stack	6-cell stack
Clustering	✓				
Wavelet transform		✓	✓	✓	
Bayesian network		✓			✓

II.3.4. Goals of this work

The essential objective of this work is to achieve the detection of SOFC system faults in the early stage. In our study, the tested stacks are all in small size, composed by 3, 5 or 6 single cells, serving for laboratory investigation. Unlike the large-scale SOFC systems where the stack operating temperature could be ensured by the heat released from the electrochemical reactions taken place inside the FCs, such "short" stacks always recur to (are situated in) a furnace in order to keep their temperature in the desired range. For this kind of small-scale SOFC systems, the faults of interest could be gas leakage in the inlet manifold (or due to untight pipes), furnace failure, fault of temperature control, too high load current, load rejection and desulphurization failure. They are usually the problems difficult to capture by normal sensors. In the framework of the GENIUS project, these failures were generalized to several improper operating conditions in which the stacks were tested.

However, it is not recommended to experiment the stacks in severe operating conditions that may lead the FCs to rapid degradation and thereby disable the stack acting as a sensor for system fault detection. Moreover, rapid degradation can greatly shorten the testing time and limit the time for the data generation and acquisition, resulting in incomplete database and information loss. In addition, the cost of experiments would also rise. Therefore, it is

preferable to operate the FC stack in the conditions that are mildly biased from the rated one, so as to ensure the availability of the data of interest and prolong the test time on a single FC stack as much as possible.

In this work, the tests from which the validation-oriented data were originated were all carried out under this concept. The biased operating points considered in each of these tests sketch the contours of safe and tolerant conditions that the fuel cell stacks are permitted to be operated in. When the real operating point falls around the demarcation of the safe operating region, an alarm should be given by the diagnosis tool to warn that the operation of the system is proceeding towards undesired direction and a fault must have happened. Another function of the diagnosis tool is to diagnose the FC stack. Being used as a specific sensor, the state of health of the stack (or the sensor) must be confirmed beforehand.

Chapter III *K*-means clustering algorithm for SOFC off-line diagnosis

In the field of fuel cell engineering where a number of experiments are involved, large quantities of data are usually available for pattern recognition and information elaboration. In practice, most industrial data analysis is based on manual selection of variables and extraction of features. This procedure is often time consuming and subject to the expectations of the engineer so that the data may be subjectively regrouped and interpreted. In the artificial intelligence technology, a lot of techniques could be used to achieve “objective” data analysis. Unsupervised classification is a candidate method for data mining. In case where the number of patterns is known but their label (or the class’s definition) is unknown, unsupervised classification method can be used to partition hidden patterns which are homogeneous in the measured data based on their statistical regularities [Hu'09]. Then, through analyzing the data assigned to each class and according to expert knowledge, the labels (or meaning) of these patterns could be determined.

There are two classic methods of unsupervised classification: clustering and dimensionality reduction [Zheng'09]. The former aims to find patterns in a dataset containing independent, identically distributed samples [Grossman'01] while the later is essential for the compact representation of patterns [Zheng'09].

In this thesis, only clustering method is studied. It is employed to analys the polarization test data in order to implement SOFC off-line diagnostic algorithm.

III.1. Introduction of clustering analysis

In the field of data analysis for knowledge discovery, it is often encountered that a dataset contains a large number of observations for various variables. Clustering analysis can be a means to partition these observations into groups or clusters, in such a way that the profiles of observations in the same cluster are very similar and the profiles of observations in different clusters are quite distinct [Mathworks'96]. This technique is particularly useful for the extrapolation of interactions between variables (for multi-dimensional data). It allows assessing the data structure and exploring dissimilarity among the groups of observations (for

each dimension). Hissel et al. (2007) and Steiner et al. (2011) [Hissel'07, Steiner'11a] used both the clustering algorithm on the fault features' data in order to identify the indicative capability of the feature variables to the states of health of PEMFC stack. Besides, the application of clustering analysis for feature extraction and identification has also been exploited in other fields: Yang et al. (2010) [Yang'10] used it to classify the precipitation of a city, Hu et al. (2009) [Hu'09] for texture classification and Clement et al. (2002) [Clement'02] for image analysis.

Nevertheless, there is no direct measure to validate the classification results yielded by clustering analysis. In practice, one must resort to heuristic arguments for the judgment of classification quality [Zheng'09] and for the cluster labellization. In addition, clustering technique is a purely computerized procedure in which the practical significations of the variables are not considered. It is thus possible that the clustering result is not able to offer the useful information relevant to the research goal. In other words, the clustering behaviours may not concentrate on patterns of interest but waste time on discovering patterns the user has not asked for [Hung'04].

In general, raw data is highly susceptible to noise, missing values, and inconsistency. Its quality can greatly affect the data mining results. In order to improve the quality of data, raw data must be pre-processed so as to ameliorate its representativeness to the information that we are interested in. Moreover, this work can increase the efficiency of the data mining process. A basic data pre-processing starts usually from the selection of significant variables, based on the expertise knowledge. Sometimes, the considered variables of interest are not measurable and should be extracted or estimated. In addition, we must decide whether to standardize the variables in some way so that they all contribute equally to the distance or similarity between data.

Apart from the purpose of partition, clustering technique serves sometimes to arrang the clusters into a natural hierarchy. This process involves a successive grouping of the clusters so that each level of the hierarchy clusters within the same group is more similar to each other than those in different groups [Giudici'09].

There is rich literature on both hierarchical and partitional clustering methods. This chapter only focuses on the non-supervised partitional clustering technique.

III.2. Clustering algorithms

Clustering aims to partition the observations into groups so that the pair-wise dissimilarities between those assigned to the same cluster tend to be smaller than those in different clusters [Zheng'09]. In this section, two of the most representative clustering techniques are reviewed:

1) *K*-means clustering;
2) Fuzzy *k*-means clustering.

III.2.1. Basic principles

For better understanding, a simple mono-dimensional example is given to explain these two clustering methods. Give a certain data set (including only one variable). Distribute the data on an axis as shown in the Figure 3-1:

Figure 3-1 Values of variable distributed on *x* axis

The points scattering along the axis can be divided into two clusters (A and B) according to the data concentrations. Using *k*-means algorithm, the membership of all the points assigned to the cluster A is set to 1; and for other points which are grouped into the cluster B, their membership to this cluster is 0, as shown in Figure 3-2:

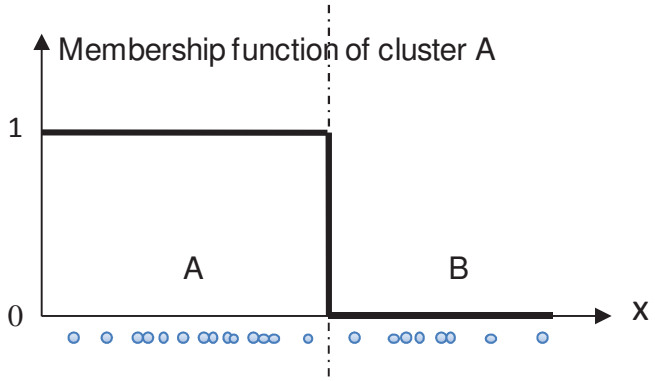

Figure 3-2 Classification by *k*-means method

In fuzzy *k*-means algorithm, a datum does not belong exclusively to a well defined cluster; instead, it is supposed to belong to all clusters but the belongingness to each of them is different. As shown in Figure 3-3, the membership of the points to cluster A is a continuous variable, which measures the degrees of belongingness.

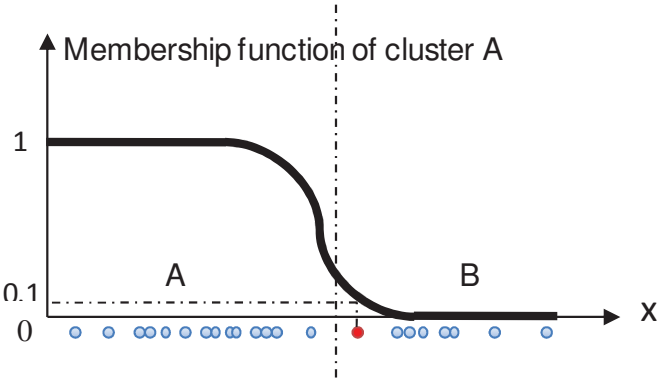

Figure 3-3 Classification by fuzzy *k*-means method

Essentially, the fuzzy *k*-means clustering algorithm is more flexible than the basic *k*-means clustering, owing to the integration of fuzzy logic theory that is usually applied for the

problems that do not require hard solutions [Nasser'06]. In sum, *k*-means technique gives hard clustering solution in which a point belongs to only one cluster, while fuzzy *k*-means discovers soft clusters by considering that a particular point can belong to more than one cluster with certain probability. Therefore, the former is also known as "hard clustering" and the later as "soft clustering".

The common ground of these two algorithms is that they are both sensitive to the initial placement of the cluster centres. With different sets of initial cluster centres, the clustering results could be different [Li'08]. In practical applications, the clustering algorithm is usually performed several times with different randomly selected cluster centres; then, the clustering results are assessed with users' knowledge to determine the best one.

III.2.2. Distance functions

Clustering technique utilizes the distance between observations to determine their similarity. There are many algorithms to measure the distance, such as the ***Euclidean distance***, the ***Manhattan distance***, the ***correlation distance***, the ***Pearson cosine distance*** and so on (refer to [Deza'09]). In this sub-section, we will introduce these distances and talk about their applications in data classification.

- Euclidean distance (**2-norm distance**):

It calculates the length of the line segment connecting two points. Suppose that there are two points (observations) $P = (p_1, p_2, \dots, p_n)$ and $Q = (q_1, q_2, \dots, q_n)$ in n-dimensional space (n variables). Then the distance from P to Q (or from Q to P) is given by:

$$d(P,Q) = \sqrt{(p_1 - q_1)^2 + (p_2 - q_2)^2 + \cdots + (p_n - q_n)^2}$$

$$= \sqrt{\sum_{i=1}^{n} (p_i - q_i)^2} = \|P - Q\|_2 \qquad \text{Eq. 3-1}$$

The drawbacks of Euclidean distance are treating all features (variables) in the same way and the tendency of large-scaled feature to dominate the others [Zou'08].

- Manhattan distance, also known as ***city-block distance*** (**1-norm distance**):

It is the sum of the lengths of the projections of the line segment between the points onto the coordinate axes.

$$d(P,Q) = \sum_{i=1}^{n} |p_i - q_i| = \|P - Q\|_1 \qquad \text{Eq. 3-2}$$

- Pearson correlation distance:

It is based on the ***Pearson correlation coefficient*** that is calculated from the sample values and their standard deviations. The data should be standardized by

$$(x - \mu)/\sigma \qquad \text{Eq. 3-3}$$

where x is a point value in one dimension, μ is the mean of data and σ is the standard deviation. This normalization is based on the assumption that distance values have a Gaussian distribution [Qian'04]. The Pearson correlation coefficient (r) between two standardized vectors $P' = \{P'_1, P'_2, \ldots, P'_n\}$ and $Q' = \{Q'_1, Q'_2, \ldots, Q'_n\}$ (the mean is 0 and the standard deviation is 1) is defined by

$$r = \frac{1}{n}\sum_{i}^{n} P'_i . Q'_i \qquad \text{Eq. 3-4}$$

which takes values from -1 (large negative correlation) to 1 (large positive correlation). The Pearson correlation distance is calculated by:

$$d(P, Q) = 1 - r \qquad \text{Eq. 3-5}$$

And thus takes values between 0 (two samples are most similar) to 2.

- Cosine distance

It measures the similarity of two vectors by the cosine of the angle (θ) between them (as shown in Figure 3-4). It is defined as:

$$d(P, Q) = \cos(\theta) = \frac{\vec{P}.\vec{Q}}{\sqrt{(\vec{P}.\vec{P})(\vec{Q}.\vec{Q})}} \qquad \text{Eq. 3-6}$$

This measure normalizes the feature vector to unit length and makes it invariant against relative in-plane scaling transformation [Zou'08]. It gives a good normalized measure of similarity ranging in [0, 1] ($\theta \in [0, \pi/2]$) but does not consider the magnitude (which is, taken into account by Euclidean distance. Consequently, the Euclidean distance (the straight line denoted with "**d**" in Figure 3-4) and the cosine distance provide similarity measures with different aspects. In [Zou'08, Zheng'09], a distance measure combining both cosine and Euclidean distances was used and it yielded a higher accuracy of data partitioning.

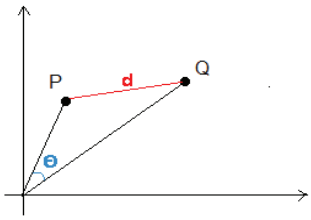

Figure 3-4 Cosine distance

III.2.3. Classification algorithms

III.2.3.1. K-means algorithm (hard clustering)

K-means algorithm was proposed in 1967 by MacQueen [MacQueen'67] and is widely used in scientific research as a classic clustering algorithm. This algorithm starts by randomly selecting *k* observations from studied dataset and treats them as initial centres of the *k* clusters. Then, each of the leaving observations is assigned to the cluster whose centre (or centroid) is nearest to the datum. After assignments of all observations in the dataset, the centre of each cluster is updated to be the mean point of all the observations assigned in the cluster (that is, its coordinates are the arithmetic mean for each dimension separately over all the points in the cluster). This centre will be repeatedly updated until the criterion function converges. The criterion for *k*-means algorithm usually uses squared error criterion function, defined by:

$$E = \sum_{i=1}^{K} \sum_{x \in C_i} \|x - c_i\|_2^2 \qquad \text{Eq. 3-7}$$

where $\|x - c_i\|_2^2$ represents the squared Euclidean distance of the point x to the centre point c_i of the *i-th* cluster. It is also known as ***arithmetic mean***. E is the sum of squared Euclidean distances of each point to the centre of its assigned cluster. It is the objective variable whose value must be minimized at the end of the clustering.

Since *k*-means is applied to a finite number of points, this algorithm can ensure the convergence of the objective E. In some cases, a small tolerance, denoted by ε, is pre-determined to set a stopping condition for the optimisation of clusters' centre: once the difference between two successive values of E is less than this small tolerance, the iteration will stop.

However, the arithmetic mean is sensitive to outliers, data errors or glitches presented in the raw dataset. Addressing to this problem, ***k*-medians clustering** is an alternative, which is well-known robust towards outliers. For this case, the Manhattan distance instead of squared Euclidean distance should be used to define the following criteria:

$$E = \sum_{i=1}^{K} \sum_{x \in C_i} \|x - c_i\|_1 \qquad \text{Eq. 3-8}$$

because the median is the point that minimizes the total 1-norm distance from all points to it [Bradley'97]. Similar to *k*-means clustering, the value of *E* in *k*-medians clustering can also converge. Nevertheless, the *k*-medians clustering is not trivially adapted to classify normalised data [Anderson'06].

III.2.3.2. Fuzzy k-means algorithm (soft clustering)

Fuzzy *k*-means algorithm was proposed by James Bezdek in 1981 [Bezdek'81] as an improvement of *k*-means algorithm. The underlying idea is that each data point belongs to all clusters with a certain degree of membership; this degree depends on the distance to each cluster centroid. Fuzzy *k*-means clustering can be implemented by 5 steps:

1) Randomly select *k* data points from a data set with *n* observations to be the initial centres of *k* clusters. A cluster-centre matrix **W**(0) is created to include these centres vectors.
2) The membership of each point to each cluster is evaluated by:

$$u_{i,j}(0) = \left(\frac{1}{\left\|\mathbf{P}_j - \mathbf{W}_i\right\|_2}\right)^{\frac{2}{m-1}} \Bigg/ \sum_{k=1}^{K}\left(\frac{1}{\left\|\mathbf{P}_j - \mathbf{W}_k\right\|_2}\right)^{\frac{2}{m-1}} \qquad \text{Eq. 3-9}$$

where

$i \text{ or } k \in \{1,2,\dots K\}$, representing the *i-th* cluster;
$j \in \{1,2,\dots n\}$, representing the *j-th* point;
m fixes the degree of fuzziness of the algorithm and $m \in [1,\infty]$ (typically =2);
P represents the data point in multi-dimensional space;
W represents the centre of cluster in the same space.

This formula normalizes memberships in unit length ($u_{ij} \in [0,1]$) and the sum of memberships of a datum to all clusters is equal to 1, like:

$$\sum_{i=1}^{K} u_{i,j} = 1 \qquad \text{Eq. 3-10}$$

3) Calculate the new cluster-centre matrix **W** by:

$$\boldsymbol{w}_i = \left(\sum_{j=1}^{n}\left(u_{i,j}{}^{m} \cdot \mathbf{P}_j\right)\right) \Big/ \sum_{j=1}^{n} u_{i,j}{}^{m} \qquad \text{Eq. 3-11}$$

4) Repeat (2) until the criteria function converges:

$$J_m(\boldsymbol{U},\boldsymbol{W}) = \sum_{j=1}^{n}\sum_{i=1}^{K} {u_{i,j}}^m \cdot \left\|\mathbf{P}_j - \mathbf{W}_i\right\|_2^2 \qquad \text{Eq. 3-12}$$

5) either until $\left|u_{i,j}(\text{iteration}) - u_{i,j}(\text{iteration}-1)\right| > \varepsilon$

6) or until $\text{iteration} > a\ maximum\ prefixed.$

III.2.4. Selection of the number of clusters

Both two clustering algorithms introduced above necessitate determining beforehand the number of clusters to retain from data. It requires the analyzer having expertise knowledge on the studied object which could help forecast the number of patterns. In practice, however, we rarely find ourselves in such a favourable position [Borgelt'06]. For example, in this work, the test from which the data were collected was made by the industrial partners who know very well the characteristics of the studied entity, while as the data analyser, we do not have much knowledge on it. In this case, the choice of clusters number seems to be a matter of trials and see. In other words, we have to cluster the given data set several times, setting a different amount of clusters for each time. To determine the best number of clusters, the classification results should be analysed to evaluate the clustering quality for each specific amount of clusters. Thus, the key issue lies in how to measure the quality of classification.

The average silhouette of the data is a useful criterion for evaluating the clustering result. The *silhouette* of a datum measures how close it is to the assigned cluster's centre and how dispersed to the neighbouring cluster's centre. A silhouette takes value from -1 (negative value implies that the datum is in a wrong cluster) to 1 (positive value implies that the datum is assigned into an appropriate cluster).

Assume the data have been classified into *k* clusters. For each datum *x*, let *a*(*x*) be the average distance of *x* to all other data within the same cluster. Then calculate the average distance of *x* to the data of another single cluster. Repeat this for every cluster and let *b*(*x*) denote the smallest average distance. The cluster relevant to this smallest average distance is called as "neighbouring cluster" of the cluster that *x* is assigned to. We define:

$$s(x) = \frac{b(x) - a(x)}{max\{a(x), b(x)\}} \qquad \text{Eq. 3-13}$$

For a silhouette *s*(*x*) to be close to 1, we have *a*(*x*) << *b*(*x*), which implies that the datum x is well matched to its assigned cluster. If *s*(*x*) is close to -1, we have *a*(*x*) >> *b*(*x*), which implies *x* would be more appropriately assigned into its neighbouring cluster. An *s*(*x*) near zero means that this datum is on the border of two natural clusters.

The average silhouette <*s*(*x*)> of a cluster is the mean value of the silhouettes of all data assigned in this cluster. It measures how appropriately (or tightly) the data has been clustered [Rousseeuw'87]. When a poor choice of cluster number is made in the *k*-means algorithm, the

average $s(x)$ will be much smaller than 1. Based on this parameter, we can easily compare the classification results and select the most appropriate cluster number.

Apart from the average silhouette, there are other cluster validation indices able to help find an appropriate number of clusters, such as the elbow method which looks at the percentage of variance explained as a function against the number of clusters, the information criterion approach which uses log-likelihood as model selection criteria including Akaike's Information Criterion (AIC) [Akaike'74] and Bayesian Information Criterion (BIC) [Schwarz'78] to estimate the value of k.

III.3. The context and the clustering-based diagnosis strategy

In the field of fuel cell engineering where a certain number of experiments are involved, large quantities of data are usually available for information elaboration. These data may have been analyzed for a specific study to which the experiments were oriented whereas its potential to other investigations may not be fully exploited. In our case for example, the data originated from the experiments for RealSOFC project* had been analyzed for the purpose of optimizing the design of SOFC stacks so as to extend their lifetime and to improve their performance in long-term operation. However, its value for the development of SOFC diagnosis technology had not been exploited. Therefore, in GENIUS project, we have firstly worked with this data, aiming at determining significant response variables that could indicate accelerated degradation in the FC stack after the occurrence of an emulated BoP fault.

Clustering technique allows the classification of data so as to separate different patterns that are not known beforehand. In this work, the data set has a large size and involves many different variables. We selected k-means hard clustering algorithm to classify system outputs (measured and extracted) data. Each of the obtained classes was then labelled to indicate one of the considered states of health of SOFC stack, e.g. the normal and the accelerated degrading state. Since the change of system operating condition can also lead to variation of the outputs, the effect of operating condition upon the stack responses has to be taken into account so as to avoid wrong judgment on the stack health. Accordingly, there would be more than two classes for the states of SOFC stack that should be considered before performing the data classification.

After the classification, each datum will be labelled by the number of its assigned class. Since clustering is a purely computerized procedure, post-classification analysis must be carried out in order to give each class practical meanings. Through analysing the data in each class, significant variables whose data have played a decisive role for the classification result could be found and considered as the feature variables to represent the state of health of SOFC stack.

In the experiments for the RealSOFC project, the SOFC stacks were tested in mildly different operating conditions, respectively. On the one hand, setting each of these conditions to be a

* Refer to the web page: http://www.real-sofc.org/

class is not necessary and may complicate data classification procedure. On the other hand, it is difficult for us to select the significant operating conditions, due to lack of knowledge on the stacks' characteristics. For simplicity, it is better to firstly classify the integrated measurements of the operating variables so that the data describing the similar operating conditions could be grouped together in a single class to study.

After classifying the operating conditions, we group the response data in the same way to see if each class of the data orients towards one the operating conditions recognized in the classification of the operating variables' data (see Figure 3-5). If yes, it means that the studied response variables do be indicative to the operating condition.

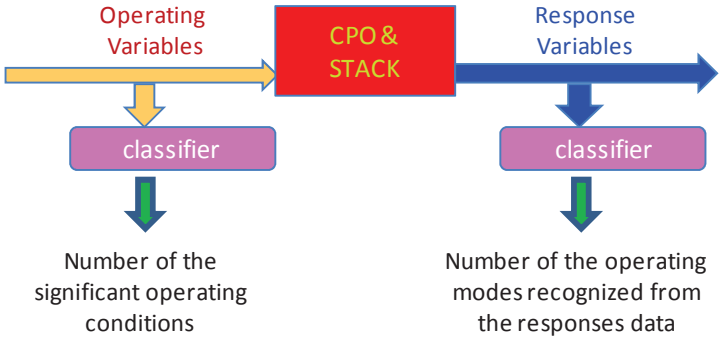

Figure 3-5 The diagnosis strategy based on the classification method

In each operating condition of interest, the stack may suffer from degradation in a long-term test. To extract this information, the responses data categorized to the same operating condition would be further partitioned to differentiate the normal and the degrading states of the stack.

After performing a classification, the data assigned in the same class must be analysed and interpreted, in order to confirm that the information retrieved from the data corresponds to the expectations of the analyzer.

III.4. Application of *k*-means clustering for SOFC stack off-line diagnosis

III.4.1. Description of the tests

The datasets used to validate the clustering based off-line diagnosis algorithm are from the RealSOFC project which aimed at increasing the understanding on the degradation mechanisms of SOFC stacks. They were collected on the HEXIS 5-cells test rig in the long-term experiments (more than 6000 hours) carried out respectively on 4 SOFC stacks of identical type and fabricated with the same technology. During each experiment, the polarization tests were repeatedly performed in order to monitor the evolution of the stack's state of health. Totally, there are 30 polarization tests in the 4 experiments.

Redox cycling and/or thermal cycling were experimentally done in the test for each stack. The former was emulated by switching off the gas and the current in a specific temperature. The

later was realized by making an abrupt reduction for the fuel supply. According to the investigation performed in the RealSOFC project, the negative impact of thermal cycling to the health of stack is greater than the impact caused by redox cycling.

III.4.2. Data preparation

III.4.2.1. Selection of significant variables

From each polarization test of a stack, we could obtain a data matrix including the temporal measurements of the stack's input and output variables. Nine variables of interest were selected and divided into two groups:

1) **Controllable operating variables**:

   Natural gas flow (g/h);
   CPO air flow (l/h);
   Cathode air flow (g/h);
   Preheating CPO (%)[*]*;*
   Preheating air (%).

2) **Measured response variables**:

   Temperature at bottom of stack (°C);
   Temperature at top of stack (°C);
   Input fuel temperature of CPO (°C);
   Output gas temperature of CPO (°C).

The first group of variables are the input of the stack (here the CPO and the SOFC stack are taken as a whole to diagnose, as shown in Figure 2-12 in Chapter 2); the second involves the responses of the stack. In addition, the current and the voltage data are picked up to plot the polarization curves (or called I-U curves).

III.4.2.2. ASR estimation

The *area specific resistance* (ASR, in unit "$m\Omega/cm^2$") and the *open circuit voltage* (OCV, in unit "mV") are two of important variables used to reflect the state of health of the stack. The ASR of a fuel cell cannot be directly measured by a sensor. However, it is possible to estimate it from I-U characteristic measurements. Generally, the middle part of the I-U curve in the region of ohmic polarization is a quasi-straight line whose slope can be roughly viewed as fuel cell's ASR, as shown in Figure 3-6.

[*] The percentage values for both the "preheating CPO" and the "preheating air" denote the ratio of the real power used by the heater to the maximal rated heating power.

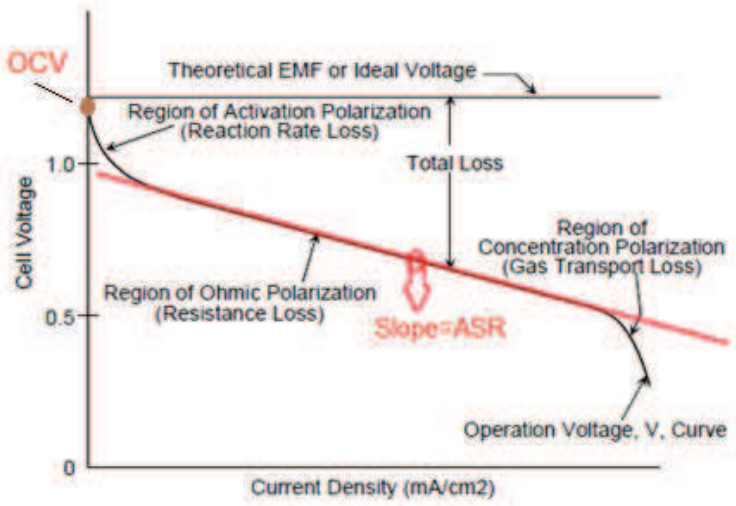

Figure 3-6 ASR and OCV given by an I-U curve*

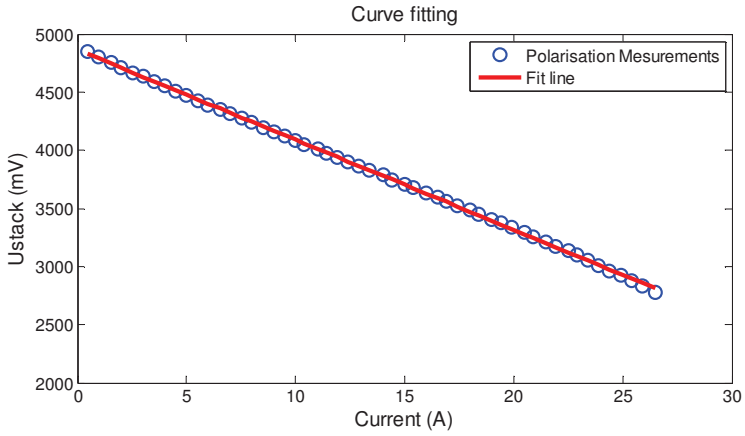

Figure 3-7 An example for the polarization curve fitting

In this work, simple linear regression was applied to estimate the slope of each available polarisation curve, based on the linear model represented by

$$y = ax + b \qquad \text{Eq. 3-14}$$

where a is the slope of the polarisation curve; y denotes the stack voltage and x is the stack current. Relying on the polynomial regression algorithm, the values of a and b can be empirically yielded from the data of an I-U curve. An example is given in Figure 3-7 to demonstrate the curve fitting result from a set of the polarization data.

III.4.2.3. Extraction of other informative data

* Source of the polarization curve and the information in the background figure: *Fuel cell handbook [electronic resource] / EG&G Technical Services, Inc*. Morgantown, WV : U.S. Dept. of Energy, Office of Fossil Energy, National Energy Technology Laboratory, 2004.

In order to learn the causes of stack degradation, it is necessary to know what the stack had experienced before every polarization test. After analyzing the entire experimental data, three parameters are calculated. They are, respectively, the *operation time* (hours), the *number of redox cycles* and the *number of thermal cycles* (total cycles from the start-up). These 3 variables' data are not involved in the dataset to classify but serve as heuristic arguments for classification result evaluation and class labelization.

III.4.2.4. Addition of a disturbing variable

In the Hexis 5-cells test rig, there are two valves to control the mass flow of the natural gas inputted to the CPO. One of them was kept closed in the experiments. However, the mass-flow sensor next to it was always active, which produced a sequence of meaningless data with small values. These data were labelled as '2nd natural gas flow' in the raw data sheet. This variable was inserted into the group of the operating variables with the aim of checking if the clustering procedure is subject to the disturbing variable.

III.4.2.5. Summary

In sum, there are in total 16 variables' data (columns) extracted from the data sheets of 30 raw polarization tests. They are divided into 3 groups:

1) Controllable operating variables' data set;
2) Response variables' data set;
3) The data set that contains the information about what the stacks had experienced in the tests, such as the emulated redox or thermal cycling or the operational time.

For simple visualization purpose, the controllable and response variables' average values in each polarization test were computed and shown in the table of Appendix-I.

In the data analysis phase, according to Figure 3-5, the k-means clustering algorithm was firstly performed on the first data set in order to find how many significant operating conditions should be considered in the diagnosis procedure. Based on the result of the first classification, the second data set was then classified to see whether the responses of the stack could reflect the system operating condition and indicate the acceleration of stack degradation happened under each of these conditions.

III.4.3. Classification results analysis

In cluster analysis, the type of measure for the distance between observations must be determined first of all. It depends greatly on what type of data do we have. The most used distance, the Euclidean distance, suffers from the disadvantage that it is sensitive to the units of measurement for the variables [Norušis'03]. If the variables are measured on different

scales, the variables with large ranges contribute more to the distance measure than the variables with small values, and thereby have a significant effect on the partitioning of the data. Moreover, the variable that has a much wider range than others will tend to dominate the classification solution [Cornish'07]. To get around these problems, each variable must be standardized to have zero for the mean value and one for the standard deviation.

Another concern is about the dependency between the clustering variables. For example, among the response variables studied in this work, the stack temperature (top & bottom) can influence two other variables considered in the clustering variable set: the ASR and the OCV of the stack. Since the clustering procedure does not differentiate the variables in a conceptual sense, if highly correlated variables are used for cluster analysis, irrelevant aspects covered by these variables will be overrepresented in the clustering solution[Mooi'11]. Accounting for this point, the factor, correlation between variables, must be also taken into account when measuring the distance between two observations. Hence, the Pearson correlation distance was chosen as the distance measure in this work. Based on it, all variables had been standardized by Eq. 3-3 before the classification.

The classifications on both the two data sets (one for the controllable variables and the other for the response variables) were executed under MATLAB by using 'k-means' function (based on *k*-means clustering method). The number of iterations was fixed to 50 (It is an empirical selection. In this work, the clustering solution became stable after 10 iterations). After each iteration, a new placement of the initial clusters' centres was randomly determined. Several values for the number of classes *k* (from 2 to 6) were tried and the best one was determined according to the average silhouette value of the classification.

III.4.3.1. For the controllable variables' data

According to the average silhouette value for the classifications on the controllable variables' data shown in Figure 3-8, two-cluster is the most appropriate choice for the number of classes *k*. The result of this classification, given in Table 3-1, implies that the first 11 polarization tests were carried out in a different operating condition from that of the rest of the tests.

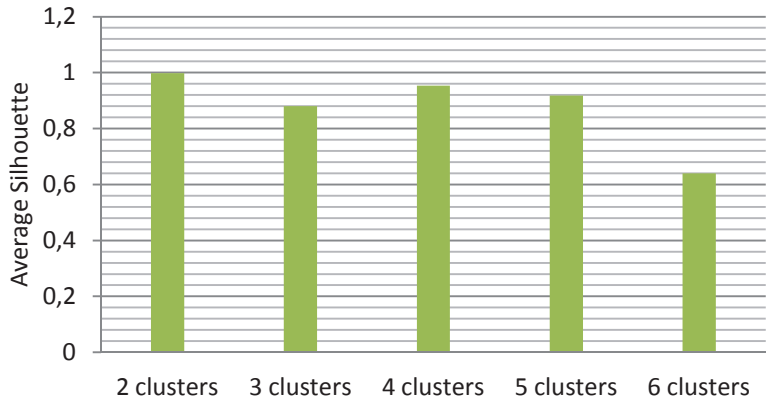

Figure 3-8 The average silhouettes of the classifications for the controllable variables' data

Table 3-1 The result of classification on the controllable parameters

		CONTROLLABLE PARAMETERS						Class No.
Stacks	test	NG flow (g/h)	2nd NG for 5 g/h Stack (g/h)	CPO Air flow (l/h)	Cathode air flow (g/h)	Preheat Air	Preheat CPO	2 clusters
HP060030	1	19,98	0,23	71,03	1001,41	24,83%	68,18%	2
	2	19,97	0,24	70,98	1001,32	28,75%	67,58%	2
	3	19,98	0,26	71,03	999,66	28,48%	68,65%	2
	4	19,99	0,26	71,06	1000,28	29,36%	68,89%	2
HP060031	5	19,92	0,07	70,61	1000,73	34,22%	40,93%	2
	6	19,92	0,10	70,61	999,45	31,68%	43,87%	2
	7	19,91	0,06	70,63	1000,22	33,74%	35,92%	2
HP060045	8	20,05	0,12	70,72	1000,31	30,36%	82,33%	2
	9	20,08	0,18	70,79	999,74	25,89%	78,35%	2
	10	20,10	0,20	70,82	999,32	23,80%	84,57%	2
	11	20,09	0,20	70,79	1000,56	24,88%	88,97%	2
HP080025	12	19,98	0,13	65,59	999,45	37,76%	46,07%	1
	13	19,96	0,15	65,61	999,48	39,46%	42,80%	1
	14	19,96	0,16	65,58	999,71	39,71%	42,64%	1
	15	19,96	0,13	65,59	999,99	39,17%	41,24%	1
	16	19,95	0,15	65,58	999,92	39,72%	42,56%	1
	17	19,97	0,15	65,59	1000,11	39,58%	41,36%	1
	18	19,94	0,13	65,59	1000,67	39,32%	40,03%	1
	19	19,97	0,15	65,58	999,32	39,41%	41,61%	1
	20	19,96	0,14	65,58	999,71	39,39%	42,24%	1
	21	19,97	0,15	65,58	999,91	39,52%	41,01%	1
	22	19,98	0,14	65,59	999,10	39,19%	40,84%	1
	23	19,97	0,13	65,59	1000,09	39,27%	39,67%	1
	24	19,96	0,13	65,59	1000,07	39,39%	40,61%	1
	25	19,97	0,15	65,57	1000,46	36,94%	43,94%	1
	26	19,98	0,13	65,59	999,92	36,81%	41,76%	1
	27	19,97	0,14	65,58	1000,31	39,15%	41,78%	1
	28	19,95	0,12	65,60	1000,28	39,15%	40,87%	1
	29	19,97	0,12	65,59	999,67	39,26%	40,33%	1
	30	19,98	0,16	65,57	999,86	39,09%	46,18%	1

It is necessary to find out the significant variable that has played a decisive role on the clustering solution so that we could easily understand the basic difference between these two classes of operating condition. Feature selection technique can help achieve this goal. It seeks to identify the variables that have the most discriminative power among the set of all the considered variables [Boutsidis'09]. Under MATLAB, there is a function called “rankfeatures” which is able to assess the significances of the variables in a two-cluster separation, relying on the absolute values of the cross-correlation coefficient between the candidate variable and all previously selected variables. This function regards the variables in the data matrix as features and ranks them by using an independent evaluation criterion which permits to assess the significance of every feature for separating two labelled groups. Owing to this function, the controllable operating variables were ranked according to their significance value relative to the solution of the classification. It turned out that the variable “CPO Air flow” held the highest ranking position, followed by the variable “Preheat CPO”. According to this result, we assert that the difference between the yielded two classes of operating condition is determined by the variation of the air flow inputted into the CPO.

In addition, the “rankfeatures” function assigned the variable ‘2nd natural gas flow’ to the last position of ranking, which implies that the classification was not disturbed by this variable’s data.

According to the numeration of the classes in Table 3-1, we labelled the Class-2 "Operating Condition 2 (OC2)" and the Class-1 ''Operating Condition 1 (OC1)". If the degradation in the stacks were accelerated, the classification on the response variables' data should produce 4 clusters to indicate 4 states of the stack: "Normal in OC1", "Accelerated degradation in OC1", "Normal in OC2" and "Accelerated degradation in OC2". In the next sub-section, we will analyse the results of classification for the response variables' data and find out the significant response indicative to the state of health of the SOFC stacks.

III.4.3.2. For the response variables' data

Figure 3-9 shows that for the response variables, the best value for the number of classes *k* should be 4. It indicates that in addition to the amount of operating modes, there are two more patterns/classes involved in this data set. This result is in accordance with the solution concluded in III.4.3.1.

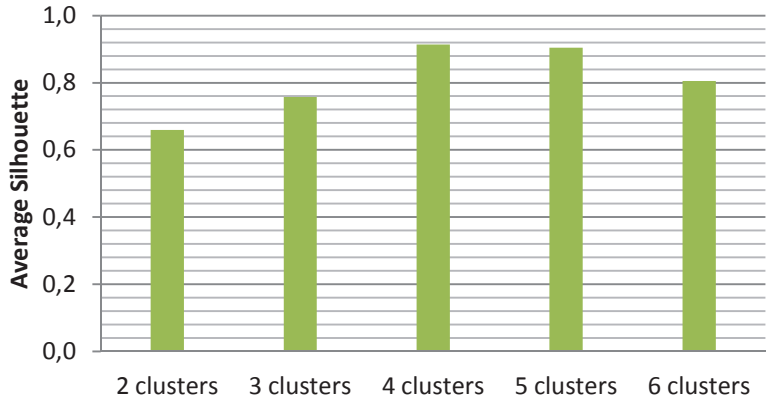

Figure 3-9 The average silhouettes of the classifications for the response variables' data

It is noteworthy that the 5-cluster classification also shows a high quality of data partitioning, for which the silhouette average value is 0.85, just a little lower than 0.86 for the 4-cluster classification. The solutions of these two classifications are given in Table 3-2. The difference between them is that in the 5-cluster classification, the test No.11 is separated from the test No. 10 and assigned into an individual class, due to a lower stack top temperature. In fact, the data of these two tests describe the same information, that is, the degradation of the stack. Merely, the degradation of the stack in the Test No.11 is severer that in the Test No.10. Therefore, we only consider 4 clusters for this data set.

For a 2-clusters classification, the solution coincides with that of the operating variables' data (see Table 3-1). However, when the number of classes is increased to 4, each of these clusters is divided into two sub-clusters, respectively. The "rankfeatures" function was used to find out the significant variable for separating the sub-clusters No.2 and No.4 as well as the one for separating the sub-clusters No.1 and No.3. As a result, it turned out that the stack top temperature and the ASR are the significant features.

Table 3-2 The solution of classifications on the response variables' data

		MEASURED PARAMETER				EXTRACTED		Stack Operation Experience			CLASSIFICATION RESULTS			
Stacks	test	T stack bottom (°C)	T stack Top (°C)	T CPO out (°C)	T CPO in (°C)	ASR (mΩ/cm2)	OCV (mV)	Operation time (hours)	Redox cycles	Thermal cycles	4 clusters	3 clusters	2 clusters	5 clusters
HP060030	1	949,33	962,62	730,77	761,05	59,17	4800,26	49	0	0	2	2	2	2
	2	949,48	961,29	722,69	761,17	69,75	4875,03	2354	0	1	2	2	2	2
	3	949,51	959,93	724,08	760,85	72,29	4844,81	4865	0	1	2	2	2	2
	4	948,44	959,90	732,87	760,43	77,55	4887,23	5471	0	1	2	2	2	2
HP060031	5	949,30	953,28	727,86	770,67	57,82	4690,39	49	0	0	2	2	2	2
	6	949,53	933,78	726,39	780,71	72,10	4767,30	2354	0	1	2	2	2	2
	7	949,61	851,47	721,93	780,13	72,97	4705,95	3690	0	1	4	2	2	4
HP060045	8	949,26	956,31	722,42	730,55	55,04	4837,18	39	0	0	2	2	2	2
	9	949,67	922,68	702,25	730,62	65,48	4942,47	3297	0	0	2	2	2	2
	10	949,70	830,05	701,40	740,55	76,89	4914,70	6065	0	0	4	2	2	4
	11	949,36	818,05	707,88	741,85	90,60	4921,11	6998	0	0	4	2	2	5
HP080025	12	849,26	857,51	720,05	774,88	92,53	4807,58	41	0	0	1	1	1	1
	13	849,44	858,11	720,45	763,36	87,62	4833,83	612	0	0	1	1	1	1
	14	849,28	858,20	719,54	760,51	86,40	4837,18	689	1	0	1	1	1	1
	15	849,47	858,40	720,76	761,88	88,08	4826,50	828	1	0	1	1	1	1
	16	849,46	858,45	719,68	761,04	85,98	4845,42	877	2	0	1	1	1	1
	17	849,41	858,61	719,13	754,76	87,44	4828,64	952	2	0	1	1	1	1
	18	849,38	858,58	719,54	754,26	89,59	4820,40	976	3	0	1	1	1	1
	19	849,42	858,51	720,11	758,81	90,52	4835,35	1000	4	0	1	1	1	1
	20	849,39	858,51	719,99	761,65	90,90	4858,24	1024	5	0	1	1	1	1
	21	849,48	858,74	719,97	758,62	93,57	4848,17	1048	6	0	1	1	1	1
	22	849,37	858,88	719,84	758,34	97,62	4841,15	1121	7	0	1	1	1	1
	23	849,35	858,97	719,48	756,23	99,86	4843,29	1145	8	0	1	1	1	1
	24	849,32	859,02	719,65	758,63	102,18	4853,36	1169	9	0	1	1	1	1
	25	849,41	858,50	720,28	770,06	138,02	4891,20	1211	11	1	1	1	1	1
	26	850,59	859,12	722,37	776,47	226,77	4867,09	1283	11	1	3	3	1	3
	27	850,35	859,18	721,04	770,97	167,86	4877,77	1313	12	1	3	3	1	3
	28	850,17	858,74	721,08	772,05	195,72	4865,87	1337	13	1	3	3	1	3
	29	850,20	858,88	720,25	769,12	216,13	4862,82	1362	14	1	3	3	1	3
	30	850,40	858,94	719,62	775,35	216,88	4899,75	1381	14	1	3	3	1	3

The result of the 4-cluster classification reveals that the degradation in the stacks HP060031, HP060045 and HP080025 had been accelerated, as explained in the paragraphs below. The information described by the third data set (including 3 variables: the operation time, the number of redox cycles and the number of thermal cycles) is helpful for explaining these incidents:

- Firstly, as has been concluded from the result of classification on the operating parameters, there are two significant operating conditions in which the stacks were tested. This result is correspondent with the solution of the clustering on the response variables' data to which the 2-cluster classification separates the tests No.1-No.11 from the rest of the tests (see Table 3-2). The feature ranking shows that the stack bottom temperature's data has a dominant effect on this classification. This implies that that the stack bottom temperature can reflect the variation in the CPO air flow rate (its data decided the solution of the classification for the operating conditions).

- Secondly, according to the third data set (information on stack operation experience), a thermal cycle had taken place in the stack HP060031 (test No.5-7) after 2354 hours of stationary operation. This event must have provoked significant stack degradation which resulted in an important temperature gradient inside the stack, because the stack top-temperature decreased from 933°C to 821°C in the following polarization test, whereas the bottom-temperature remained at the same value. In the stack HP060045, the stack top temperature also has a significant decrease in the tests No.10-11. We attribute it to the accelerated aging phenomenon of the fuel cell, because when this event happened,

the stack had been continuously operated for 6000 hours. The fact that the response variables' data in the test No.7, 10 and 11 were assigned into a single cluster (Class-4) implies that the studied variables are indicative to the state of health of the stack. We label this cluster "Severely degraded in OC2".

- The data measured on the stack HP080025 are divided into two individual clusters. This stack passed firstly 11 redox cycles during which its degradation rate was not influenced. However, it started to quickly degrade when a thermal cycle happened after 1211 hours of stationary operation. This event is indicated by the sharp increase of the ASR value after the occurrence of the thermal cycle. The classification procedure has captured the variation of the ASR value. As a result, the data in the tests No. 26-30 were assigned into another independent cluster (Class 3), being distinguished from those for the previous tests. We labelled this cluster "Severely degraded in OC1". However, differing from the accelerated degradation happened in OC2, this degradation acceleration can be only reflected by the ASR value.

  In fact, the ASR is a very useful indicator capable of reflecting the fuel cell degradation. According to its values, all the first three stacks were actually degraded during the operation. However, the *k*-means algorithm had only found out the degradation in the stack HP060031 and in the stack HP060045, while the degradation in the first stack was not diagnosed. This can be attributed to the difference of the degradation mechanisms for these stacks. Since the significant temperature gradient was present in both the stacks HP060031 and HP060045, they might suffer from mechanical damage such as delamination between cell components. In contrast, the stack HP060030 did not have significant temperature gradient; its degradation may be relative to other mechanisms.

- Finally, the data observed in the tests where the stacks were in the good state (Test 12-25 and Test 1-6, 8-9) are correctly assigned into the other two clusters which indicate the normal operation in "OC1" and "OC2", respectively.

III.4.4. Analysis of the silhouettes of the classified data

As introduced in the sub-section III.2.4, the silhouette of a datum measures how close it is to the assigned cluster's centre and how dispersed it is to the neighbouring cluster's centre. This parameter can give us insight into the performance of the clustering.

Figure 3-10 illustrates the mean of silhouette value for the classified response observations in each polarization test. The 4 colours indicate the 4 labelled classes, respectively. According to these silhouette values, we can conclude that the 1st stack (HP060030) remained in good state of health throughout the experiment whereas the other 3 stacks were severely degraded during the experiments.

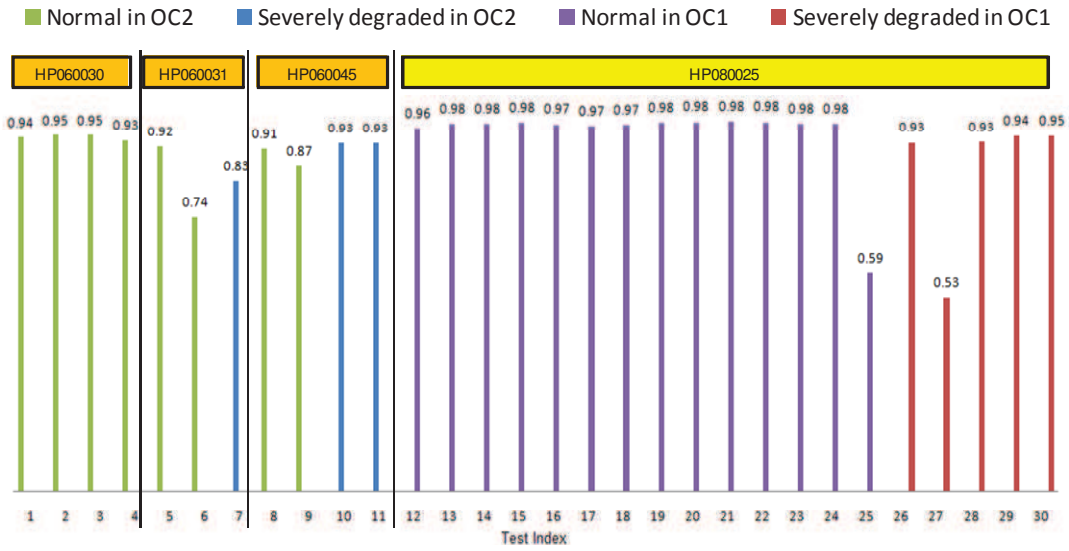

Figure 3-10 The silhouettes of the response variables' data classified into 4 clusters

For the stack HP060031, its silhouette value for the class "Normal operation in OC2" shows a decline of 20% in the second polarization test, which indicates the state of the stack is less well correspondent to the normal state. It implies a considerable degradation having occurred in the stack, due to the occurrence of a thermal cycle. Then, after continuing to operate for another 1200 hours, the stack's degradation became more and more severe. The same analytical result can be yielded according to the silhouette value (up to 0.83) of the Test-7 for a different class, which implies the significant disagreement between the observations in this polarization test and those of the former two tests (Test-5 & 6).

For the stack HP060045, the degradation is mainly attributed to the aging mechanism. During the first 3000 hours of operation, the silhouette values of the first two polarization tests (Test-8 & 9) are quite close, which indicates that the state of health of the stack was stable in the earlier operating period, just like the class label describes. However, severe degradation of the stack appeared in the terminal phase of the operation (after 6000 hours). That is the reason why the observations of the polarization tests (Test-10 & 11) in this period are separated into the class of "stack degradation".

For the stack HP080025, its degradation is mainly attributed to the thermal cycling that accidently took place after 1200 hours of continuous operation. Before this incident, the stack's state of health was reasonably stable and showed insusceptible to the redox cycling, because the silhouette values for the tests carried out during this period are nearly identical. However, after the advent of a thermal cycle, the silhouette value (for Test-25) decreases about 40%. The data of the sequential tests (Test-26 to 30) are assigned into another class, indicating that the stack had been severely degraded. Among these tests, the silhouette value of the Test 27 is 40% less than those of the other tests due to its much lower ASR value. It proves the dominant effect of ASR on this classification solution. In addition, even through the observation in Test-25 is assigned to the class "Normal operation in OC2", its relatively low silhouette value implies that the state of health of the stack had started to change. In this case, the silhouette variable shows potential as a prognostic indicator.

III.5. Conclusion

In this chapter, an algorithm is proposed to implement SOFC system off-line diagnosis. This algorithm is based on the *k*-means clustering technique serving for hard-classification on the stacks' response data. The application of feature ranking technique is exploited to analyse the classification result and find out the significant response variables indicative to the state of health of SOFC stack in different operating conditions. The parameter "average silhouette" is computed to assert the classification quality and determine the natural number of clusters within the studied datasets. The silhouette for the data of each polarization test is also studied.

The algorithm is validated by using the data of polarization tests from the RealSOFC project. This dataset involves 4 patterns, defined as follow (see Table 3-3):

Table 3-3 The patterns within the dataset for validation

	Pattern 1	**Pattern 2**	**Pattern 3**	**Pattern 4**
Operating condition	OC 2	OC1	OC1	OC2
State of health of the stack	Normal	Normal	Severe Degraded	Severe Degraded

Based on the classification result, we conclude that the thermal cycling is very harmful to the health of SOFC. Only one thermal cycle is able to provoke significant acceleration to SOFC stack degradation. In contrast, the investigated stacks seem insusceptible to the redox cycling. Moreover, in one of the studied operating conditions, the difference between the stack's top and bottom temperatures is found being able to indicate the degradation of the stacks. This implies that the profile of the stack internal temperature is quite relevant with the observed degradations. Finally, it is found that the silhouette value of the datum to their assigned class has potential ability to demonstrate the degrees of the stack degradation, which is useful in the fuel cell prognostic application.

Chapter IV Wavelet transform based algorithm for SOFC system online diagnosis

In this chapter, another diagnosis method based on wavelet-transform signal analysis is introduced. The wavelet transform technique has been employed and greatly developed in the field of mechanical system diagnosis [Paya'97, Peng'04, Bartelmus'09] . Here, we use it to realize online detection of the BoP fault and the failure inside the SOFC stack/cells.

For a FC stack operated in galvanostatic mode, it is considered that its voltage signal involves rich information regarding the operating condition and the state health of the cells. However, such significant information is often not readily available in the raw temporal signals. To address this problem, the signals should be transformed to another representation so that the desired information could become more noticeable and easy to extract.

In our case, since the occurrence of the fault may affect the stationarity of the system process, the wavelet transform technique pointing to non-stationary signal analysis was selected as the basic method for the signal treatment.

It is noteworthy that the signal processing cannot solve the diagnosis problem but is the first phase in the whole process of diagnosis. The wavelet transform contributes to representing the signals in another manner such that effective and sensitive fault indicators could be easily discovered and extracted from the new representation of the signal.

Steiner et al. (2011) [Steiner'11a] had successfully used the wavelet transform to decompose signals in order to find out effective fault features for the state of health of PEMFC stack. However, the application of this method for the SOFC and system diagnosis has not been exploited. Hence, the emphasis of this chapter focuses on studying how to use the wavelet transform to implement SOFC system diagnosis. The determination, extraction and validation of SOFC system's fault indicators are presented following an introduction to the wavelet transform technique.

IV.1. Introduction to wavelet transform

IV.1.1. Basic principles

Wavelet Transform (WT) belongs to the multi-resolution analysis method class. It is similar to the Short Time Fourier Transform (STFT), implemented by means of multiplying the signal with a window function. These methods aim at mapping a signal into a two-dimensional function of time and frequency. They can extract, from a temporal signal, the information about both when and at what frequencies a single event occurs.

The difference between STFT and WT mainly lies in their windowing technique. In STFT, the window function is invariable, keeping the same window for all frequencies [Polikar'96a]. In WT, however, the window function can be varied based on a "mother wavelet" function, denoted by "Ψ". Owing to this feature, the wavelet analysis allows the use of long-term intervals where we want more precise low-frequency information, and shorter regions where we want high frequency information [Misiti'09].

The term "wavelet" means a small wave. The smallness refers to the condition where the function is of finite length. The wave refers to the condition where this function is oscillatory [Polikar'96b]. The term "mother" implies that the wavelet is the basic waveform for the other wavelets derived from this mother wavelet function.

The continuous WT is defined by:

$$C(u,s) = \langle f, \Psi_{u,s} \rangle = \frac{1}{\sqrt{s}} \int f(t).\psi^* \left(\frac{t-u}{s}\right) dt \qquad \text{Eq. 4-1}$$

where *f*(t) is the original signal and *C(u,s)* denotes the transformed signal; *u* and *s* denote respectively the **translation** and **scale** parameters.

The translation parameter is related to the location of the window, as the window is shifted along the time axis of the raw signal. It corresponds to time information in the transform domain. The scale parameter is proportional to 1/frequency. Similar to the scale used in maps, high scales (low frequency) correspond to a non-detailed global view of the signal. It is related to the frequency of the wavelet and low scales (high frequency) correspond to a detailed view. The variation of the scale results in a scaling action (either dilate or compress) on the mother wavelet, which will yield a set of window functions (wavelets). Larger scales correspond to dilated (or stretched out) mother wavelet and small scales correspond to compressed mother wavelet.

For a pair of *(u,s)*, *C(u,s)*, also known as wavelet coefficient, measures the similarity between the corresponding wavelet and the windowed section of the signal. The higher its value is, the more similar they are. Once the mother wavelet is chosen, the computation starts with *s*=1 and continues for the increasing values of *s*. In other words, the continuous WT starts from high frequencies and proceed towards low frequencies.

After having selected the mother wavelet, a continuous WT can be completed by repeatedly performing the following steps:

1. Place the wavelet at the beginning of the signal at the point which corresponds to time t=0 (see Figure 4-1-a). The wavelet function at s=1 is multiplied by the signal and then integrated over all times. The result of integration is then multiplied by the constant number $1/\sqrt{s}$ for energy normalisation purpose. The final result is the value of the transformation at time u=0 and scale s=1.
2. The wavelet at scale s=1 is shifted towards the right until the location $u=u_1$ (see Figure 4-1-b); compute $C(u_1,1)$ with Eq. 4-1. This procedure is repeated until the wavelet reaches the end of the signal. As a result, a vector of wavelet coefficients for the scale s=1 will be obtained.
3. Then, s is increased by a small value to get a new scale value s_1, which results in a stretched-out wavelet (see Figure 4-1-c). Repeat the Step 2 to obtain another vector of wavelet coefficients.
4. Step 3 is repeated for every value of s.

When the process is completed for all desired values of s, the continuous WT of the signal has been completed.

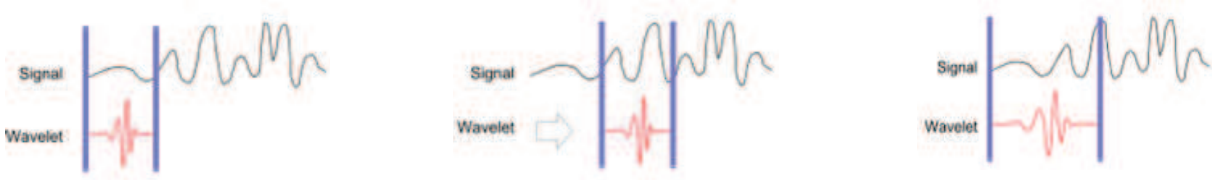

(a) (b) (c)

Figure 4-1 The translation and the scaling of the wavelet [Misiti'09].

IV.1.2. Discrete wavelet transform

Calculating wavelet coefficients at every possible scale and position leads to a great amount of work and generates a huge amount of data, which is not always necessary. In order to make the analysis much more efficient and just as accurate, the scales and positions can be chosen based on powers of two—the so-called dyadic scales and positions, defined as:

$$u = k.2^j, \qquad s = 2^j, \qquad j \epsilon N^+, \qquad k = 1, 2, \dots, \frac{N}{2^j} \qquad \text{Eq. 4-2}$$

where N is the length of the digital signal. In this case, the transformed signal is a function of j and k. This transformation belongs to discrete wavelet transform, in which the time parameter is discretized with respect to the scale parameter in a variant sampling rate [Polikar'96c].

For j = 1, discrete WT is equivalent to a practical filtering algorithm. As illustrated in Figure 4-2, the digital signal (S) in length of N is inputted into a low-pass and a high-pass filter, respectively. The output signals are then downsampled (one point out of two is sampled), producing two subsignals. The one obtained from the low-pass filter is the ***approximation*** of the original signal and the one from the high-pass filter is known as the ***detail*** of the signal.

The approximation subsignal corresponds to the low frequency (or high scale) band of the original signal while the detail subsignal corresponds to the high frequency (or low-scale) band.

For $j > 1$, the discrete WT can be implemented by simply iterating the above decomposition process, with successive approximations being decomposed in turn (as in Figure 4-3), so that the signal is broken down into many lower resolution components. After each level of decomposition, the sampling frequency is reduced by half. Note that the discrete WT can consist of $\log_2(N)$ stages at most. In other words, the decomposition levels allowed for a signal equals to the number of iterations that the signal length N could be divided by 2 repeatedly.

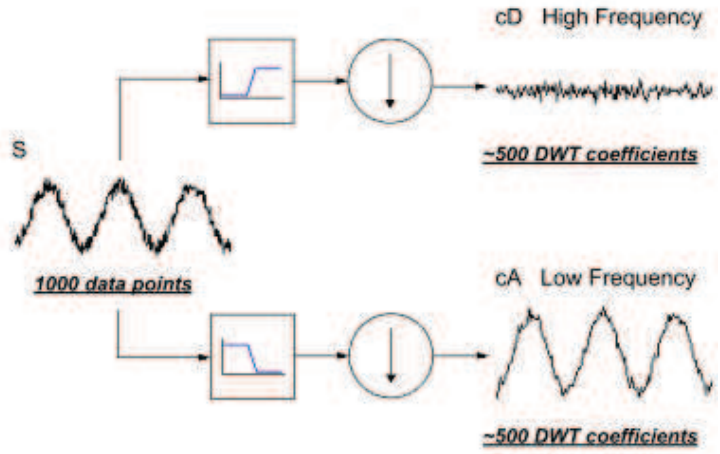

Figure 4-2 Schematic diagram of one-stage filtering [Misiti'09]

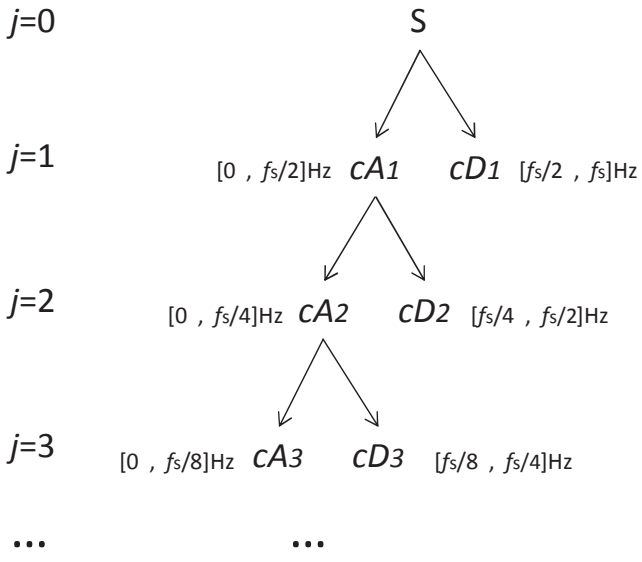

Figure 4-3 Discrete wavelet decomposition tree

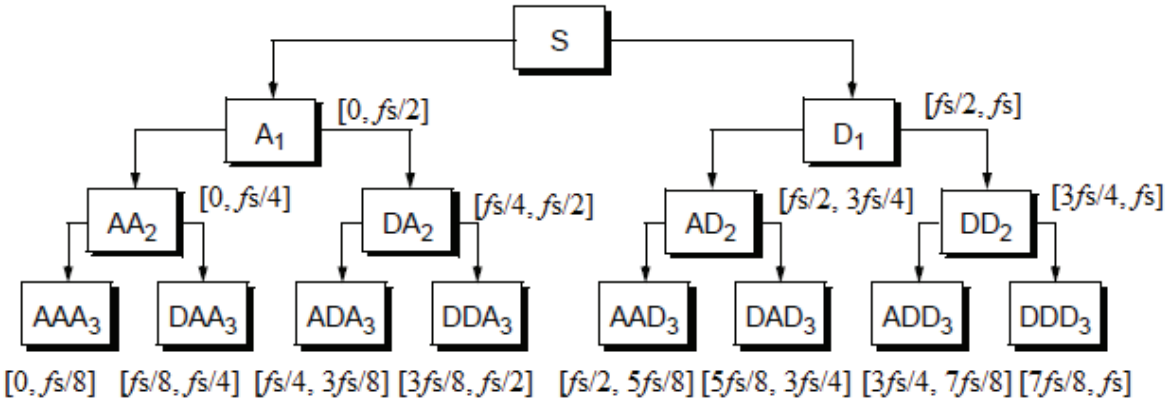

Figure 4-4 Wavelet packet decomposition tree for a digital signal sampled in frequency f_s [Misiti'09]

IV.1.3. Wavelet packet transform

As the WT decomposes only the approximation signals, some problems may be encountered in applications if the important information is located in higher frequency domain [Steiner'11a]. To solve this problem, a solution is to use Wavelet Packet (WP) transform which decomposes not only the approximation subsignals but also the detail ones (as shown in Figure 4-4). This transformation leads to a large number of detail signals over a ser of frequency bands divided equally and being narrower than those in the discrete wavelet transform.

IV.2. Discussions

The WT is just a method for signal decomposition. It cannot solve the diagnosis problems. In diagnosis application, the objective of signal decomposition is to enable the analysis of the signal over different frequency bands so as to find out the significant signal components or features relevant to the identification of the fault.

Before ploughing into the fault diagnosis by using WT, it is necessary to consider some questions concerning which type of signals (steady or transient) to analyse, what kind of indicators to extract (wavelet coefficient-based, singularity-based or wavelet energy-based) and which method (discrete WT or WP transform) to use for signal transformation. These questions contribute to a deep view into the application of the WT based diagnosis method. Answering them beforehand could help us have a clear train of thought and a specific goal in the discovery of effective fault indicators. In the following paragraphs, discussions on these 3 questions will be given. The reasons justifying the answer to each of them will be clarified.

IV.2.1. About the selection of signals to analyze

The WT can be used to treat both steady-state and transient signals. According to the design of the diagnostic strategy in this work, the action of fault detection aims at capturing the happened fault, by means of comparing the stack's post-fault response with the afore-fault or reference one so as to determine the occurrence of the fault.

In practice, a FC system fault such as gas leakage may lead to a continuous decline of the FC voltage until the fault is found out and corrected. In laboratory experiments, however, this kind of faults is usually emulated by artificially changing the FC operating condition to a specific one. Thus, for a laboratory research, the investigated fault is actually referring to a faulty operating mode/condition applied on the FC stack rather than a faulty action. Accordingly, it is reasonable to select FCs' steady signals under different operating conditions as the investigated object. Comparing with transient signals, they can more exactly represent the state of stack at a certain operating point.

In addition, due to the safe operation design integrated in the system control, a contrived variation on an operating parameter may lead to the change of other operating parameters settable by the automatic control system, aiming to restrict FC stack to operate in safe range so as to avoid serious stack failure and accidental system shut-downs. For instance, a man-made decrease at the input fuel flow rate may activate the control unit to automatically modify the current density in order to protect the stack from overload operation; a designed reduction of the input air flow rate may result in a reaction of the control unit to decrease the stack temperature. Due to such chain activities from the control system, the stack will pass a relatively long time before reaching steady state at the new operating point.

The transient FC voltage signal obtained during this period presents the dynamic evolution of the FC operating condition. It reflects the integration of the effects caused by a series of modification on the operating parameters. In order to figure out the individual influence of a fault on the FC voltage signal, the pure effect caused by this fault of interest (ex: modification of fuel flow) upon the FC behavior must be separated from that originated from other factors (ex: current density modification). However, it is often difficult to implement by the study on the transient signal. By contrast, investigating the stationary signals could get round this difficulty, simplifying the problem to a comparative study, i.e. comparing the stack's states before and after the advent of fault.

In sum, the voltage signals to study in this work should be the ones obtained when the whole FC system restores its stationarity after an operating-condition-change manipulation.

IV.2.2. About the property of the indicators

In Chapter 2, three categories of WT-based indicator adopted for diagnosis purpose have been enumerated and introduced. The singularity based indicators, essentially relying upon the singularity points in the signals to implement fault indication, are generally obtained from non-stationary signals. Now that the steady-state signals have been determined as the only

investigated object in this work for indicator research, the singularity-based diagnosis method is not applicable in our case.

As for the wavelet coefficients based method, it leads usually to a large volume of feature parameters. Since the wavelet coefficients are only a representational manner for a signal and carry no physical signification, the users usually have to use classification technique to analyze these parameters in order to achieve fault discrimination. This method requires users to empirically define relevant thresholds for the wavelet coefficients in order to separate the fault-free area. In our work, due to the lack of the expertise knowledge on the studied FC stack, it is very hard for us to correctly determine these thresholds. Hence, the wavelet coefficients based method is not applicable for our case, either.

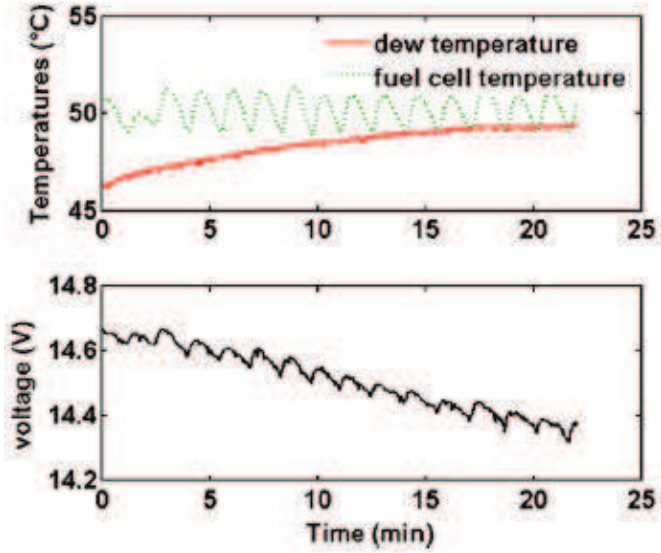

Figure 4-5 The decline of PEMFC stack voltage caused by experimental membrane flooding [Steiner'11a]

The wavelet energy based indicator seems to be a potential selection. A successful example has been made by Steiner et al. (2011) [Steiner'11a] who used wavelet energy parameters to establish two feature vectors for detecting flooding phenomenon occurred in a PEMFC stack. Through performing clustering analysis, the indicative capability of these features was proven effective. It is noteworthy that in their investigation, there is only one fault (FC flooding) under study. It was artificially created inside a PEMFC stack operated in nominal condition. This fact implies that the features' discriminative capability for distinguishing the good and the bad state of the stack is limited only to the case where the FC is operated in the rated/nominal condition. From their experiments, it was found that the decrease of the FC voltage linked to the FC flooding (emulated by increasing the inlet gases dew point temperature) was quasi-linear and proceeding in an oscillating manner as shown in Figure 4-5. In other words, the oscillation observed in the decreasing trend of the voltage signal is related directly to the flooding phenomenon. Based on this feature, Steiner and the co-workers put their efforts on the characterization of the oscillating behaviour present in the voltage signal's trend component. Based on the WP transform, they extracted the approximation subsignal from the raw voltage signal for fault indication, because the former involves the oscillating

component of the signal. That is why at the end of this research paper, the feature extraction was only carried out on the approximation wavelet packet (i.e. the packet 7 declared in the article). The finally validated feature vectors consisted of the normalized wavelet energy values in this significant packet.

Relatively being more complex in our case, however, the FC stack is operated continuously in different (normal and abnormal) operating conditions. This means that our fault indicators must permit to distinguish 3 basic cases of operation, i.e.

1) The fault-free case: the whole FC system is operated properly;
2) BoP fault: the FC stack is operated in an improper condition but the health of the stack is at the normal state.
3) FC failure: one or several FCs in the stack has a serious degradation or has been broken so that the stack could neither be used as a sensor for system state diagnosis nor continue to work for power generation.

In addition, in the experiments contributed to the GENIUS project, there are as many as 17 operating points of interest (including the nominal one) having been tested. Taking into account the FC failure case, there are at least 18 modes of operation to consider. In this case, the oscillation present in the voltage trend signal is not likely to be discriminative enough for distinguishing all these operating modes.

Furthermore, it has been determined that only steady-state signals are under investigation, which signifies that the analysed signals should be stable at a certain voltage value and thus their trend signal is much likely to be a smooth average line. In this situation, we must turn the focus from the approximation subsignal (the oscillating component of the signal) to the detail subsignals (the fluctuating part of the raw signal).

The fluctuating behaviour of a detail subsignal at some frequency band can be synthetically described by its wavelet energy. Based on this parameter, every investigated mode of operation, being represented by a voltage signal of FC, could be characterized by the distribution of the wavelet energies over different frequency components of this signal. As long as the high-frequency fluctuations of the steady-state signals observed in the normal and the faulty cases are distinguishable, we could adopt them to indicate the state of health as well as the operating condition of the FC.

Following this idea and based on the practical situation of this work, the wavelet energy present in the high-frequency components of the signals (i.e. detail subsignals obtained from WT) will be used for fault indicators establishment.

IV.2.3. About the selection of the signal transform method

Selecting the discrete WT or the WP transform as the signal processing method requires considering 3 factors:

1) The sampling rate of the available signals;
2) The signals' length;
3) The computing time permissible for a complete transformation.

The first factor limits the richness of the information that a signal contains. In the field of signal analysis, it is widely believed that the higher the sampling rate is, the more exactly and in detail the signal can describe the information. Because the physical and electrochemical processes inside the FC occur very fast, the major information on the FC behaviours should lie in high frequency bands. Unfortunately, in the available database of , the maximal sampling rate for the signal measurement is only 3 Hz (on FCLAB's test bench) and even less (1Hz for the VTT system). With such a low sampling rate, the information available in the signal about FC stack behaviours is very limited. If the WP transform is used to process the signal, the detail component of the signal where the significant information locates will be decomposed as well, resulting in a set of refinedly separated detail subsignals (see Figure 4-4), that is, the "details of the detail" which are often not useful for the study of low-frequency sampled signals. From the point of view of information theory, the super-decomposition on the detail leads the similar information to being dispersed over more discrete frequency bands, making them less noticeable and even covered by interfering noises. As a result, the extraction of fault-relevant information will become very difficult. That is the reason why the WP transform method is not suitable for this work.

As for the other two factors, i.e. the signal length and the computing time required for signal transformation, there is some relationship between them. For a steady signal, its length determines the redundancy of the digital representation (i.e. the signal) for the information. For our case where the signal data were collected at low sampling rate, the longer the signal is, the more information could be captured from the signal, and thereby the easier for us to learn about the symptoms of the state of the stack.

Nevertheless, a long signal means a long extra time needed for accurate enough measurement of the symptoms, which leads to a considerable delay for the diagnosis. Fortunately, the selected discrete WT algorithm is very simple and can be implemented rapidly. In comparison with WP transform, discrete WT can economize at least 50% of computational time (refer to Figure 4-3 and Figure 4-4).

IV.3. The diagnostic method

Generally, the measured steady voltage signal of FC involves fluctuations (refer to the signal *S* in Figure 4-7). When FC is operated in normal conditions, these fluctuations are regarded as random noises that exist universally in electrical signal. Their presence is unavoidable and could be considered as a natural phenomenon. However, when the state of the FC system is abnormal, unwanted fluctuations will appear in the FC's response signal, superposing directly on the afore-mentioned natural ones. These interfering fluctuations can lead to changes of the fluctuating energy distribution of the signal. So, as long as being able to recognize the

variation of the signal's high-frequency fluctuations, the change of the state of system could be detected.

Suppose that the frequency spectrum of the FC's voltage signal appears as presented in Figure 4-6-a in normal operating conditions and as presented in Figure 4-6-b in a faulty condition. Comparing them, we can find that the faulty condition has provoked shifting of the centre of the dominant high-frequency band from 50 Hz to 68Hz. If the sampling frequency for signal measurement is high enough (ex: 100Hz), the diagnosis problem could be solved according to the location of the dominant high-frequency component of the signal on the frequency axis. Nevertheless, in case where the sampling frequency is very low, for example 1 Hz in our case, the available spectrum of the voltage signal will be only restricted to the range of frequencies below 1Hz, excluding the significant frequency band relevant to the faulty condition.

Zooming in the low-frequency area of these two spectra (see Figure 4-6-c and Figure 4-6-d), we can still observe the difference between them in the frequency band of [1/16, 1] Hz. Merely, it is not as obvious as that in the dominant frequency band. To utilize such unapparent difference to indicate the faulty condition, it must find an effective way to singularize this difference.

The idea is to calculate the spectral energy for each frequency value and analyze the energy distribution over the whole frequency band of interest. As spectral energy equals to the square of amplitude, it permits to amplify the difference between the two studied spectra.

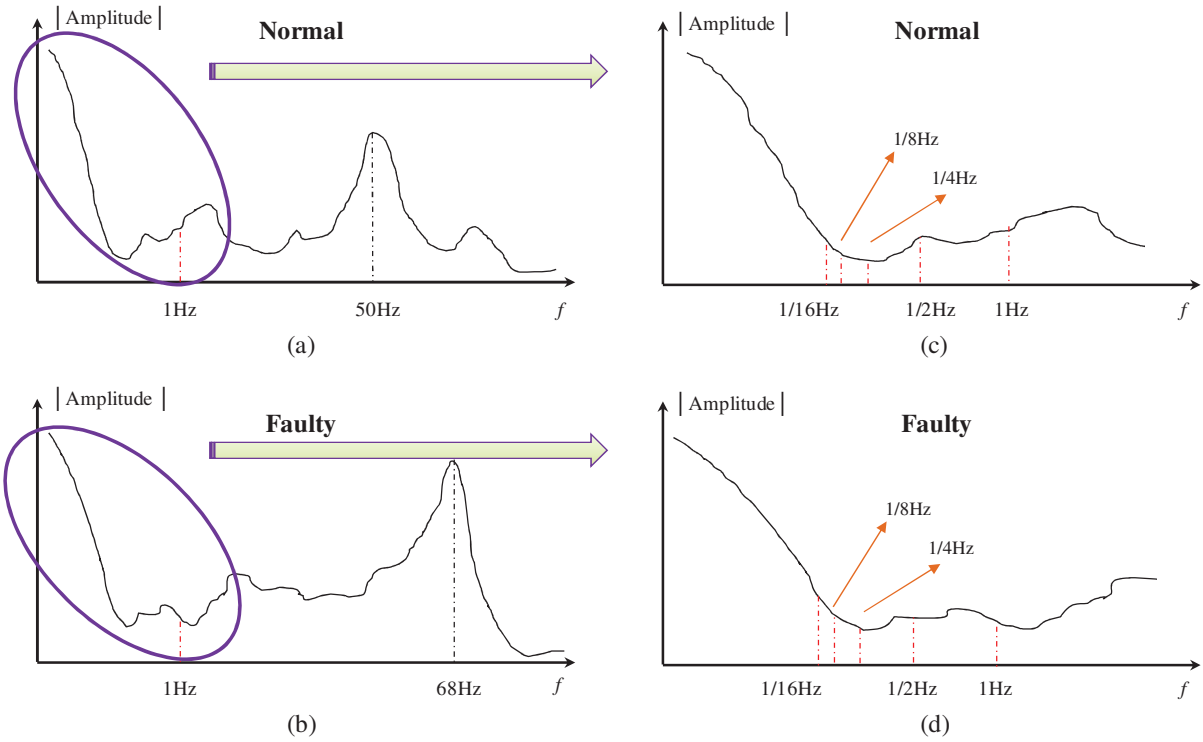

Figure 4-6 An example of the different spectral distributions of signal in the normal and the faulty conditions; (a) the spectral of a signal for the normal condition; (b) the spectral of a signal for the normal condition; (c) and (d): the zooms for the low-frequency part of the spectrum in (a) and in (b).

Performing a 4-level discrete WT on a FC's voltage signal sampled in 1Hz, the frequency band [1/16, 1] Hz will be dyadicly divided into 4 sequential bands, i.e. [1/2, 1] Hz, [1/4, 1/2] Hz, [1/8, 1/4] Hz and [1/16, 1/8] Hz. Under the normal condition, the spectral curve (see Figure 4-6-c) is smooth and thus the variation of the amount of energy lying in these bands should follow a decreasing order because the bandwidth becomes narrower and narrower. By contrast, the form of the spectral curve in the faulty condition (see Figure 4-6-d) reveals some differences, which may lead to the change in the energy distribution over these 4 frequency bands. Accordingly, the key to solve the fault detection problem lies in revealing and quantifying the energy distribution of the signal under study.

In the field of WT, there are three kinds of parameters that could be applied to analyze the energy distribution of signals: **relative wavelet energy**, **total wavelet entropy** and **relative wavelet entropy**. In the diagnosis application, we can use them as feature variables to indicate the studied fault.

IV.4. The indicative variables and their definitions

According to the principle of discrete wavelet transform, it can dissect the steady signal into essential part and fluctuation. The fluctuating part is then stripped off and the essential part further dissected into even more essential parts and fluctuations on them, and so on, as shown in Figure 4-3. For n-levels decomposition, n approximation components and n detail components of the signal S (sampled in f_s Hz) can be obtained during the transform. In WT field, each of these components is represented by a vector of wavelet coefficients, denoted by cA_j (for the approximation component) or cD_j (for the detail component) where j denotes the number of the transform level, and is related to a specific frequency band. The wavelet coefficients in cD_j, calculated at the scale 2^j and the position $k.2^j$, are denoted by $C_j^d(k)$.

It is possible to remap these wavelet-coefficients described components back to the time-domain space through inverse wavelet transform. As a result, a group of subsignals (denoted by a_j or d_j) of the original signal could be obtained.

Figure 4-7 gives an example to illustrate the result of a 5-level discrete WT on a steady voltage signal composed of 2000 samples. The sampling time for measuring this signal is 1s. The curve a_5 is the approximation subsignal obtained at the decomposition of the final level, relevant to the frequency band of 0-1/32 Hz. It is a smoother set of time series, consisting of the essential part of the raw signal and the lowest frequency oscillations. The following curves (d_5 to d_1) are the detail subsignals obtained at the decompositions of the 5 levels. They illustrate fluctuating behaviours of the analysed signal at higher frequency bands that have different widths and don't interlap ($d_1 \rightarrow$[1/2 , 1]Hz; $d_2 \rightarrow$[1/4 , 1/2]Hz; $d_3 \rightarrow$[1/8 , 1/4]Hz; $d_4 \rightarrow$[1/16 , 1/8]Hz; $d_5 \rightarrow$[1/32 , 1/16]Hz).

In this subsection, three WT-based variables are introduced to characterize fluctuating behaviors of signal.

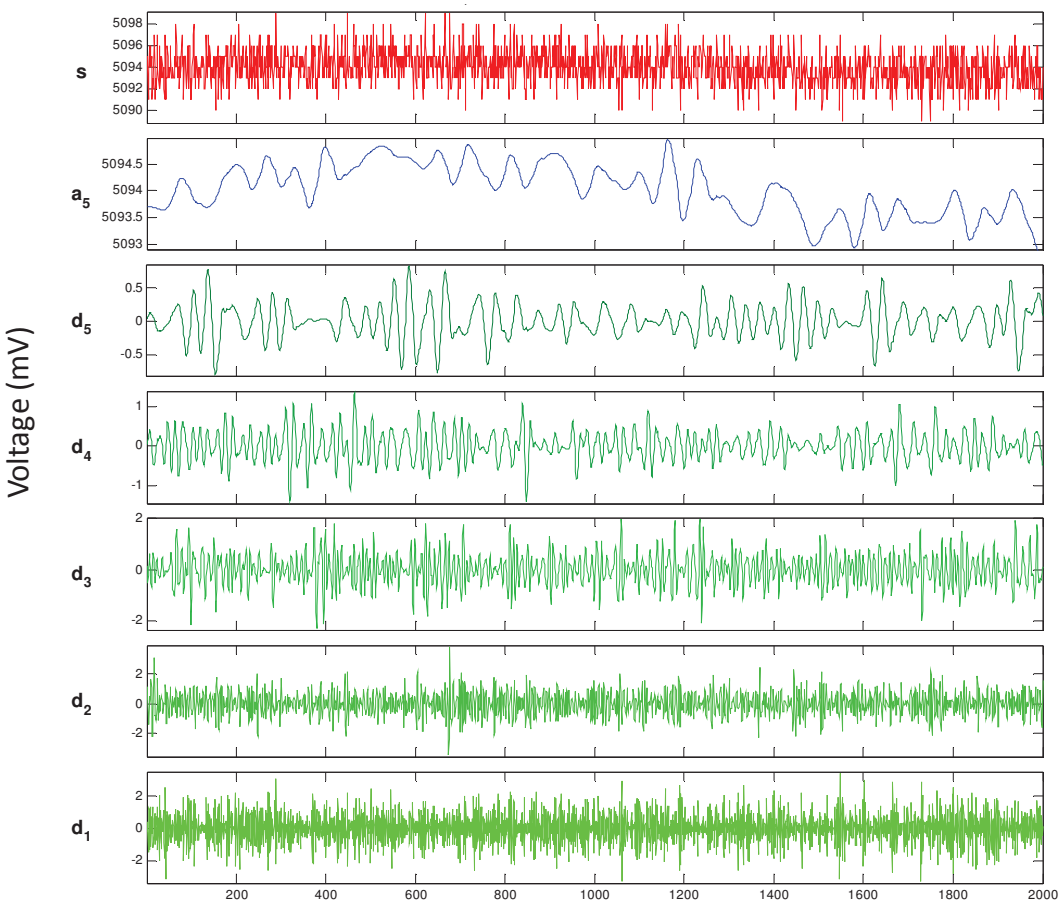

Figure 4-7 An example to show the results of a 5-level discrete WT on an SOFC's voltage signal (the original signal: **S**)

IV.4.1. Wavelet energy and its normalization

In the time domain, the energy of a signal is the sum of the squares of its time-series values. Similarly, the energy of a subsignal obtained from discrete WT is the sum of squares of its wavelet coefficients. Therefore, in the field of WT, this energy is also known as *wavelet energy*.

For a detail subsignal at level j, its energy, denoted by E_j^d , can be computed by

$$E_j^d = \sum_k \left| C_j^d(k) \right|^2 \qquad \text{Eq. 4-3}$$

where *d* signs that the calculated energy is contained in a detail subsignal and *j* is the number of decomposition level.

By summing up all energies of the detail subsignals, the value of the total energy of fluctuations in the studied raw signal is produced (as expressed in Eq. 4-4). Based on it, each of detail subsignals' energy can then be normalized into the percentage form (denoted by p_j^d in Eq. 4-5), called as *relative wavelet energy*.

$$E_{tot}^{d} = \sum_{j}\sum_{k}\left|C_j^d(k)\right|^2 = \sum_{j} E_j^d \qquad \text{Eq. 4-4}$$

$$p_j^d = \frac{E_j^d}{E_{tot}^d} \qquad \text{Eq. 4-5}$$

The wavelet energy of a detail subsignal measures the strength of fluctuation of the original signal at the relevant frequency band. Normalizing it to the relative wavelet energy is favorable to study the signal's energy distribution over discrete frequency bands.

IV.4.2. Total wavelet entropy

The Total Wavelet entroPy (TWP), denoted by S_{WT}, originates from the Shannon entropy theory that applies the notion of entropy to measure the amount of information contained in a signal. In this work, we use it to measure the degree of order/disorder of the energy distribution in the fluctuation components of the studied signals [Rosso'01]. The TWP is a function of relative wavelet energies, defined as

$$S_{WT} = -\sum_{j} p_j^d * \ln\left(p_j^d\right). \qquad \text{Eq. 4-6}$$

A small value of TWP indicates that the energy distribution is in a high degree of regularity.

IV.4.3. Relative wavelet entropy

The Relative Wavelet entroPy (RWP) measures the degree of similarity of the energy distribution between in two different signals. It is expressed as the summation of wavelet coefficients within a selected frequency range over the time [Emre Cek'10], formulated by

$$S_{WT}(p|q) = \sum_{j} p_j^d * \ln\left(\frac{p_j^d}{q_j^d}\right) \qquad \text{Eq. 4-7}$$

where q_j^d denotes the relative energy of the *j*-th level detail subsignal of a reference signal. In this work, the voltage signal measured in the nominal condition is taken as the reference signal. The RWP is positive and vanishes when $\{p_j^d\} \equiv \{q_j^d\}$.

IV.5. Application

IV.5.1. Prepare the signals to study

Four groups of SOFC cell voltage signals are prepared for indicators validation.

1) The first group of signals are picked up from the 1st round test on the VTT system. They are all measured at the steady state. Each of them corresponds to an operating condition. Throughout this test, there is no severe degradation observed in the cells. The signals are used for the validation of the WT-based parameters' indicative capability to the FCs' operational condition in the case where the stack is fuelled with pure hydrogen.

2) The second group of signals are from the 2nd round test on the VTT system. At the beginning of this experiment, one of the cells (the Cell 3) in the stack was accidentally broken. This event provoked an unknown effect upon the performance of its adjacent cell—the Cell 4. The polarization curves shown in Figure 4-8 demonstrate this undefined effect. Except this, however, neither the proceeding of the experiment nor the performance of other cells was influenced by this incident. Therefore, the second group includes only the voltage signals of the good-state cells (the Cell 1, 2, 5 and 6). They also serve to assess the performance of the indicators in terms of distinguishing the normal/tolerant operating conditions from the harmless ones for the SOFCs that are operated with reformed natural gas.

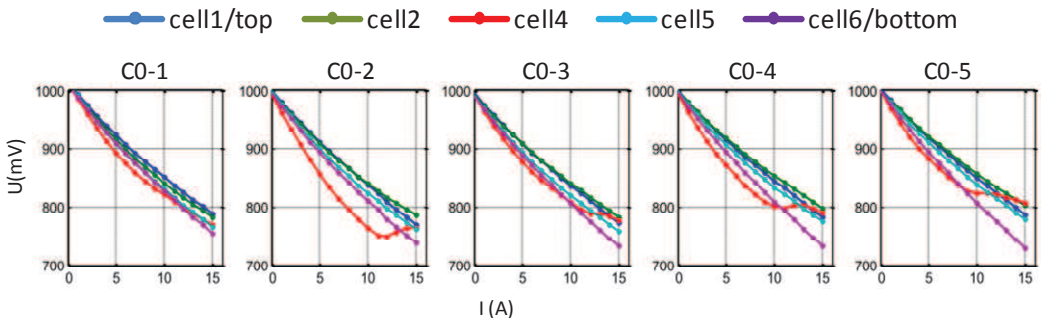

Figure 4-8 The polarization curves of the good-state cells measured in the 5 repetitions of nominal operating condition

3) The voltage signals of the broken cell and one of the good-state cells (the Cell 1) in the 2nd round test on the VTT system are gathered in the third group. They serve to evaluate the indicators' ability of recognizing the state of health of the FC under various operating conditions. For simplicity, we consider only two states of health for the SOFCs: "good" or "broken".

4) The fourth group involves the voltage signals measured at different time on a cell in the 3-cell SOFC stack stationarily operated on the FCLAB's test bench. This cell had progressively degraded in the proceeding of the test. They are used to see whether the indicator is able to reflect the degrading process of the cell.

On the VTT's test bench, the sampling frequency for signal measurement is 1Hz; on the FCLAB's test bench, it is 3Hz. For the signals from the 1st round test on the VTT test bench, each of them consists of 2000 time-series samples while for the signals from the 2nd round experiment, the length of signals is reduced to 1200. This design aims to see if the fault symptom could be captured by a shorter signal measurement. The shorter the analyzed signal,

in the lower delay could the diagnosis start after a fault takes place. As for the signals from the FCLAB's test bench, since their sampling frequency is relatively higher, they should theoretically contain more detailed information on the state of health of the stack (because this information usually locates in high frequency band). Thus, the length of these signals could be further reduced. Their length is fixed to 800.

IV.5.2. Implementation of signal decomposition

The analysis on each signal starts with a 5-level discrete WT which is automatically implemented by using the "dwt" function under Matlab. The selected mother wavelet is the Daubechies 4 (or 'db4') [Daubechies'92], as shown in Figure 4-9. The 'db4' WT can redistribute the energy of a signal and compress most of energy in the final obtained approximation subsignal [Walker'08]. After performing the 'db4' WT on each signal, we can obtain a series of detail subsignals which are represented by a vector of wavelet coefficients, respectively. Each of them contains an amount of energy. It is from these detail subsignals that the parameters described in Section IV.4 are extracted.

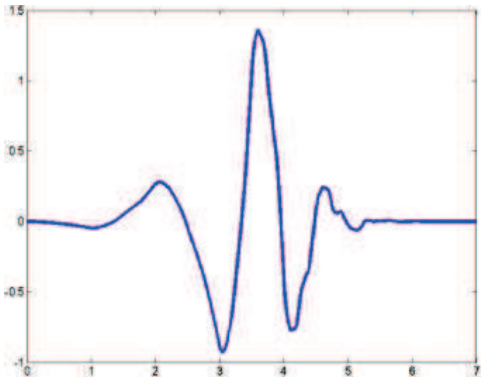

Figure 4-9 Daubechies-4 wavelet

To examine the performance of the indicative variables, the essential work is to confirm if the wavelet energy distribution in the fluctuating components of a cell voltage signal is capable of indicating the operating condition and the state of health of the FC.

IV.5.3. Results

IV.5.3.1. For the 1st group signals

In the experiments carried out on the VTT system, the stack was operated continuously in 17 operating conditions (the nominal one is denoted by C0; the bias ones are denoted by C + the experiment number declared in Table 2-1) through modifying the inputs of the FC stack. The test started in the nominal condition and then repeatedly returned to this operating point after having operated in every 4 bias conditions. In order to provide a direct view to the SOFC's operating state in these conditions, we joined together the stack's steady voltage signals

measured in every operating condition and represented them on the same axes in the real experimental order, as shown in Figure 4-10.

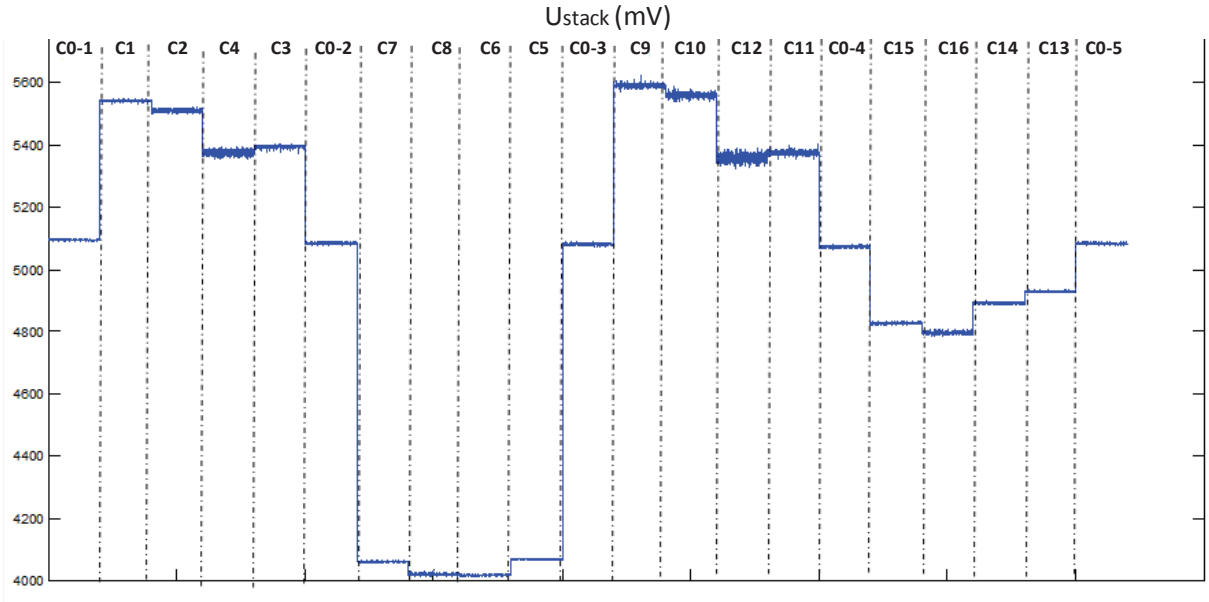

Figure 4-10 Stationary signals of the stack voltage in 20 tests (from VTT 1st test round data)

a. The Relative Wavelet Entropy (RWE) values:

Figure 4-11 gives the calculated RWE values of the detail subsignals of the cells for different operating conditions. Analyzing the diagrams of the last row, we can find that the variation of the energy in the detail subsignal obtained at each level of decomposition follows a progressively descending trend when the stack is operated in the nominal condition. In other words, with the proceeding of the wavelet transformation level after level, the filtered-out detail/fluctuation component of the signal contains less and less energy. According to the RWE value, nearly a half (50%) of fluctuation energy is contained in the 1st level detail subsignal which is related to the frequency interval of [0.5, 1] Hz.

However, in several bias operating conditions such as C4, C10, C11 and C12, this frequency band is not in dominant place. Instead, the fractions of energy lying in the different frequency bands (that is, in the subsignals of different levels) are very close to each other. Here we transform the operating parameters' numerical values corresponding to these 4 conditions into qualitative values (see Table 4-1) for generalization. This gives prominence to the innate character of the studied conditions.

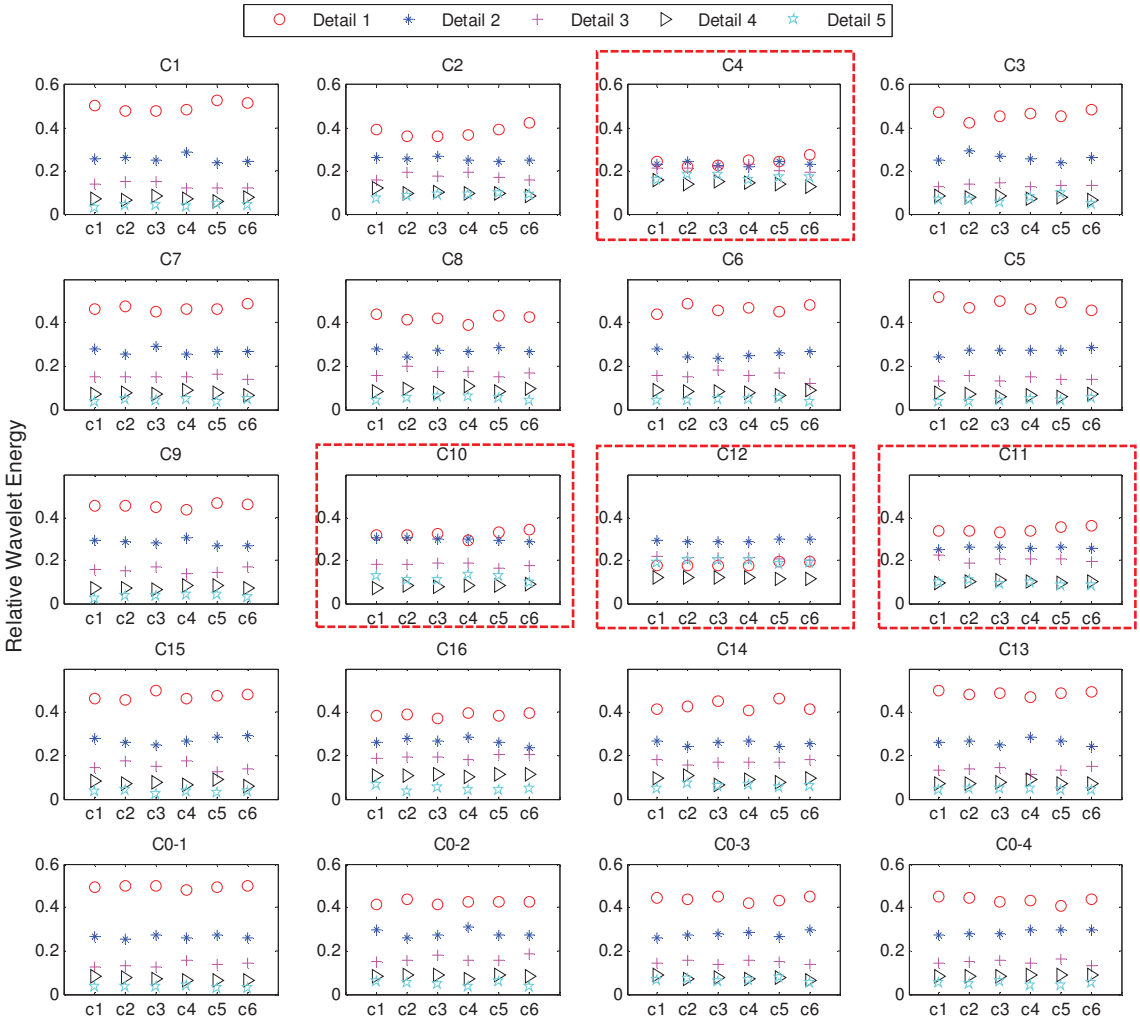

Figure 4-11 The RWE values of the detail components in the cells' voltage signals associated to different operating conditions

Table 4-1 The undesired operating conditions

Condition	T_f	J	FU	AU
4	LOW	LOW	HIGH	HIGH
12	HIGH	LOW	HIGH	HIGH
10	HIGH	LOW	LOW	HIGH
11	HIGH	LOW	HIGH	LOW

Based on our expertise on SOFC degradation mechanisms, the variable *FU* is considered to be strongly linked with FC degradation. At high *FU*, the partial pressure of fuel can locally be close to zero due to the dilution of reaction product. In such case of local fuel depletion and high water vapour concentration, the fuel atmosphere is no longer reductive, leading to a local

reoxidation of the nickel anode. Moreover, this phenomenon can easily occur in low-loading situations where the fuel flow is kept at a low level to meet the requirement of constant fuel utilisation. Accordingly, C4 and C12 can be viewed as critical operating conditions which are harmful to the health of SOFC.

In addition, C10 and C11 represent commonly a high-temperature situation, especially in C11 where both T_f and FU are at their high level, which risks of accelerating the degradation of FC. In C10, the air utilization is high and the current density is low, which implies that the air flow rate is at a very low level. This condition is harmful for the stack in a large-scale system where the air flow should be kept at a relatively higher level than needed in order to remove the produced heat in the stack. Therefore, both of these two conditions are undesired.

b. The Total Wavelet entroPy (TWP) values:

Figure 4-12 demonstrates the evolution of the TWP values of the cell voltage signals along the shifting of the operating condition. The last 4 points at the end of each curve correspond to the TWP values in the 4 repetitions of experiments in the nominal condition. Among, the maximal one determines the height of the dash lines. It is easy to observe that for every cell, the TWP point at the harmful conditions (C4, C10, C12 and C11) goes beyond its criterion line.

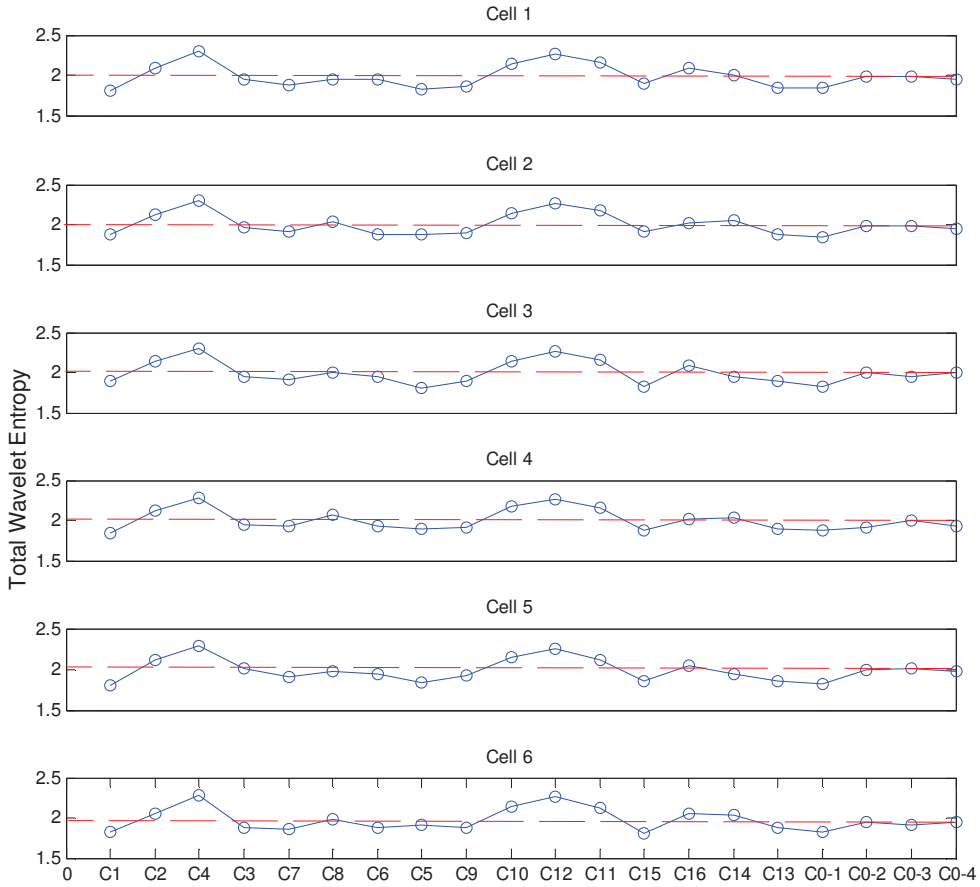

Figure 4-12 The TWP values in the bias and the nominal operating conditions for every cell

In addition, the value of TWP at C2 is also higher than the value obtained in the nominal condition. C2's qualitative description (see Table 4-2) implies that this condition may be related to the part-loading state of the system. Although this has no negative effect upon the FC, from the efficiency point of view, this operating condition is still undesirable for a power system. However, this aspect is out of the scope of our research.

Table 4-2 The operating parameters for C2

Condition	T_f	J	FU	AU
2	LOW	LOW	LOW	HIGH

c. The Relative Wavelet entroPy (RWP) values:

Figure 4-13 illustrates the varying process of the RWP values of the voltage signals with the shifting of the operating condition. These plots demonstrate that RWP is able to make prominent the critical operating conditions (i.e. C4 and C12).

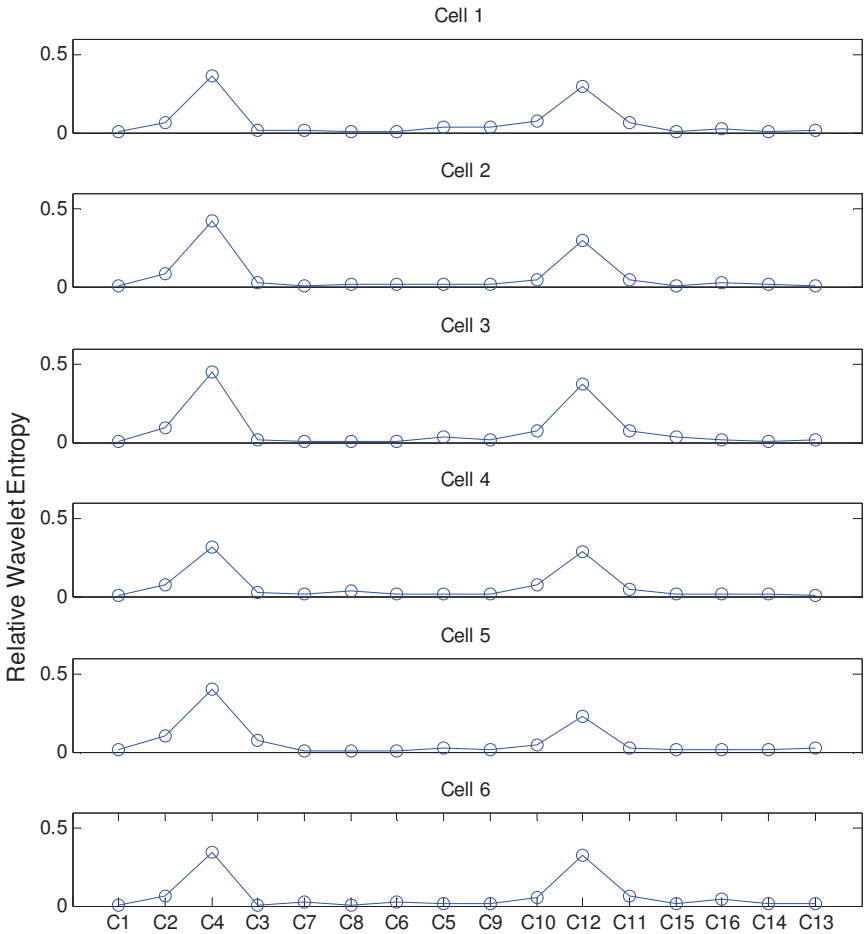

Figure 4-13 The RWP values of the voltage signals measured in the16 bias operating conditions for every cell

IV.5.3.2. For the 2nd group signals

The stack tested in the 2nd round experiment on the VTT's test bench experienced 16 bias operating points, plus the nominal one. The operating parameters' numerical values corresponding to these points are listed in Table 4-3 following the order of tests. Their qualitative values are the same as those considered in the 1st round experiment. So, we could pre-determine C4, C12, C10 and C11 to be undesired operating conditions beforehand. Then, we analyze the values of the indicative parameters extracted from the signals of this group in order to see if these parameters are able to reveal the abnormal operations on the FCs.

Table 4-3 Operating conditions for the 2nd test round in VTT (listed in the real condition shifting order)

Operating condition	T_f [°C]	J [A/cm2]	FU	AU
C0-1	760	0.3	0.5	0.235
C10	790	0.2	0.4	0.300
C6	730	0.4	0.4	0.300
C4	730	0.2	0.6	0.300
C16	790	0.4	0.6	0.300
C0-2	760	0.3	0.5	0.235
C1	730	0.2	0.4	0.170
C13	790	0.4	0.4	0.170
C7	730	0.4	0.6	0.170
C11	790	0.2	0.6	0.170
C0-3	760	0.3	0.5	0.235
C9	790	0.2	0.4	0.170
C2	730	0.2	0.4	0.300
C8	730	0.4	0.6	0.300
C15	790	0.4	0.6	0.170
C0-4	760	0.3	0.5	0.235
C12	790	0.2	0.6	0.300
C3	730	0.2	0.6	0.170
C5	730	0.4	0.4	0.170
C14	790	0.4	0.4	0.300
C0-5	760	0.3	0.5	0.235

a. The RWE values

According to the RWE values shown in Figure 4-14, we can see that the distribution of the wavelet energy in the voltage signals of the mixture gases-fuelled SOFC cells also follows a regularly decreasing rule when the stack is operated in the nominal condition. By comparison, we can pick up 5 bias operating conditions in which the cell signals' RWE distribution looks abnormal. They are the pre-determined undesired/critical operating conditions (C4, C12, C10 and C11) and C1. The later is meant to a part loading condition of system (refer to the values of the operating parameters given in Table 4-4). Since only short stacks are studied in this

research, we put the emphasis onto the recognition of the critical operating conditions, that is, C4 and C12.

Table 4-4 The qualitative value of the operating parameters in C1

Condition	T_f	J	FU	AU
1	LOW	LOW	LOW	LOW

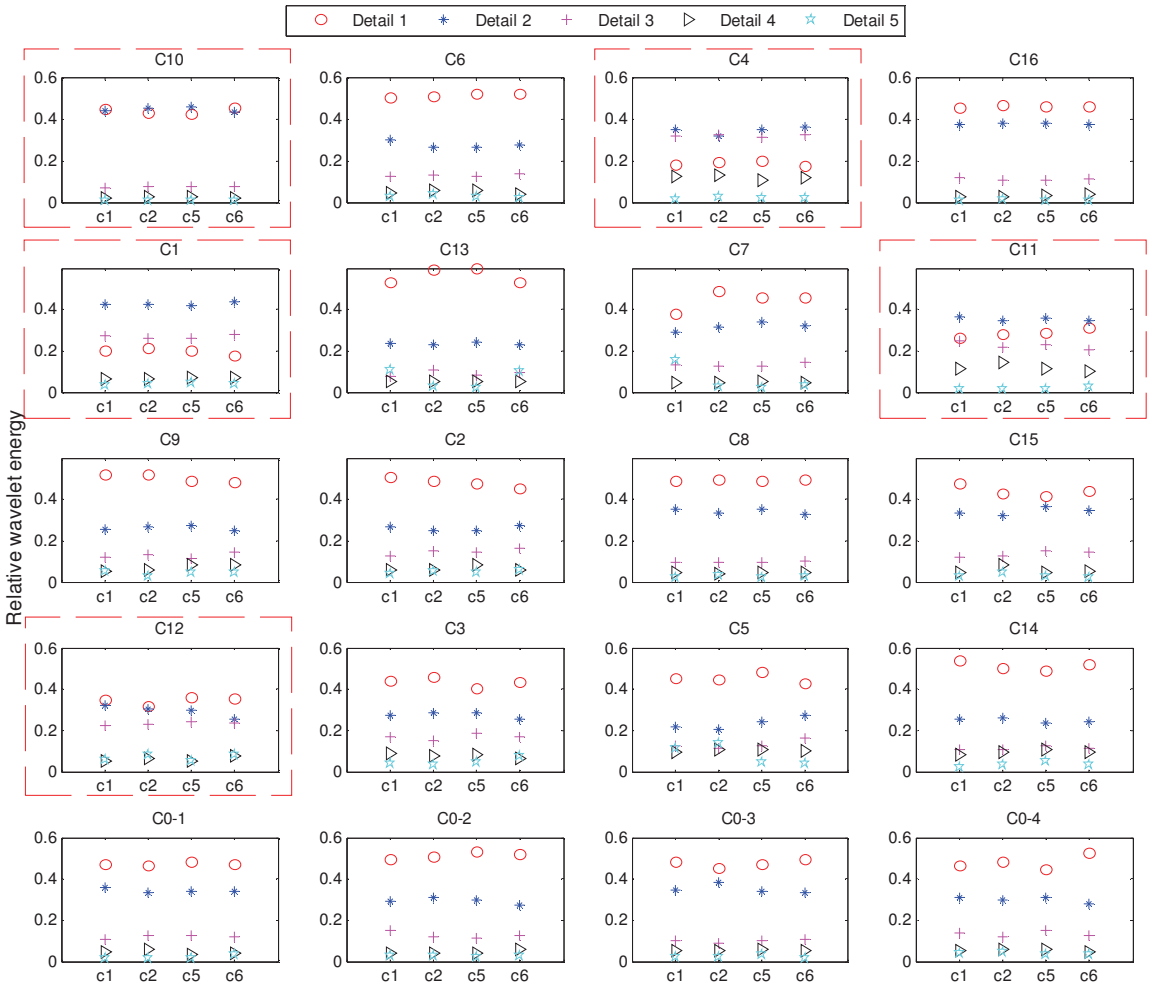

Figure 4-14 The RWE values of the good-state cells' signals (c1, c2, c5 and c6) under different operating conditions

b. The TWP values

The TWP values for each of the good-state cells under different operating conditions are calculated and given in Figure 4-15. From the last four points of each curve, we can see that in this test, the cells' TWPs in the normal operating condition (C0) are not as stable as in the 1st round test (refer to Figure 4-12). A dash line is plotted for each curve to indicate the maximal value of TWP in C0. We can obverse that for each cell, the points that locate above

this line are different. Especially for the Cell 6 where the majority of the TWP values are higher than this threshold, it is unreasonable to say that the operating conditions relevant to these values are all unsuitable for this cell. Hence, we conclude that the TWP is not representative and indicative to the abnormal operating condition of the SOFC stack tested in the 2nd round test where emulated reformed natural gas was provided as the fuel.

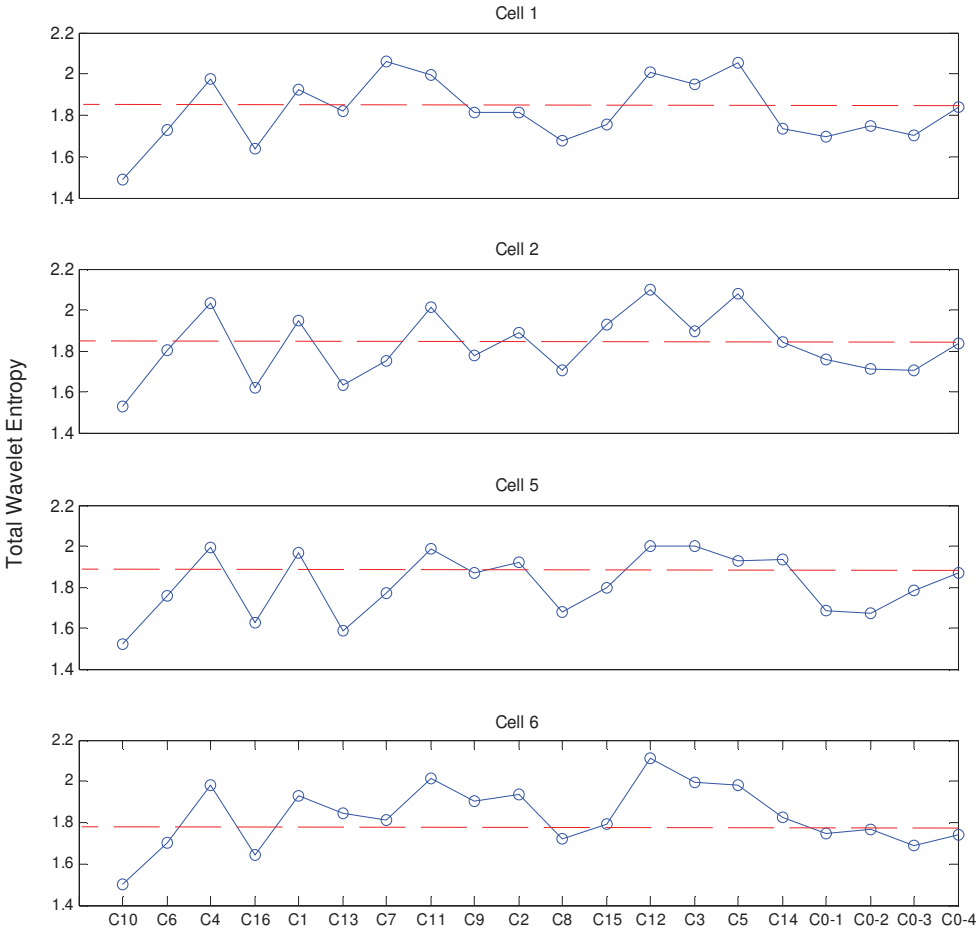

Figure 4-15 The TWP values for the good state cells under different operating conditions

c. The RWP values

For the 1st group signals, we have seen that RWP is a perfect indicator to the critical operating conditions C4 and C12. However, for the 2nd group signals, the indication of this parameter is not enough straightforward. As illustrated in Figure 4-16, the critical conditions that the RWP indicates for Cell 1 are differing from those for other cells.

Focusing onto the distributions of RWE of the signals (re-see Figure 4-14), we can observe that the details of the first 3 levels take up the biggest part of the wavelet energy. By contrast, the energy contained in the details of the other levels is relatively insignificant. It means that the detail subsignal 4 and 5 may not contain useful information on the state of FC and therefore should not be taken into account in the RWP value's calculation. Otherwise, they might influence the real value of RWP. For example, in C7 (see Figure 4-14), the RWE of the

5th detail subsignal of the Cell 1 is unreasonably higher than those of the other cells, which decreases the RWE of the detail subsignals of the 1st and the 2nd level. This phenomenon can also be found in the signals of Cell 1 and Cell 2 when operated in C5. Accordingly, it is necessary to re-compute the RWP for each signal by only considering the details of the first 3 levels.

Figure 4-17 illustrates the optimized RWP values. This time, the RWP effectively differentiates the critical conditions C4, C1, C11 and C12 from other moderate bias operating conditions. However, it is not capable of indicating the C10 (which has been pre-determined as one of the critical operating conditions).

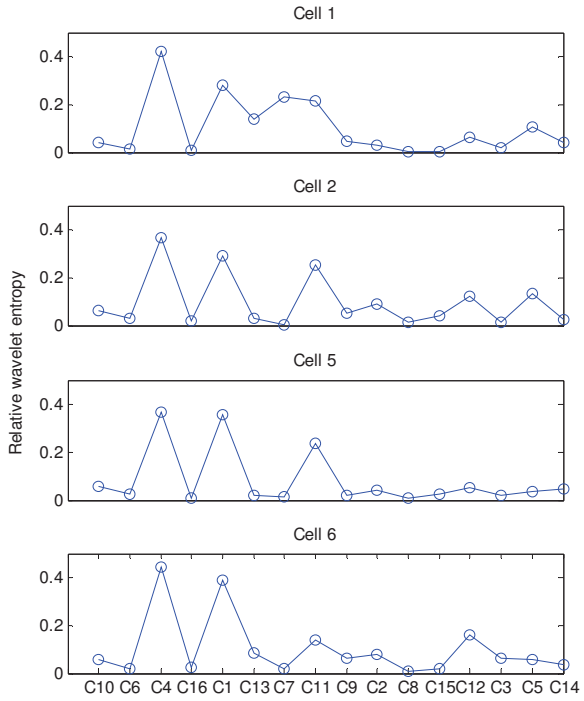

Figure 4-16 The RWPs in the 16 bias conditions (5 details)

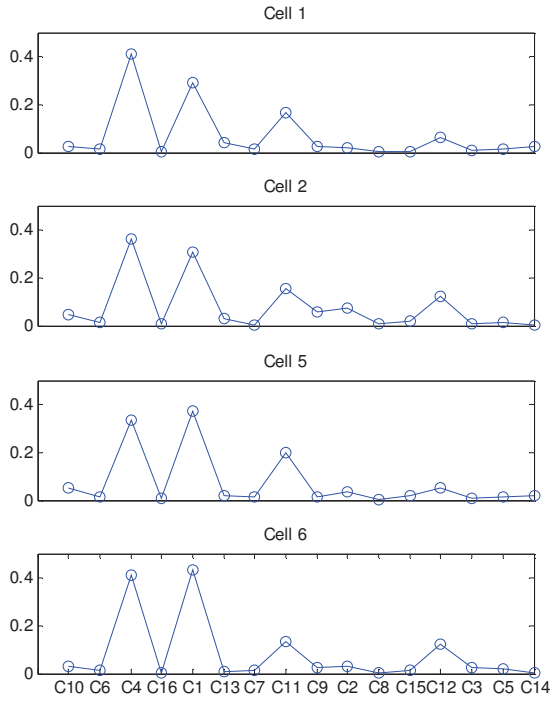

Figure 4-17 The RWPs in the 16 bias conditions (3 details)

IV.5.3.3. For the 3rd group signals

The 3rd group signals describe the performance of a broken cell in different operating conditions. Figure 4-18 gives the polarization curve of the cell when it was in a good state and operated at the nominal point, as well as 4 polarization curves measured after the cell was broken. They illustrate the cell's degradation procedure.

The polarization curve in C0-3, measured when the system returned the third time to the nominal condition, reveals a performance recovery phenomenon in the cell. (For comparing, the slope of the curve in C0-2 is up to 250 mΩ while decreases to 50 mΩ in C0-3). This may be attributed to the positive effect of some moderate bias operating condition that the cell had experienced before the operating condition was reset to the nominal one.

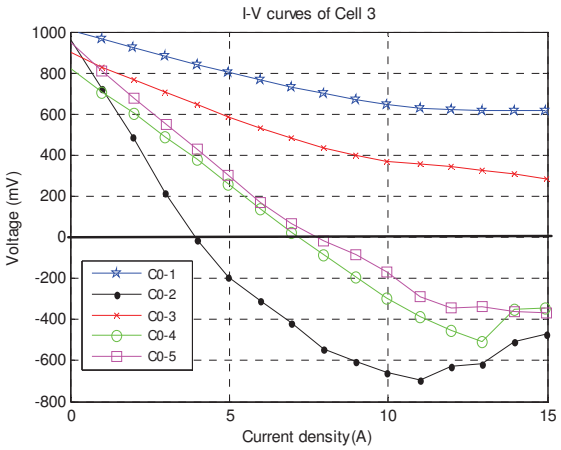

Figure 4-18 The polarization curves of Cell 3 in the 5 repetitions of the nominal condition

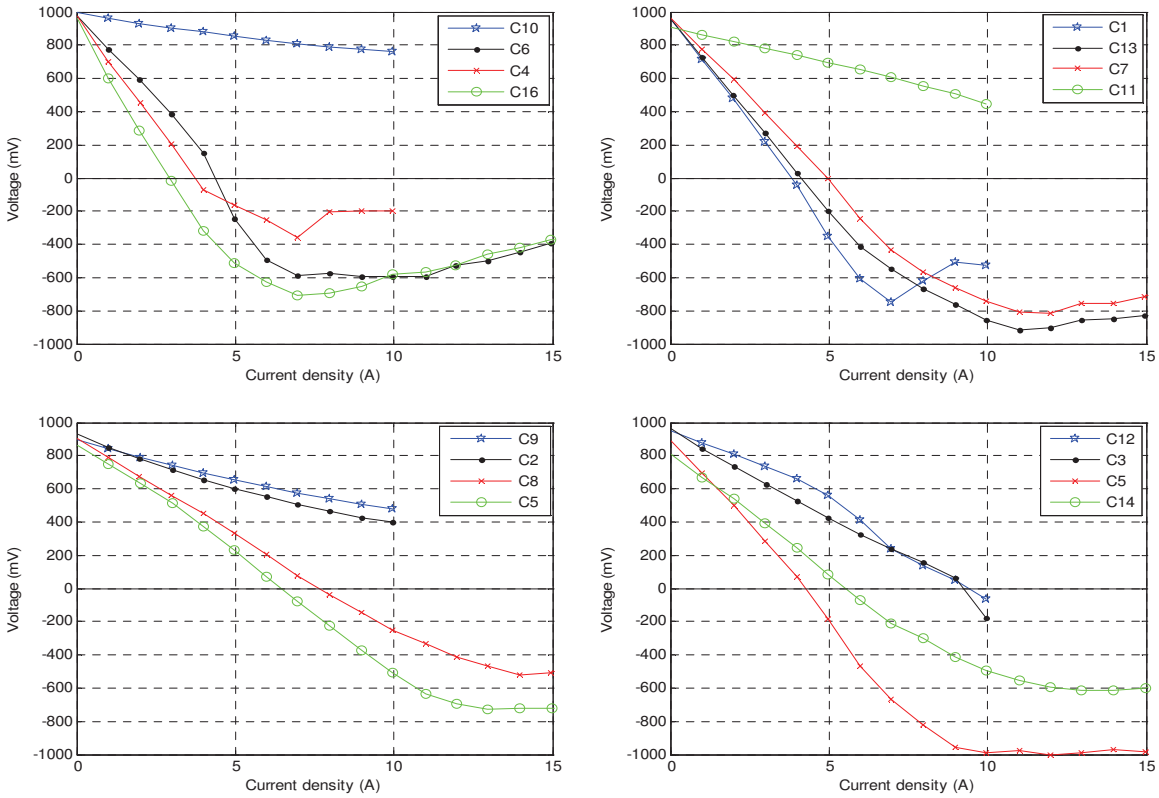

Figure 4-19 The polarization curves of the Cell 3 measured when the operating condition (load current excluded) was set at each of the bias operating points

Figure 4-19 gives the polarization curves measured while the operating condition was set at each of the bias operating points. It shows that the cell was broken after C10. The 4 operating conditions that were tested between C0-2 and C0-3 are C1, C13, C7 and C11. In Figure 4-19, we can see that the slope of the polarization curve in C11 is much smaller (about 25 mΩ) than those in other conditions (which are above 200 mΩ), implying that the cell is partly recovered. In addition, after C11, the cell's performance had been staying in a recovered state in C9 and C2 until the operating condition was shifted to other points. However, the reason to explain such a temporal recovery is unknown.

The Cell 3's voltage signals in the investigated operating conditions are sequentially shown in Figure 4-20. Their RWE, TWP and RWP values are given and analyzed in the following paragraphs.

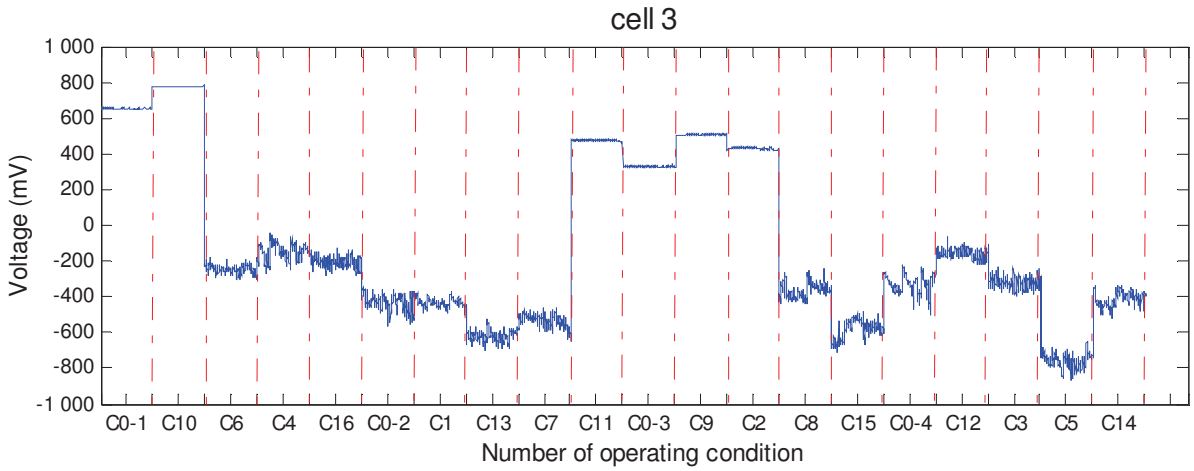

Figure 4-20 The voltage signals of the Cell 3 in the different operating conditions

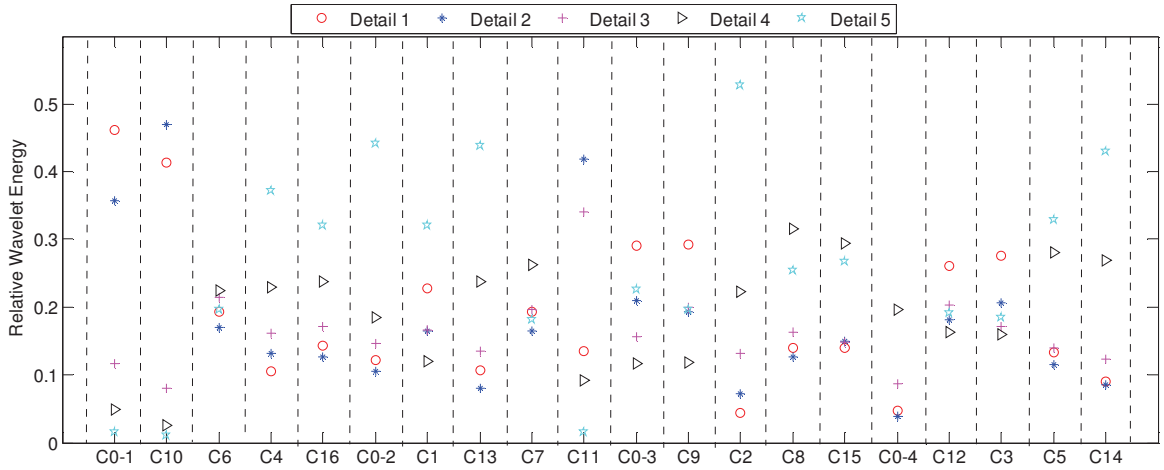

Figure 4-21 Distribution of wavelet energies in the Cell 3's voltage signals for the different operating conditions

a. The RWE values

The RWE values of the studied signals are illustrated in Figure 4-21. We can observe that the distributions of wavelet energy of the signals in C0-1 and C10 are identical to those of the good-state cell. In other words, the RWE values indicate that at the beginning when the cell was operated in these two conditions, it was at the good state of health. This indication is in accordance with the fact demonstrated by the polarization curves in Figure 4-19. Moreover, the RWE values demonstrate that from C6, the wavelet energy distribution in the voltage signals becomes greatly disordered. This suggests that the cell was operating abnormally. However, it is not possible to confirm the type of fault (system fault or FC failure) according

to the RWE values. To solve this problem, we can calculate the TWP value of the signals in order to quantitatively analyze the wavelet energy's distributions.

b. The TWP values

Figure 4-22 gives the TWP values of Cell 3's signals. For comparison, the TWP points of the Cell 1's signals are plotted in the same axes as well. The horizontal dash-dot line indicates the TWP value of the cell 3' signal when it was in a good state and operated in the nominal condition (C0-1). We can see that, except for C10, all of the TWP points of the Cell 3 for the other bias conditions locate above this reference line. In addition, they are higher than the TWP points of the good-state cell, i.e. the Cell 1, except for C11 where the health of Cell 3 was partially recovered. Nonetheless, it is still hard to quantitatively differentiate the system fault, that is, the improper operation from the cell failure by TWP.

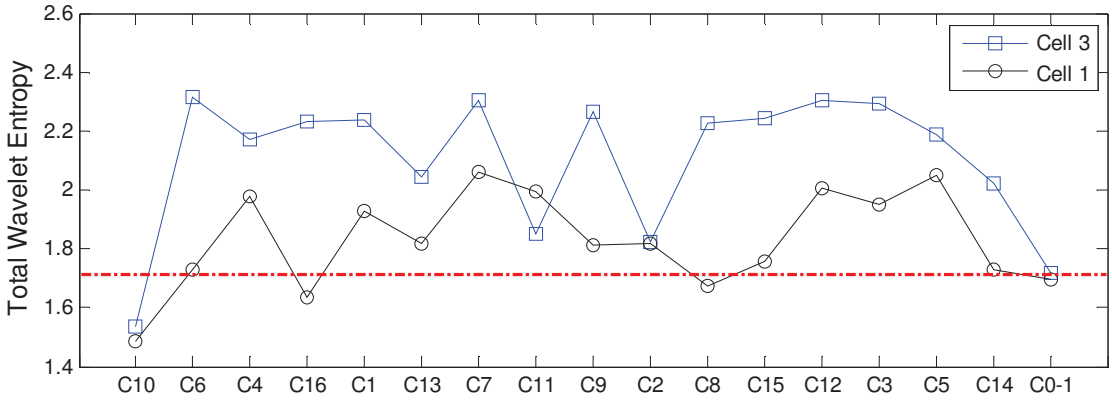

Figure 4-22 The TWPs for the degraded cell (Cell 3) and the good-state cell (Cell 1) in the different operating conditions (5 details)

c. The RWP values

In Figure 4-23, the RWP values of the signals for both Cell 3 (the broken cell) and Cell 1(the good cell) are illustrated in the same axes. We can observe that in all the operating conditions that Cell 3 experienced after C10, the RWP points of Cell 3's signals are all higher than those of Cell 1's. Their values are generally greater than 0.5. As for C10 in which Cell 3 remained in a good state of health, its signal's RWP is identical to that of Cell 1's.

Additionally, in C0-3 where the polarization curve of Cell 3 demonstrates that the performance of this cell was partially recovered, the RWP value is greatly smaller than in C0-2 and C0-4 for which the cell was severely damaged.

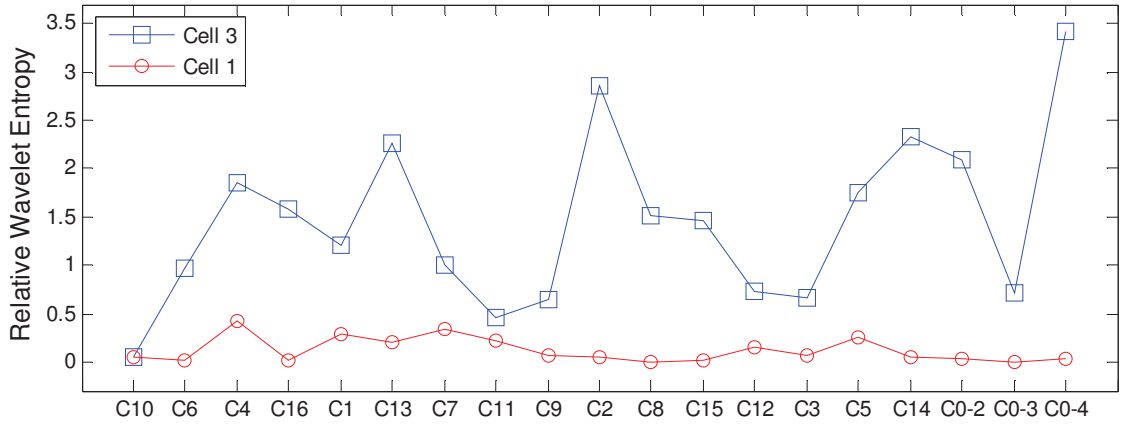

Figure 4-23 The RWPs for the degraded cell (Cell 3) and the good-state cell (Cell 1) in the different operating conditions (5 detail subsignals considered)

Looking back to the raw signals of Cell 3 shown in Figure 4-20, it is easy to find that the amplitudes of the fluctuations in the negative signals are obviously larger than those in the positive signals. If this phenomenon is related to the nature of the voltage sensor, a question should be considered: is the perturbation in the sensor or the state of the FC that the RWP really reflects? Since our aim is to diagnose the early fault of FC which usually contributes to reducing the voltage rather than reversing, it is necessary to further validate the indicative capability of RWP to the state of health of the cell whose voltage remains positive.

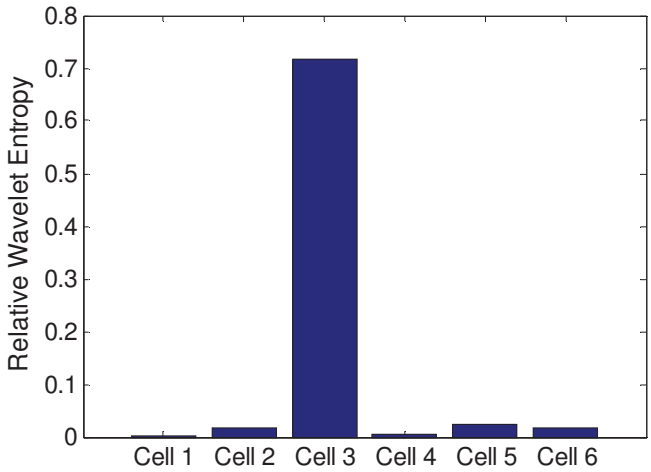

Figure 4-24 The RWP values of the 6 cells' signals measured in C0-3

To meet this requirement, a comparison between the good-state cells' and the degraded cell's signals in C0-3 is made (because the Cell 3's signal in C0-3 is positive and does not have obvious large-amplitude voltage fluctuations). The RWP values of these signals are illustrated in Figure 4-24. Comparing to the good-state cells, the RWP of the broken cell's signal is one order of magnitude greater, up to 0.7. Therefore, this parameter is indeed able to differentiate the state of health of SOFC.

IV.5.3.4. For the 4th group signals

The voltage signals in the 4th group are shown in Figure 4-25. All of them were measured on a 3-cell SOFC stack for the same operating condition. From the polarisation curves showed in Figure 4-26, we can see that this stack had progressively degraded during the experiment.

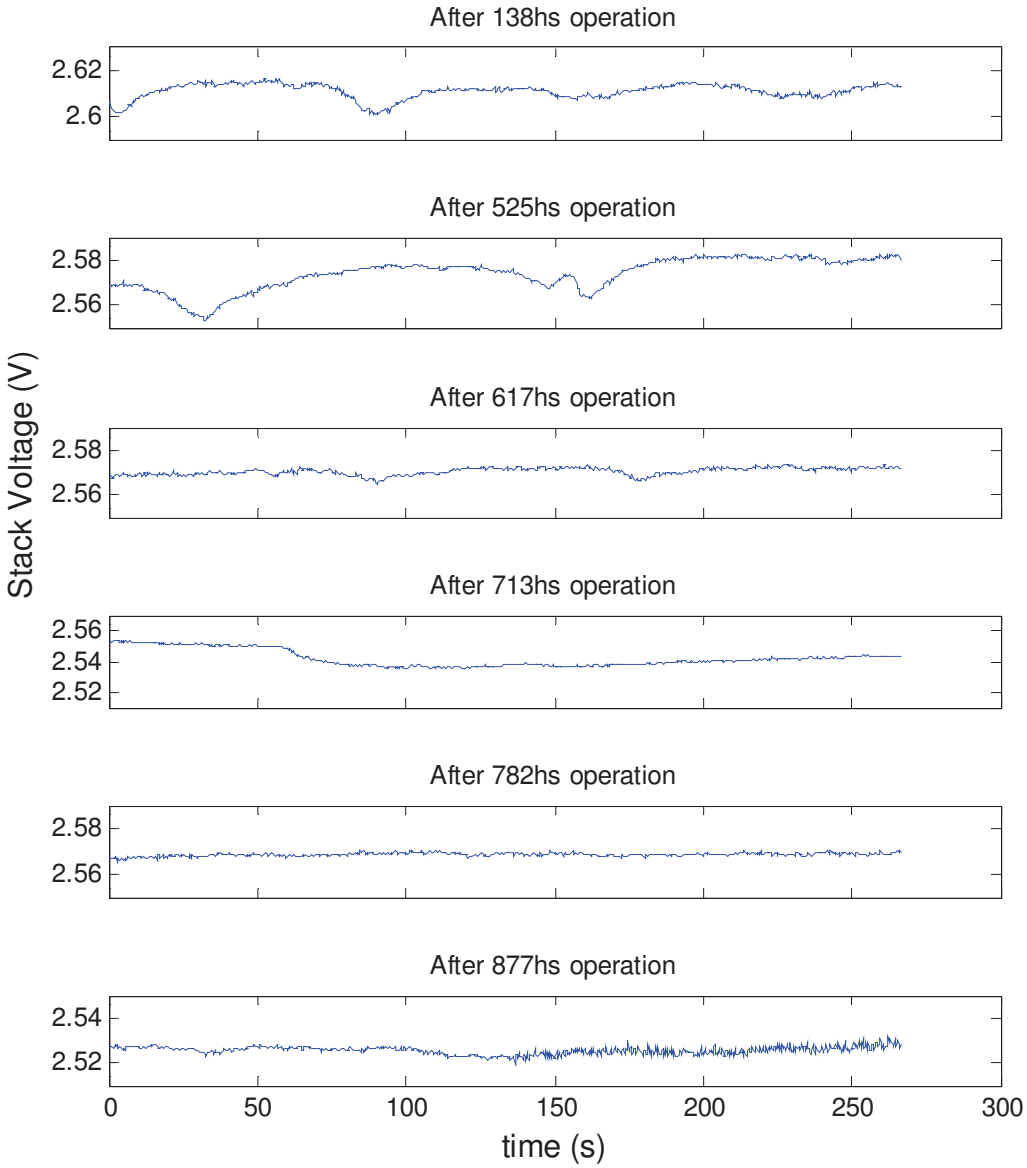

Figure 4-25 The voltage signals of a progressively degraded SOFC stack measured at different time when operated in an specific condition (T_s=770°C and I=6A).

The RWP values of these signals are calculated through treating the first signal as the reference. They are plotted along the measurement time and shown in Figure 4-27. We can find that the evolution of the RWP value follows an increasing trend which is similar to the degrading process of the stack that is implied by the polarization curves shown in Figure 4-26. Accordingly, we can conclude that RWP is an effective indicator to the state of health of the SOFC stack.

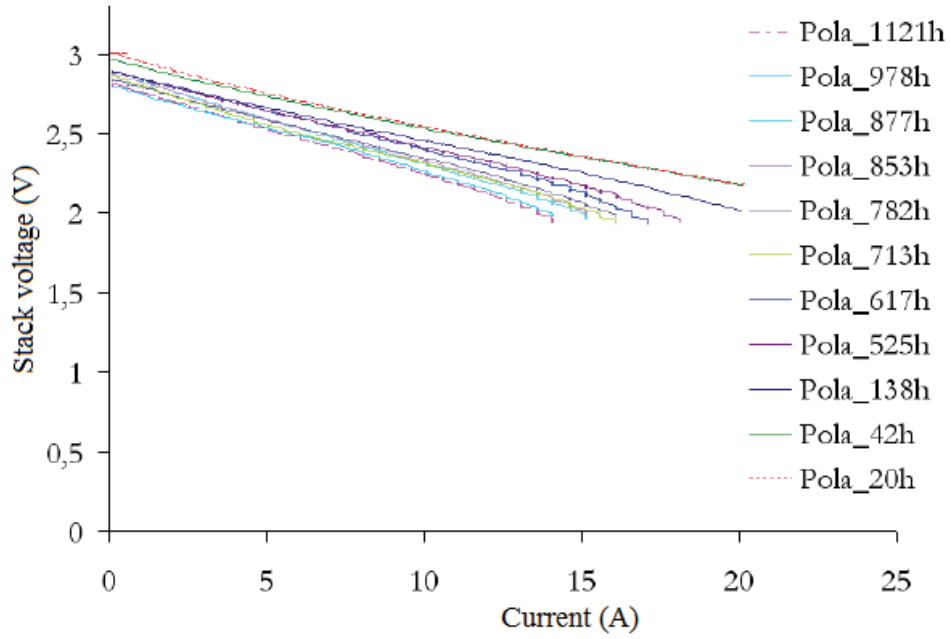

Figure 4-26 Polarization curves of the SOFC stack

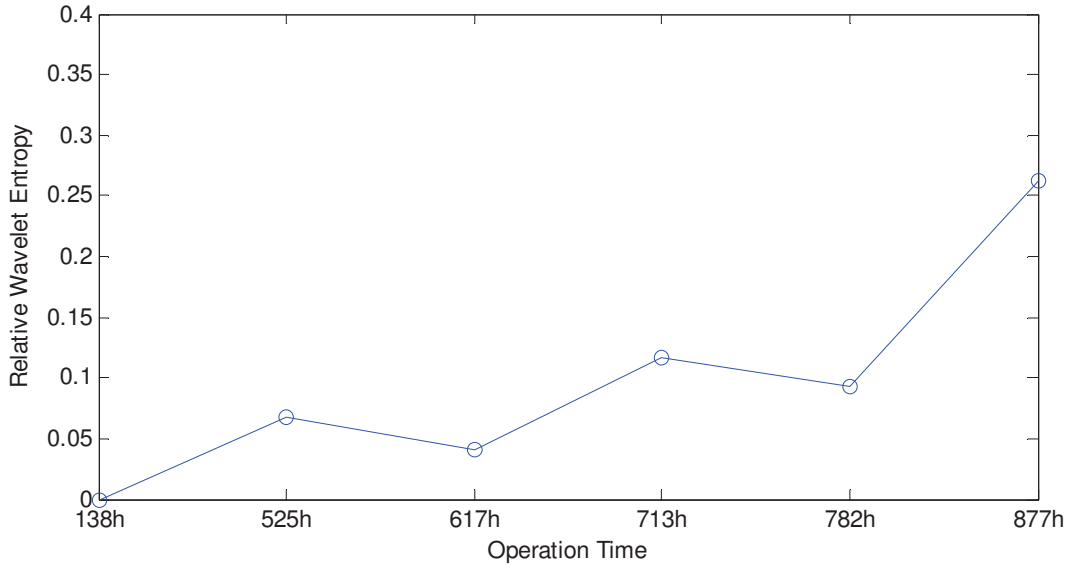

Figure 4-27 Evolution of the RWP value of the degraded stack's voltage signal

IV.6. Conclusion

In this section, the WT based diagnostic method was introduced and used on 4 groups of signals with the purpose of studying its application in the fuel cell system diagnosis. Three parameters (RWE, TWP and RWP) were extracted from the signals and analyzed in order to validate their capability of indicating the operating condition as well as the state of health of SOFC.

For the 1st group of signals, through comparing the energy distribution (described by RWE values) of the signals in the bias operating conditions and those in the nominal operation, 4 conditions were picked up and viewed as undesired operating conditions. Among them, 2 critical ones could be effectively indicated by the signal's RWP value. Numerically, the TWP permits to distinguish all of the 4 deprecated conditions from the tolerant ones. However, this parameter is less discriminative than the RWP. Then, the capabilities of the RWE and the TWP to indicate undesired operating conditions are also validated by the 2nd group signals, which demonstrates that the investigated WT based diagnostic method is generic for different SOFC systems (in our case, the 1st and the 2nd group signals are from two different experiments on the same test bench. The difference of the experiments is that one used pure hydrogen as the SOFC's fuel while the other used emulated reforming gases). However, for the 2nd group signals, the significant frequency band is only restricted to the frequency range between 1/8Hz and 1Hz, instead of the range [1/32, 1] Hz as for the 1st group signals. It was found that over the later frequency range, the RWP values were not discriminative for differentiating the undesired operating conditions from the normal/tolerant ones. Consequently, before carrying out the diagnosis, it is important to analyze and precisely determine the significant frequency band that is relevant to the fault.

The 3rd and the 4th group signals were used to validate these 3 parameters' capability of indication to the damaged or degraded SOFC/stack. Through comparison, we conclude that the RWP is the most effective indicator for the state of health of SOFC. It permits not only to find out the damaged cell in a SOFC stack but also reflect the degrading process of a stationarily operated SOFC.

Finally, by comparing the results of analysis on the 2nd and the 3rd group signals, 2 threshold values (i.e. 0.05 and 0.5) could be yielded to divide the RWP values into 3 classes, each of them indicating the state of health of the SOFC, that is:

1) Normal operation for the interval [0, 0.05];
2) Abnormal operation for (0.05, 0.5];
3) Stack broken for (0.5, ∞).

In this diagnostic method, RWE mainly serves for the analytical phase, helping confirm if the measured signal contains useful information on the state of SOFC and determine the significant frequency band relevant to the fault.

As for TWP, although it is not as effective as RWP for fault indication, this parameter is able to reflect the deviating process of the operating condition from the nominal/desired operating point. It is thus useful for tracking the variation of the system operation.

Chapter V Bayesian network based algorithm for SOFC system online diagnosis

For a FC system, generally, the operating point of the system is characterized by a series of input variables of the FC stack, such as the load current density, the furnace temperature (for short stack), the fuel and air flow rates, etc. The measurement on these variables can provide information useful for checking the current operating condition of the system. Hence, in most cases, the system monitoring is implemented by relying on the specific sensors pointing to their measurements. However, in some cases such as gas leakage in the inlet manifold of FC, the sensor may not be able to detect the problem if it is located in the upper stream of the faulty location.

Under the concept of using the FC stack as a sensor for the system diagnosis, the FCs' outputs are considered being able to reflect the actual operating state of the system. When a system-level fault occurs, the operation for the FC stack will deviate from the nominal condition, which leads to abnormal FC responses.

In Chapter 4, the wavelet transform based diagnosis algorithm has been validated being able to recognize the normal and the abnormal responses of FC and giving the location of fault (in the BoP part or in the FC itself). However, it cannot provide more detailed information on the state of the system such as the operating parameters so that the engineers could determine relevant remedial measures.

To solve this problem, it is necessary to develop an intelligent meta-model capable of mapping the FC response to the corresponding input such that we could obtain an insight on the current system operating condition.

For complex systems (such as fuel cell systems), an analytical model is often not available or is too complex to be used in diagnosis. Such systems are currently supervised by a human operator who has to find the fault by means of his experience about the process behaviour. Such experience does not refer to quantitative measurements but includes assertions about operating conditions or sequences of operating points, which can be represented by sequences of symbols. Typically, process diagnosis uses alarm messages rather than numerical measurement data [Lunze'02]. Consequently, from a diagnosis point of view, it will be more

useful if the model could provide qualitative information on the operating parameters rather than numerical value. Thus, discrete Bayesian network approach was selected in this research for the model establishment.

In this chapter, the theory of Bayesian approach will be firstly introduced. Then, we will talk about how to use a Bayesian model to solve diagnosis problems. For the application, a Bayesian network (BN) based meta-model will be built and then tested by using two groups of experimental data, respectively. The results will be given and analysed at the end.

V.1. Introduction to Bayesian network (BN) and Bayesian approach

A BN model can serve for two different applications, either as a knowledge basis or as a reasoner; the former encodes what we know while the later acts on the knowledge basis to answer queries of interest [Darwiche'09]. As a knowledge base, BN is usually used for prediction, calculating the probability of the results given a cause; in contrary, for reasoning purpose, it is used as a diagnostic support to infer the corresponding cause as a symptom is observed. Note that the reasoning process requires the prime knowledge base acting as speculative foundation.

For diagnosis purpose, the BN model serves as a reasoner and its construction leads thereby to two targets: 1) build a knowledge base about the input-output causal relationship of the studied entity and 2) enable automated reasoning.

V.1.1. Configuration of BN

A BN is a representational device that is meant to organize one's expert knowledge on a particular aspect of the studied problem. It relies on the basic awareness that the independence forms a significant aspect of beliefs and that it can be interpreted relatively easily using the language of graphs [Darwiche'09]. It consists of two components as shown in Figure 5-1, one qualitative and another quantitative. The former, shown as a directed acyclic graph (DAG), corresponds to the structure of BN, demonstrating the features/variables of interest (represented by nodes) and conveying information about the causalities between them (represented by arrows). The arrow from X1 to X2, for example, implies a direct causal influence of X1 on X2; thereby, we say that X1 is a parent of X2 and conversely, X2 is a descendant of X1. The quantitative part, known as conditional probability tables (CPTs), quantifies these causal relationships by conditional probabilities (CPs) derived from a sample dataset. The CP measures the probability in the occurrence of a certain event when knowing its relative event(s) has (have) happened.

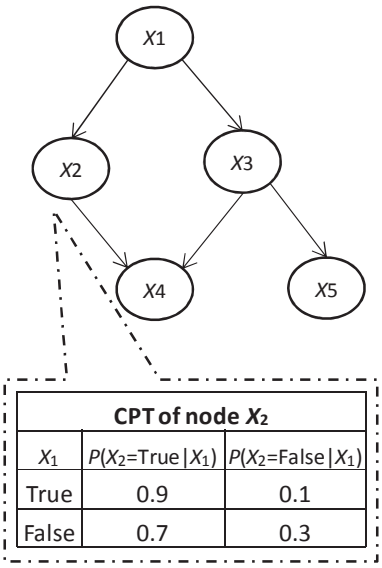

CPT of node X_2		
X_1	$P(X_2=\text{True}\|X_1)$	$P(X_2=\text{False}\|X_1)$
True	0.9	0.1
False	0.7	0.3

Figure 5-1 An example of Bayesian network

Taking the Figure 5-1 as an example, the CPT for variable X2 provides the probability of each value of X2 and every instantiation* of its parent X1. For example, Pr(X2=True|X1) denotes the probability of occurrence of the event that X2 is true when having known the value of X1. For Boolean variable, it must have

$$\Pr(\mathrm{X2}|\mathrm{X1}) + \Pr\left(\overline{\mathrm{X2}}\middle|\mathrm{X1}\right) = 1. \qquad \text{Eq. 5-1}$$

This equation implies that when X1 happens, there are only two possible values for X2.

In fact, CPTs are consequence of BN parametrization. Hence, BN is usually mathematically represented by a pair (G, Θ), where G denotes a DAG and Θ is a set of CPTs for each variable/node. We also use $\theta(\mathrm{X}|\mathbf{U})$ to denote a single CPT that lists CPs between a variable X and its parents **U**. Note that the size of a CPT is exponential in the number of parents **U**.

V.1.2. Baye's theory

With a BN, if a cause is given, it is easy to infer the possible effect(s) by following in a top-down way the causal chains defined in the DAG and then to ascertain the most possible value for it/them based on computed conditional probabilities. In another case, however, where a mediated event like X2 in Figure 5-1 for example, instead of the primary cause, is given, we may also consider X5 as an effect other than X4. The reason is that having known X2 = true (X2 happens), we trust that X1 has very likely happened and thus following the chain X1 → X3 → X5, it is "reasonable" to consider that X5 is possible to occur. Such a prediction involves a reasoning behaviour from X2 to X1, which leads to calculating Pr(X1|X2); yet the CPTs provide only causal conditional probabilities while the inverse ones are unknown. Bayes' theorem allows us to implement this calculation. It is defined as follows:

* An assignment of values to a network variable is called an instantiation of a variable..

Given two events E and F such that Pr(E)≠0 and Pr(F)≠0,we have

$$\Pr(E|F) = \frac{\Pr(F|E)\Pr(E)}{\Pr(F)} \text{ or } \Pr(F|E) = \frac{\Pr(E|F)\Pr(F)}{\Pr(E)} \quad \text{Eq. 5-2}$$

These formulae imply that Bayes' theorem supports both causal (top-down) and evidential (bottom-up) reasoning. However, the common usage of Bayes' equation is when the event E is perceived to be a cause of the event F because the belief in an effect given its cause, Pr(F|E), is usually more readily available than the belief in a cause given its effect, Pr(E|F).

It is worth noting that in BN, both Pr(E|F) and Pr(F|E) are the **subjective probabilities** instead of the relative frequency of the occurrence for an event. According to the probability theory, the relative frequency is computed with a subset of data which is randomly sampled from the complete outcome population. For example, in a trial of flipping a two-sided coin, there are two possible outcomes, "head" and "tail'. Repeating this trial 1000 times, the obtained 1000 outcomes must include "heads" as well as "tails". Differing from this example, for an improperly operated SOFC, the eventual faults that may occur are usually unknown. In one experiment, there might be 4 events/symptoms that could be observed while in another identical experiment, there might be 7. Neither of the outcomes yielded from these two identical experiments is able to represent the outcome population. For this case, the probability of an event that is computed with the data from one of the experiments expresses actually the **degree of belief** in the occurrence of the event for this individual experiment. In BN, it is this kind of probability that is used to measure individualistic uncertainty.

When we collect the data from a test on a FC system, the values for FC input will not be randomly sampled from a population in statistics; rather we design the tests so as to let FC operate in specific operating conditions, because the test's objective is to obtain the corresponding output space given an input of interest. For this case, the relative frequency is not available to depict the occurring probability of a specific output.

Fortunately, BN meta-model can address this circumstance. It describes a subjective probability distribution based on a careful analysis of the situation, such like a physical model which is usually built under a series of pre-defined assumptions. Just because of this, BN is quite attractive in the case that the experiment is designed for a specific purpose. Finally, it is worthy to note that even if the probabilities in a BN are not the actual relative frequencies but the estimates, a CPT can be still obtained from relative frequency data [Neapolitan'03].

V.1.3. Inference based on BN

Consider a situation where there is an entity characterized by a group of features, and where some of these features have a direct influence on the others. For example, in our research, the SOFC is the studied entity, its operating point is interpreted by a set of feature parameters, i.e. the operating variables (the input of SOFC, e.g. current density, gas and air flow rates, furnace temperature, input flow pressure, etc) and the FC response variables (the output of SOFC, e.g. voltage, output flow pressures, stack temperature, etc.). Among, some of the operating

variables have direct influence on the responses while others have indirect influence. Moreover, some output variables of the FC possess also direct influences on other outputs in an uncertain domain. For example, the furnace temperature could determine the stack temperature while the later is one of the important factors capable of determining the FC's output voltage. So, the furnace temperature possesses an indirect effect upon the FC performance through the stack temperature.

We wish to determine the actual state of this entity referring to the measurements of these variables, whereas some measurements are not reliable. In this situation, we would set up a BN and use Bayes' theorem to make a probabilistic inference for the states of uncertain variables, relying on the certain ones. Essentially, this activity aims to obtain the marginal probability distribution (MPD) for a subset of network variables. The MPD can be viewed as a projection of the joint distribution on a smaller set of variables [Darwiche'09].

In the field of statistics, given a sample space for a set of independent random variables, we could translate it to a joint probability distribution (JPD) of events. Conditioning on a given state of a variable, this JPD should be updated because the awareness on this variable may decrease our belief in some events whereas increase that in others. Such updated JPD is known as a posterior probability distribution. As shown in the last column of Table 5-1, the probability for each instantiation is modified based on the joint probabilities listed in the third column, given the new information "Y1 is true". Owing to this information, our belief on the instantiation No.3 is greatly increased while at the same time, we believe that the instantiations No.5 to No.8 are not possible to happen for sure.

Table 5-1 An example of a JPD

Instantiation	Y1	Y2	Y3	Pr(.)	Pr(.|Y1=TRUE)
1	TRUE	TRUE	TRUE	0.056	0.236
2	TRUE	TRUE	FALSE	0.017	0.072
3	TRUE	FALSE	TRUE	0.163	0.688
4	TRUE	FALSE	FALSE	0.001	0.004
5	FALSE	TRUE	TRUE	0.615	0
6	FALSE	TRUE	FALSE	0.067	0
7	FALSE	FALSE	TRUE	0.009	0
8	FALSE	FALSE	FALSE	0.072	0

In practice, however, the interesting variables are not always independent. Instead, one variable may have an effect upon one or several variables. Indeed, Bayesian network is favourable to model the causal relationship between the variables. It is not impossible but inefficient to represent the causal relationship between all the information of the specific

domain in real world [Hwang'11]. Therefore, in a BN, the variables are supposed to be conditionally independent, under which the JPD for the network instantiation z can be obtained by multiplying all network parameters that are compatible with z, as the following definition:

Given a Bayesian network (G, $\boldsymbol{\Theta}$), over a set of n random variables, X={X_1, X_2, …, X_n}, the joint probability for a network instantiation z=(x_1, x_2, …, x_n) is given by

$$\Pr(X_1 = x_1, X_2 = x_2, \dots, X_n = x_n) = \prod_{i=1}^{n} \Pr\left(X_i = x_i \middle| X_j = x_j \text{ for each } X_j \text{ which is a parent of } X_i\right) \quad \text{Eq. 5-3}$$

Each multiplication factor at the right side of Eq. 5-3 can be determined with the help of DAG and their value can be found in one of the CPTs. This formula is based on the chain rule and the conditional independence in probability theory. The independence is the underlying assumption of Bayesian network. It is particularly important to Bayesian inference and usually used in three cases: in a BN,

1) If two nodes X_1 and X_2 are independent of each other, we have

$$\Pr(X_1 , X_2) = \Pr(X_1) . \Pr(X_2) \quad \text{Eq. 5-4}$$

2) If two nodes have the same immediate parent node(s), for instance, there is a chain X_4 ← X_3 → X_5, they are conditionally independent given the state of the direct parent node, i.e.

$$\Pr(X_4|X_3 , X_5) = \Pr(X_4|X_3) \quad \text{Eq. 5-5}$$

3) For any non-descendant node, it is conditionally independent of its non-direct parent nodes given the states of all its direct parent nodes. For the example in Figure 5-1, we can have

$$\Pr(X_4|X_1 , X_2 , X_3 , X_5) = \Pr(X_4| X_2 , X_3) \quad \text{Eq. 5-6}$$

Given a joint distribution of a set of variables X={X_1, X_2, … , X_n}, the MPD over a subset of X, i.e. X'={x_1, x_2, … , x_m} where m ≤ n, can be obtained by summing the joint probabilities of all instantiations to the complementary set of X', that is, X"={x_{m+1}, x_{m+2}, … , x_n}, formulated by

$$\Pr (x_1, x_2, \dots, x_m) = \sum_{X_m, X_{m+1}, \dots, X_n} \Pr(x_1, x_2, \dots, x_n) . \quad \text{Eq. 5-7}$$

Take Table 5-1 as an example, we can obtain

$$\Pr(Y1 = \text{true}, Y2 = \text{true}) = \Pr (Y1 = \text{true}, Y2 = \text{true}, Y3 = \text{true})$$

$$+ \Pr(Y1 = \text{ture}, Y2 = \text{true}, Y3 = \text{false}) = 0.056 + 0.017 = 0.073$$

When being conditioned on a certain evidence *e*, the MPD, known as Marginal Posterior Distribution (MPD), is computed by the equation:

$$\Pr(x_1, x_2, \dots, x_{\mathrm{m}}|\mathrm{e}) = \sum_{x_{\mathrm{m}}, x_{\mathrm{m+1}}, \dots, x_{\mathrm{n}}} \Pr(x_1, x_2, \dots, x_{\mathrm{n}}|\mathrm{e}) \qquad \text{Eq. 5-8}$$

V.1.4. Parameterization of BN by data learning

The quantitative dependencies between variables are specified by a set of parameterized conditional probabilities which finally determine the JPD over all variables of BN. Given the BN structure, the goal of this part is to learn the set of parameters $\boldsymbol{\theta}$ of the BN from a database. The basic method of parameter learning from complete data is Maximum Likelihood (ML) parameter estimation.

Assume we have a data set $\boldsymbol{d}$ of N independent observations (samples) over m discrete variables $[\mathrm{X}_1, \mathrm{X}_2, \dots, \mathrm{X}_{\mathrm{m}}]$: $\boldsymbol{d} = \{S^{(1)}, S^{(2)}, \dots, S^{(N)}\}$ and $S^{(i)} = (x_1^{(i)}, x_2^{(i)}, \dots, x_m^{(i)})$. The likelihood of observing the given data set $\boldsymbol{d}$ equals to the product of the conditional probabilities of all the observations given the parameters $\boldsymbol{\theta} = \{\theta_1, \theta_2, \dots, \theta_m\}$:

$$\Pr(\boldsymbol{d}|\boldsymbol{\theta}) = \prod_{i=1}^{N} \Pr\left(S^{(i)}\middle|\boldsymbol{\theta}\right) \qquad \text{Eq. 5-9}$$

The parameters are unknown and we wish to estimate them from data. Given BN structure G, the ML learning focuses on the problem of estimating a single $\boldsymbol{\theta}$ which maximizes the likelihood $\Pr(\boldsymbol{d}|\boldsymbol{\theta})$. Equivalently we can maximize the log-likelihood:

$$\mathcal{L}(\theta) = \log \Pr(\boldsymbol{d}|\boldsymbol{\theta}) = \sum_{i=1}^{\mathrm{N}} \log \Pr\left(S^{(\mathrm{i})}\middle|\theta\right) = \sum_{i=1}^{\mathrm{N}} \sum_{j=1}^{\mathrm{m}} \log \Pr\left(x_j^{(\mathrm{i})}\middle|\theta_j, S_{\mathrm{PA}_j}^{(\mathrm{i})}\right)$$

$$= \sum_{j=1}^{\mathrm{m}} \mathcal{L}_j(\theta_j) \qquad \text{Eq. 5-10}$$

where $S^{(i)}{}_{\mathrm{PA}j}$ is the i-th observation of $\mathbf{X}_{\mathrm{PA}j}$, the parent variables of X_j. Each $\mathcal{L}_j$ can be maximized independently as a function of $\boldsymbol{\theta}_j$ [Ghahramani'03]. It is worthy to note that the likelihood function is positive while the log-likelihood function is negative. However, maximizing these two functions are equivalent. $\boldsymbol{\theta}_j$ is the conditional probability table for X_j given its parents.

The distribution of conditional probability estimate $\boldsymbol{\theta}_j^k$ for the k-th instantiation of $(\mathrm{X}_j, \mathbf{X}_{PAj})$ is asymptotically normal and can be approximated by a normal distribution:

$$\mathcal{N}\left(\Pr\left(x_j\middle|x_{PA_j}\right), \frac{\Pr\left(x_j\middle|x_{PA_j}\right)\left(1-\Pr\left(x_j\middle|x_{PA_j}\right)\right)}{N.\Pr\left(x_{PA_j}\right)}\right), \qquad \text{Eq. 5-11}$$

where each Pr(.) is computed from the training data set in statistics. This formula implies that the variance of the estimate $\boldsymbol{\theta}_j^k$ will decrease as the size N of the data set increases.

V.2. Conception of a BN model for FC system diagnosis use

The WT based diagnosis algorithm proposed in the last chapter is capable of differentiating the normal and abnormal operating conditions as well as the good and poor state of health of FC. However, it is not able to provide other information such as the value of operating variables. To face this drawback, we developed another diagnostic algorithm based on Bayesian network which serves for estimating the significant operating parameters.

In practical application, the developed Bayesian network is treated as a model. It is used to map the measurements of the electrical variables of the FC to a relevant operating condition. The input variables of this model are the FC's current density and the voltage response. The outputs will be a group of feature parameters that could characterize the operating condition of the FC. For simplicity and being intuitive, each variable in the model is designed to have qualitative values, such as "low", "normal", "high" or "very high". Comparing with numerical value, qualitative value corresponds better to the way of human thinking. It allows offering straightforward information to the expert so that the later is able to quickly make a decision on the actual state of the supervised FC system. In addition, using this kind of linguistic variables is favourable to the generalizability of the model for different types of SOFC.

Since the estimation performed by the BN model is an inference process, the input variables are also known as **evidential variables**. The output variables, representing the questions to answer, are called **query variables**. Differing from traditional models that yield a precise value to a variable, the BN model estimates the conditional probability for each value of the query variable. The value that has the maximal probability will be picked up to be the answer of the query.

For different diagnostic goals, the FC's BN based model would be applied in the different manners. When being used to position the BoP fault, each of query variables in the BN model could be related to the state of certain equipment integrated in the system. For instance, the furnace temperature variable can be regarded as an indicator to the state of the heater; the flow rate of input fuel can reflect whether gas leakage happens at the inlet manifold. When the diagnosed object is the entire FC system, all query variables, together, should be viewed as a feature vector to indicate the state of the overall system.

For our case, the BN model is mainly used to infer in real time the details on the actual operating condition of the FC stack. This information is favourable to track the system's operational activity and predict its evolution. The model will be parameterized with the

datasets from the 1st round test on the VTT test bench contributed to the GENIUS project and from the experiment of a 6-cell SOFC stack on the FCLAB's test bench, respectively. These two tests were both designed to operate the FC stack in mild operating conditions in order to avoid fast FC degradation. Therefore, the obtained experimental data actually outline a limited safety operational range for the studied FC stack. Using them to parameterize the BN, the later will become a knowledge base to mathematically represent such safe operation space. In other words, the BN has learned the information contained in the data. For an input that lies in this space, the BN model can infer a significant response with the relevant knowledge that it has obtained. While given an input locating outside of this space, the model will not be able to recognize it and as a result, it will set the probability of each instantiation of query variables to zero. In simulation application, this is a null response. However, for diagnosis purpose, this output implies that the FC stack is being operated in an unsafe condition. Owing to this feature, hence, the BN model can also serve for system diagnosis use.

Following this conception, a Bayesian network model was built up. The process of its establishment will be presented in the next section. It is worth noting that this BN model is designed only for purpose of recognizing FC stack's operating condition. In other words, it is oriented to system fault diagnosis. In case that the FC stack is damaged, this model will become ineffective for the diagnosis purpose, because one of its inputs, i.e. the stack's voltage, is no longer relevant to the operating condition but greatly influenced by the current state of health of the FC.

V.3. Establishment of the Bayesian network

V.3.1. Preparation of the experimental data

The performance of a BN model depends greatly on the network structure as well as on the quality of experimental data and their formalization. In this work, two datasets are prepared for the BN's structure learning and parameterizations. One is originated from the signals measured in the 1st round test of the VTT system; the other is from the 6-cell SOFC stack's test on FCLAB's test bench.

Table 5-2 The operating conditions of the 1st round test in VTT (listed in the real condition shifting order; T_f: furnace temperature; J: current density; FU: fuel utilization; AU: air utilization)

Operating condition	T_f [°C]	J [A/cm2]	FU	AU
C0-1	760	0.3	0.5	0.4
C1	700	0.1	0.4	0.3
C2	700	0.1	0.4	0.5
C4	700	0.1	0.6	0.5
C3	700	0.1	0.6	0.3
C0-2	760	0.3	0.5	0.4
C7	700	0.5	0.6	0.3
C8	700	0.5	0.6	0.5
C6	700	0.5	0.4	0.5
C5	700	0.5	0.4	0.3
C0-3	760	0.3	0.5	0.4
C9	820	0.1	0.4	0.3
C10	820	0.1	0.4	0.5
C12	820	0.1	0.6	0.5
C11	820	0.1	0.6	0.3
C0-4	760	0.3	0.5	0.4
C15	820	0.5	0.6	0.3
C16	820	0.5	0.6	0.5
C14	820	0.5	0.4	0.5
C13	820	0.5	0.4	0.3
C0-5	760	0.3	0.5	0.4

V.3.1.1. The 1st dataset formalization (the 1st round experiment on VTT's test bench)

In VTT's 1st round test, the SOFC system was continuously tested in 17 operating conditions. These conditions were shifted from one to another by on-line modifying the 4 operating parameters' value (see Table 5-2). All operating point transitions were done gradually, by "small" step-wise changes. In order to have more operating points, the steady state values measured at these steps were picked up and combined with the data obtained during polarization curve measurements to compose an experimental data set. This data set was then randomly divided into two groups, one used as the training data for BN structure learning and parameterization and the other for the model validation. The training dataset involves 46000 samples; the validation dataset has 15400 samples.

V.3.1.2. The 2nd dataset formalization (6-cells SOFC stack on FCLAB's test bench)

In FCLAB, the SOFC stack was tested under different operating temperatures and load current densities while the other controllable parameters (such as the gases flow rates) were kept constant [Gay'12]. The hydrogen stoichiometry is set to 1 and the air stoichiometry is 2. For implementing these experiments, the fuel cell stack operated 8 hours every day in the tested condition when being fed by pure hydrogen. Then, it was manipulated in stand-by mode for the other 16 hours, being provided with a mixture of gases consisting of 5% H_2 and 95% N_2. The flow rate of the fuel (pure H2) is 1.8 NL/min and 8.6 NL/min for the air flow rate. The experimented stack temperature varied between 700 °C and 805°C, increasing or decreasing in a step wise of 15°C. Under every pre-designed stack temperature, a polarization measurement was manually carried out, through either increasing or decreasing stepwise the current density between 0A and the maximal value, as summarized in Table 5-3. Moreover, the SOFC stack had also been steadily operated in 78 operating points under various current density and stack temperatures (see Table 5-4).

Table 5-3 Polarization curve measurement under different stack temperatures (6-cell SOFC stack on FCLAB's test bench)

T_{Stack} / Current	700 °C		715°C		730°C		745°C		760°C		775°C		790°C		805°C	
0-3A/3-0A	✓			✓	✓			✓		✓	✓		✓			✓
3-6A/6-3A	✓			✓	✓			✓		✓	✓		✓			✓
6-9A/9-6A	✓			✓	✓			✓		✓	✓		✓			✓
9-12A/12-9A	✓			✓	✓			✓		✓	✓		✓			✓
12-15A/15-12A	✓				✓											
15-18A/18-15A	✓				✓										✓	
18-21A/21-18A			✓		✓		✓	✓		✓	✓			✓	✓	
21-24A/24-21A					✓		✓			✓	✓			✓	✓	
24-27A/27-24A							✓			✓	✓			✓	✓	
27-30A/30-27A										✓	✓			✓	✓	

Additionally, the effect of the stack temperature evolutions upon the fuel cell performance had been investigated. The temperature was manually varied (upwards or downwards) in some constant current density value or in a range, as indicated in Table 5-5. Since these experiments covered rich operating points, the measurement data from them are involved in the training data set as well.

Table 5-4 The 78 designed stationary operating conditions

T_{Stack} / Current (A)	700°C	715°C	730°C	745°C	760°C	775°C	790°C	805°C
0	✓	✓	✓	✓	✓	✓	✓	✓
3	✓	✓	✓	✓	✓	✓	✓	✓
6	✓	✓	✓	✓	✓	✓	✓	✓
9	✓	✓	✓	✓	✓	✓	✓	✓
12	✓	✓	✓	✓	✓	✓	✓	✓
15	✓	✓	✓	✓	✓	✓	✓	✓
18	✓	✓	✓	✓	✓	✓	✓	✓
21		✓	✓	✓	✓	✓	✓	✓
24			✓	✓	✓	✓	✓	✓
27				✓	✓	✓	✓	✓
30					✓	✓	✓	✓

Table 5-5 Testing data from 12 experiments
(the symbol "→" indicates the varying direction of the temperature)

T_{Stack} / Current	700°C	715°C	730°C	745°C	750°C	760	775°C	790°C	805°C
21A-0A		→							
12A							→		
						←			
15A		→				→		→	
18A	→			←			←		
23A-12A		←							
30A						←		←	

V.3.2. The state of health of the stacks

Since the FC stack is used as a sensor to examine the state of the system, its state of health throughout the system diagnosis process should not have considerable variation. Otherwise, the evolution of the stack responses can also be related to a stack failure, which will influence the judgement on the system state.

Figure 5-2-a demonstrates the polarization curves measured at the five nominal operating points before, during and after the test on VTT system. From the slope of these curves, we can find that the stack's performance does remain reasonably well constant throughout the test. The average standard deviation at each *I-U* point is less than 7mV.

As for the test performed in FCLAB, only two repetitions of polarization measurement were carried out. The *I-U* curves are plotted and shown in Figure 5-2-b. From these curves, we can see that the SOFC stack did not degrade but showed improved performance after 216 hours of operation. However, the reason why this phenomenon could occur is unclear. (There may be a change of the micro-structure of the cells.) A significant stack temperature hysteresis effect can be observed in the polarization curves. For the earlier polarization measurement, the difference of the stack voltage measurements in the current interval between 15A and 20 A is up to 400mV. For the other one (after 216 hours), the maximal difference of the voltage measurements keeps the same but happens in the range of current from 18A to 23A.

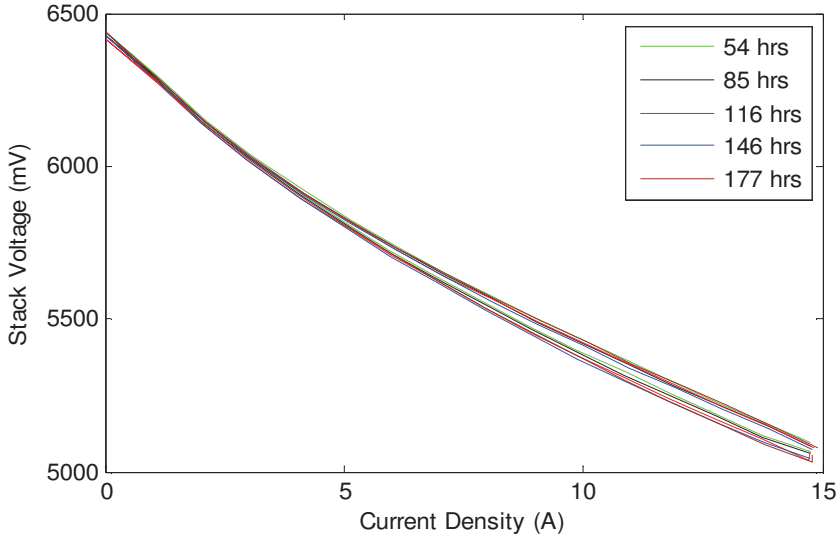

(a)

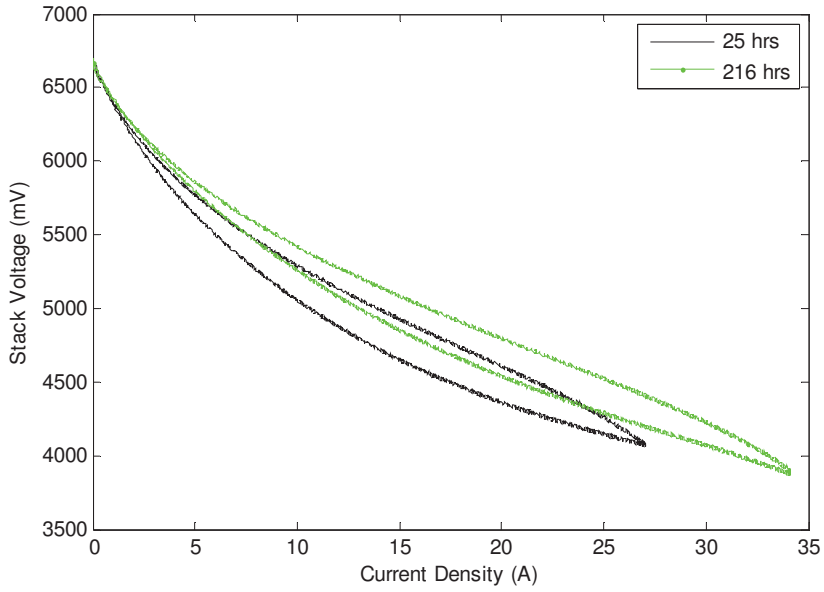

(b)

Figure 5-2 The *I-U* characteristic curves measured at different operating time (t_0= after start-up phase). (a) In VTT: in nominal condition of T_f=760°C, FU=50% and AU=27.75%; (b) In FCLAB: in nominal condition of T_f=750°C, F_{H2}=1.8NL/min and F_{air}=8.5NL/min.

V.3.3. Determination of the network variables and structure

V.3.3.1. The BN variables

The network's variables can preliminarily define the scope of study. They are used to represent the features that characterize the system state in the domain of interest. Under the galvanostatic control, the voltage of the stack, easily and cheaply measurable, is one practical variable for deducing FC operation. Under regular operating conditions, the voltage depends greatly on the load current density but can be also influenced indirectly by other inputs such as hydrogen and air flows and the furnace temperature.

Since the BN serves as a meta-model of the SOFC, the network is designed to have three layers: the upper layer represents the input side of the SOFC stack and the variables in this layer are directly operated by the system; the middle layer is related to the FC operating conditions and the bottom layer represents the output side. The variables in each layer are listed in Table 5-6. In the application of the BN, U and I (the evidential variables) are provided to the model as evidences for operating parameters' state estimation.

Table 5-6 BN variables determination

Upper layer	Stack Current (I)	H_2 flow rate (F_{H2})	Air flow rate (F_{air})	Furnace temperature (T_f)
Middle layer	Fuel utilization (FU)	Air utilization (AU)	Stack temperature (T_s)	
Bottom layer	Stack voltage (U)			

V.3.3.2. The BN structure

Determining the BN structure is equivalent to defining the causal relationships between variables. It can be completed by hand and with expert knowledge about the studied system. In the field of artificial intelligence, some algorithms for structure learning are available to automate the BN structure definition. This kind of algorithms repeatedly executes a seeking procedure in order to search and specify a set of network variables as the direct causes (or parents) for a certain variable. Riascos et al. (2007) [Riascos'07] used respectively Bayesian-score (K2) algorithm and Markov Chain Monte Carlo (MCMC) algorithm to learn Bayesian networks for the purpose of PEMFC diagnosis. They combined the network structures obtained by these two algorithms and optimized it with the expert knowledge. K2 is a search-and-score algorithm and requires initially setting an order of the nodes to which the quality of the network structure is sensitive. MCMC algorithm searches the best network graph in a set

of samples from the structure space. Details about these two algorithms can be found in [Cooper'92] and in [Pearl'00].

In our work, the network structure was determined with the knowledge and experience on the diagnosed systems. K2 algorithm was used to construct a Bayesian network from the dataset of records. This network served as a reference to validate the causalities defined in the expertise-based network and find implicit dependencies between the variables. The final BN structure is shown in Figure 5-3.

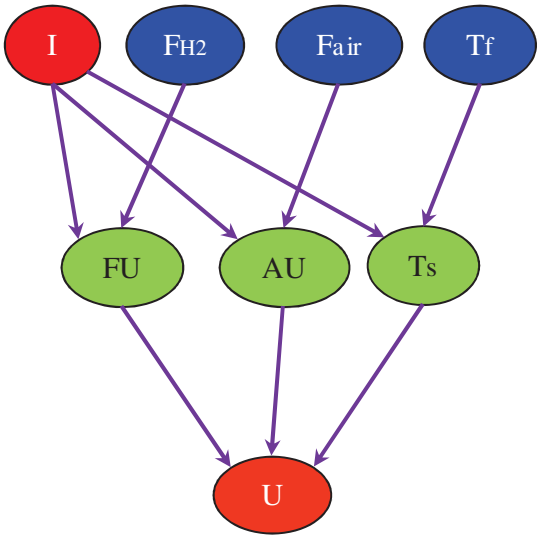

Figure 5-3 The structure of the proposed BN model

Note that the variables in the first layer are considered independent between each other because of the fact that their values are set in the experiments by the system control unit. The association between I and T_s is due to heat production of ohmic resistances in the stack. Even after data discretization, this relation could still be found out by using K2 algorithm. However, the known impact of F_{air} upon T_s was not observed in the network learnt by K2 algorithm because it is insignificant for a short stack and was not present in the experimental dataset. Therefore, the dependence between these two variables was neglected. It is noteworthy that since the Bayesian network is used as a knowledge base retrieved from the data, the determined relations between the variables of the network should be in accordance with the information represented by the training data.

V.3.4. Discretization of the data

Before being used to fit the BN model, the prepared two groups of data should be respectively discretized because the BN involves only discrete variables, which is also known as discrete BN. This raises a question that should be answered in advance: how many distinct values/intervals to define for each variable? The solution is usually unapparent and should be found in the context of specific examples [Darwiche'09]. Computing time and accuracy issues should be taken into account because a great number of values for query variable may result in a long time of network parameterization as well as poor accuracy in reasoning. Wasterlain

et al. (2010) [Wasterlain'10] had tried and compared three different classification methods, namely the segmented tree [Hartigan'79], the manual discretization and the *k*-means clustering algorithm, in the construction of a naïve BN classifier used for PEMFC diagnosis. For their study, the classification rates of these methods were 91.2%, 89.2% and 88.2%, respectively.

In our investigation, the data discretization was carried out manually according to the practical situation of the systems. For the operating variables, the faulty modes of operation that may cause SOFC degradation were taken into account. Larrain et al. (2006) [Larrain'06] had reported that the degradation rate of SOFC was mostly dependent on stack temperature. They proposed hence to minimize the stack temperature to 750°C or lower in order to decrease the FC degradation rate. Tu et al. (2004) [Tu'04] also discussed the advantage of operating temperature below 800°C with respect to the cost of stack and BoP, the capability of thermal cycle and the reduction of corrosion rate in long-term operation.

In addition, for a short time, Larrain et al. (2006) and Comminges et al. (2012) [Comminges'12, Larrain'06] believe that fuel shortage is the principal cause of stack degradation even in unloaded conditions. Therefore, according to these investigations, the fuel utilization factor should be kept in a narrow range during the FC operation, on the one hand for maintaining the system efficiency and on the other hand for extending the stack lifetime.

In this work, the safe operating temperature range for a SOFC stack was determined between 720°C and 780 or 790°C for the temperature variable. The normal fuel utilization was defined in the range between 45% and 55%.

For our case, the design of query variables' discretization is based on the design of experiments as well as according to the literature research presented in the previous paragraphs. These variables were discretized around the center domain (the rated value). The number of distinct values for each query variable was limited to 5. The labels were defined as low/center/high or very-low/low/center/high/very-high (Refer to Table 5-7 & Table 5-8).

Table 5-7 Query variables discretization for VTT's data

	Very low	**Low**	**Center**	**High**	**Very high**
F_{H2} **(Nl/min)**	< 0.4	[0.4,0.9)	[0.9,1.5)	[1.5,2.2)	>=2.2

	Low	**Center**	**High**
F_{air} **(Nl/min)**	< 5	[5, 10)	> = 10
***Tf* (°C)**	< 730	[730, 790)	> = 790
***FU* (%)**	< 45	[45, 55)	> = 55
***AU* (%)**	< 15	[15, 30)	> = 30
***Ts* (°C)**	< 720	[720, 780)	> = 780

Table 5-8 Query variables discretization for FCLAB's data

	Very low	**Low**	**Center**	**High**	**Very high**
F_{H2} **(Nl/min)**	< 0.4	[0.4,0.9)	[0.9,1.5)	[1.5,2.2)	>=2.2

	Low	**Center**	**High**
F_{air} **(Nl/min)**	< 7.1	[7.1, 9.9)	> = 9.9
***Tf* (°C)**	< 700	[700, 780)	> = 780
***FU* (%)**	< 45	[45, 55)	> = 55
***AU* (%)**	< 15	[15, 30)	> = 30
***Ts* (°C)**	< 720	[720, 790)	> = 790

Table 5-9 Evidential variables discretization

Interval label	***I* (A)**	***U* (V)**
1	< 3	< 4
2	[3, 6)	[4, 4.3)
3	[6, 9)	[4.3, 4.6)
4	[9, 12)	[4.6, 4.9)
5	[12, 15)	[4.9, 5.2)
6	[15, 18)	[5.2, 5.5)
7	[18, 21)	[5.5, 5.8)
8	[21, 24)	[5.8, 6.1)
9	[24, 27)	[6.1, 6.4)
10	> = 27	> = 6.4

For the discretization of the evidential variables (i.e. *I* and *U*), it is better to design a larger number of distinct values for each of them. From pattern recognition point of view, such design leads to refined discretization/classification which is favourable to discrimination

ability of the evidence variables in terms of the heterogeneity between classes and the homogeneity within the classes. As a result, the input (evidence) could have higher directivity to the corresponding pattern. However, differing from the query variables, it is not necessary to give descriptive statement to the distinct values of the evidential variables. In this work, we have designed the same discretization rules of evidential variables for the FCLAB's and VTT's data sets (see Table 5-9).

V.3.5. Parameterization of the BN model with the experimental data

With the BN approach, the dependencies between variables are quantified by parameterized conditional probability distributions (CPD). The computation of CPDs is a process of BN parameterization based on data learning. The basic method of parameter learning from complete data is Maximum Likelihood (ML) parameter estimation. Details about this method can be found in [Ghahramani'03].

In this work, we used this method to estimate the BN parameters from the discretized training data. For the BN prepared for the FCLAB test bench, the training dataset included 28000 samples; and for the VTT system, there were 46000 samples. The parameterization procedure was carried under Matlab, using the Bayes Net toolbox available in [Murphy'07].

V.4. Results and analysis

V.4.1. Validation of the BN model

In the model validation, the values of I and U were inputted into the BN as evidences to compute the posterior probability distribution over the distinct values of every query variable based on Eq. 5-2 and the formula introduced in Section V.1.3. The junction tree algorithm is available in the Bayes Net toolbox, which allows transforming the graph of the network into an appropriate data structure and performing the probability computation for the inference exactly and efficiently (refer to [Darwiche'09] for details). Finally, the value having the maximal probability was selected as the estimated state for the variable. An example on the SOFC operating parameters estimation based on this BN model is given in Appendix-II.

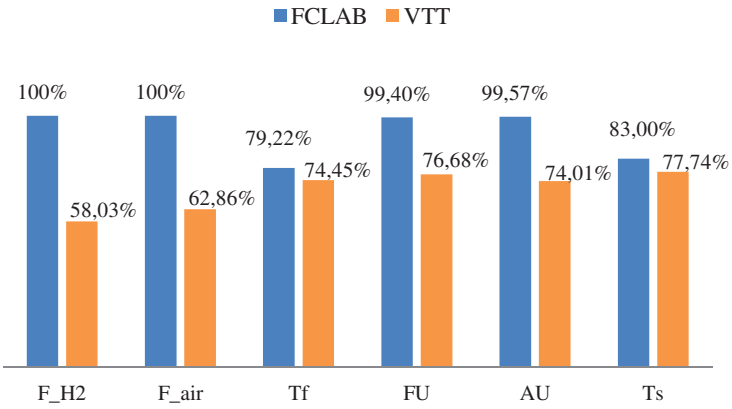

Figure 5-4 The estimation accuracy of the BNs

The ratio of correct estimates for every query variable is shown in Figure 5-4. 15400 samples from VTT database and 12000 samples from the FCLAB 6-cell stack experimental database were used for the validation. Because the fuel and air flows were maintained constant in the FCLAB test bench, the estimation by the BN model showed a perfect accuracy, up to 100% for these variables. By contrast, the estimation accuracy on T_f and T_s were lower since the stack was operated under varying temperature conditions. For the VTT system, all of operating parameters are variable, which leads to a greater number of operating conditions. Some of them may correspond to the same (I, U) pair whereas the BN model can only associate the given/measured (I, U) pair to a single operating condition. This issue will be further analyzed and discussed in the next sub-section.

The adaption of the model in diagnosis application depends on the fault(s) that the users intend to diagnose. As discussed in Chapter 4, the operating modes with high *FU* and high stack temperature are considered as the fault to diagnose. Among the testing data from VTT system, there are 1449 samples related to this faulty operating mode. We used these samples to validate the diagnostic ability of the BN model. As a result, the ratio of accurate diagnostic is about 67%.

V.4.2. Analysis

Generally speaking, the established BN model plays a role of knowledge base which depicts the information contained in the training data with causal relationships and utilizes the probability theory for the causalities quantification so that inference based on this knowledge base could be achieved by means of computation. In order to examine the goodness of the model in knowledge representation, we can compare the information of the training data with the knowledge represented by the model so as to analyze their accordance.

In this work, the discrete BN is used to estimate SOFC operating variables given the value of I and U. It is thus equivalent to projecting the (I, U) point to a specific space of the SOFC's operating conditions.

According to the severity ranking of SOFC degradation phenomena yielded from the DESIGN (**Degradation Signatures Identification for Stack Operation Diagnostics**) project[*], the parameter *FU* is recognized as an important source of failure or severe performance degradation: it indeed causes anode oxidation. At high *FU*, the partial pressure of fuel can locally be close to zero since the fuel is diluted by the produced steam. In case of local fuel depletion and high water vapour concentration, the atmosphere at the anode side is no longer reductive, leading to a local reoxidation of the nickel anode. In addition, according to VTT, T_s is also an important parameter that should be closely supervised during the operation.

Therefore, we put our efforts on studying the performance of the BN model for *FU* and T_s estimations. For easier understanding, we designed an I-O (Input-Output) map to reveal the mapping relations between each of these two query variables and the evidential variables that are modelled by the BN, by using a 2D I-U plant grid with colours (see Figure 5-5). For comparison, the discretized training data are illustrated in the same way.

V.4.2.1. Projection of *FU* on the I-U grid

Figure 5-5 displays the I-U planes which are divisionalized into a rectangular grid according to the evidential variables' discretization rules (see Table 5-9). In Figure 5-5-b, the coloured rectangular paves compose a region that the training data locate. In Figure 5-5-a, there is the same coloured region on the grid, which implies that the BN model has well learnt the scope of the SOFC operation that is described by the training data. The coloured region includes 3 colours, each of which corresponds to a state of the studied variable: the blue represents the low level; the gray-blue for the central level and the light blue (cyan) for the high level. Comparing with the I-U measurements obtained in the different operating conditions (shown by coloured symbols), we can find that the edge of the coloured region outlines a zone that involves all the polarization curves. In case that all the I-U measurements are obtained when the SOFC stack is operated in normal mode, this zone can be considered as a representation of the safe operating range for the SOFC whereas the dark region (paved by gray rectangles) is relevant to the improper operations.

In Figure 5-5-a, the majority of rectangles are related to the low *FU* conditions while two are assigned to the conditions with normal *FU* and the other two rectangles at high current density are relevant to high *FU*. However, according to the training data, the distribution of the *FU* values on the I-U grid is very different.

From Figure 5-5-b, we can see that the value of *FU* in some rectangles (in hot colours: red, orange, yellow and light green) is ambiguous, especially at high current densities where a I-U pave is relevant to two or three different states of *FU*. This is due to the fact that the limited variation of the *FU* (from 40% to 60%) emulated in the test did not provoke considerable change upon the stack performance. The polarization points measured at different *FU* values

[*] Refer to http://cordis.europa.eu/projects/rcn/97933_en.html

prove it. We can see in Figure 5-5-a that the green circular symbols relevant to the low *FU* generally overlap with the yellow triangular symbols correspondent to the high *FU*.

Since the case of fuel starvation was not well experimented, the BN model has only learned the information on the system when being operated in a narrow range of *FU* variation in which the variation of the stack voltage is not apparent. Comparing Figure 5-5-a and Figure 5-5-b, it is easy to know that the estimation mistakes made by the BN model mainly take place when the diagnosed system is fully loaded.

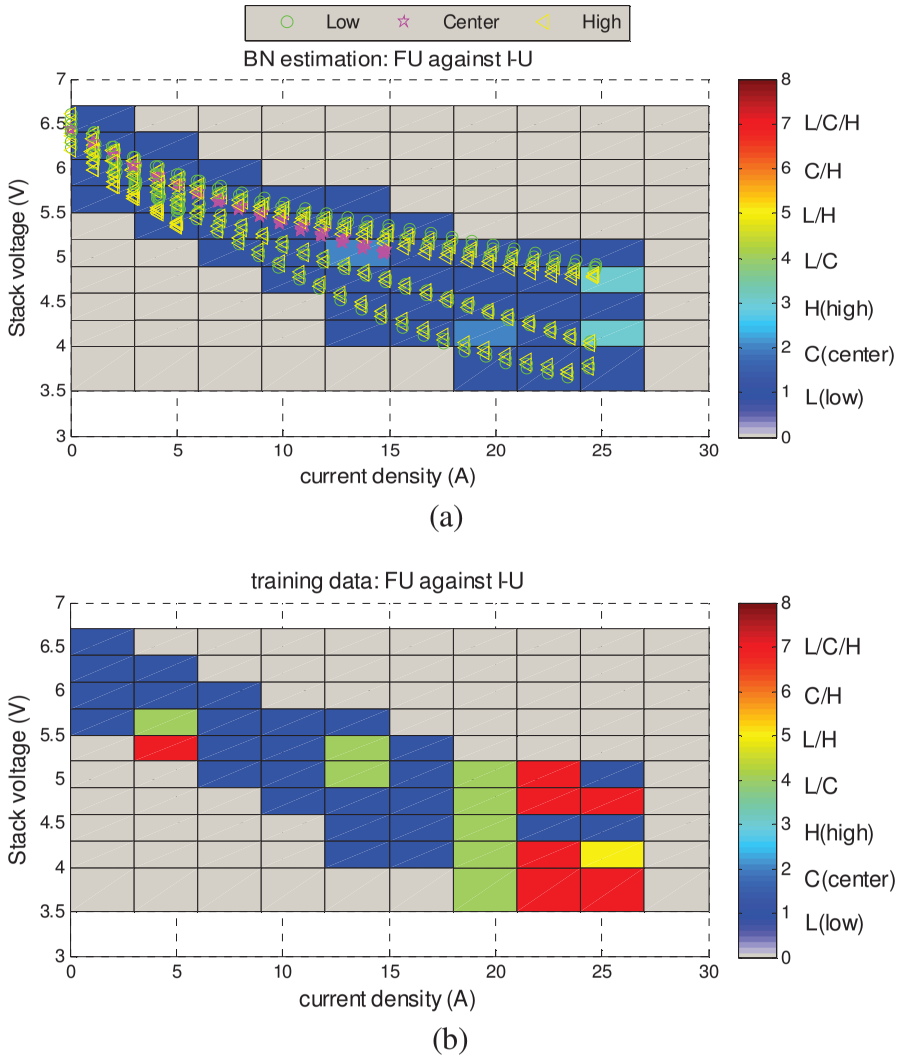

Figure 5-5 (a) The BN estimated distribution of FU values & (b) The real distribution of FU values on the I-U grid with a colormap

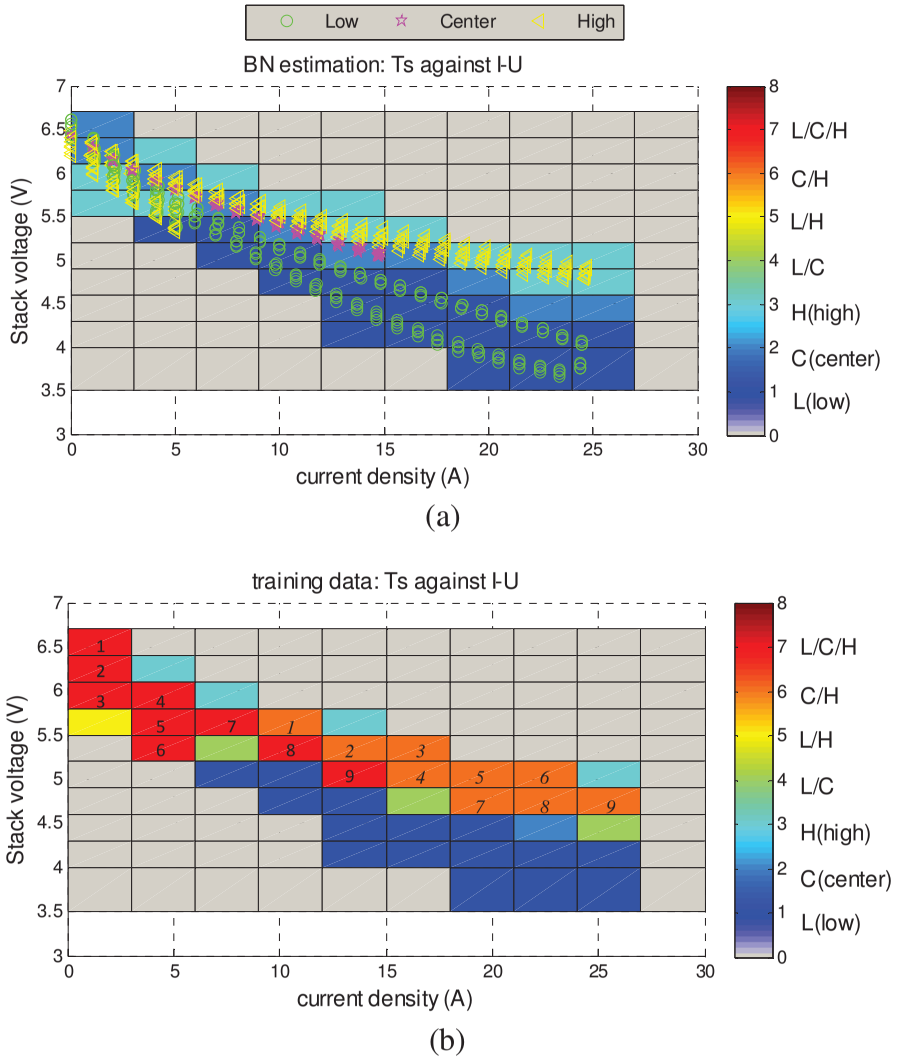

Figure 5-6 (a) The BN estimated distribution of T_s values & (b) The real distribution of T_s values on the I-U grid with a colormap

V.4.2.2. Projection of T_s on the I-U grid

In Figure 5-6-a, the I-U points (represented with different symbols) measured at different stack temperatures are quite distinguishable. The stack performance at high temperature is much better than at low temperature, due to the reduction of the ohmic loss in the electrolyte as well as in the improved contacts between the cell and the interconnect.

Being trained with these distinct I-U measurements, the BN model is able to divide the tested operation area (that is, the entire coloured region) into 3 parts; each of them corresponds to a temperature range and has a similar form with the relevant I-U curve tendency (see Figure 5-6-a).

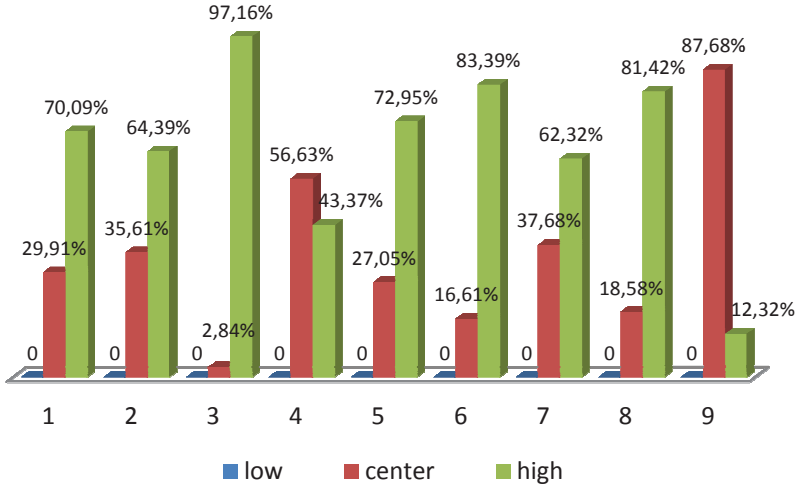

Figure 5-7 Histogram of the probability distributions over T_s values for the orange paves of the I-U grid

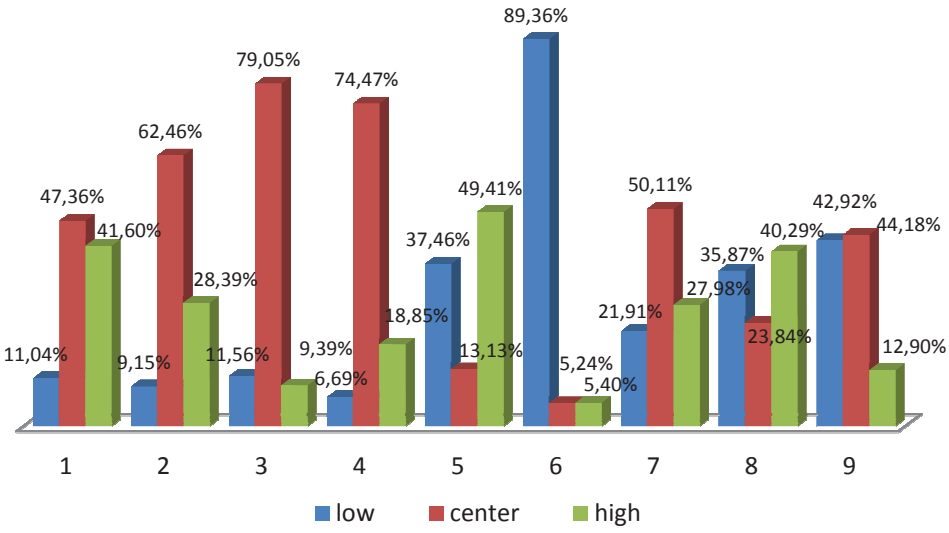

Figure 5-8 Histogram of the probability distributions over T_s values for the red paves of the I-U grid

Referring to Figure 5-6-b, we can find that when the stack current is greater than 8A and has a higher voltage, the value of T_s is hard to be determined between the centre and the high level (the orange zones labelled by italic numbers). Fortunately, the BN model can compute the probability for each level. The probability distributions over the stack temperature's values related to the orange rectangles are illustrated by a histogram in Figure 5-7. We can see that, apart from the pave No.4, the probabilities of the 3 T_s levels in the other cases are discriminative enough so that the users could easily determine the value of T_s.

However, for the red area of the I-U grid in Figure 5-6-b (labelled by bold numbers) where the current density is lower, the value of T_s is hard to determine, because the I-U measurements in this area are overlapped. The probability distributions calculated by the BN model reveal this overlapping further. In Figure 5-8, we can see that, except for the red paves No. 2, 3, 4, 6 and 7, it is difficult to determine the T_s's value for other I-U paves since the probabilities for two of the three values (low/center/high) are very similar. For example, in the red pave No.1, the probability that T_s is at the center level is very close to the probability for T_s at the high level. Wrong estimation may thus be encountered when the measured I-U point falls in this kind of zones.

V.5. Conclusion

In many cases, the degradation of a fuel cell originates from improper operation. The sensors used to measure the operating parameters may be not reliable when a system fault has happened. Under the requirement of GENIUS to diagnose the fault with no additional sensors, this problem can be addressed by developing an on-board diagnosis algorithm to recognize the system operating conditions.

Following this idea, a static discrete BN was built for SOFC system fault diagnosis. Two tests were carried out respectively on FCLAB's and VTT's test benches on HTceramix 6-cell short stacks. The network structure (the same for the two considered SOFC systems) was determined upon expert knowledge about the SOFC system. It was validated with the experimental data sets obtained from the two systems by applying the K2 structure learning algorithm. Then, the BN was parameterized by using the ML parameter learning method to fit the discretized experimental data sets, respectively. The final discrete BN models were found to be capable of estimating the values of the operating variables based on the stack electrical output measurements, that is, only the current density and the stack voltage.

For simple fault detection use, the BN model is able to outline a zone on the I-U plane to indicate the safe operation scope for the SOFC stack, based on the training data. When the I-U measurement lies outside this zone, the model will output null probability distributions for all query variables to declare that the SOFC stack is operated in an abnormal mode. For early fault diagnosis use, the operating conditions with high FU and high T_s were considered as faulty mode in our work to diagnose. The ratio of right diagnostic for the VTT system was about 67%.

Finally, a three-dimensional I-O map (a two-dimensional grid plane covered by coloured paves) was proposed to illustrate the mapping relation between the (I, U) pair and a single operating variable that is modelled by the BN. This map is a useful tool for the estimation and analysis of the BN model's performance.

Conclusions and perspectives

1. Summary of findings and conclusions

Durability is one of the crucial issues for the practical application and commercialization of fuel cell (FC) technology. A great amount of research efforts has been and continues to be made on the improvement of FCs or stacks' design and materials in order to increase their effective lifetime in stationary operation. On the contrary, the influences of system component failures upon the durability of FC have not been given enough attentions. In this context, an EU project RealSOFC* had been performed to study the degradation in solid oxide fuel cell (SOFC) stacks as a function of the operating conditions. Following it, another EU integrated project GENIUS was proposed to achieve SOFC system diagnosis, accomplishing the detection and identification of improper operating conditions.

The work of this thesis was carried out in the framework of GENIUS project which asserts the usage of the SOFC stack as a sensor for system diagnosis implementation. This thesis investigates non-destructive diagnostic methodology for different SOFC systems on the basis of data mining, signal analysis and statistical modeling. The ultimate objective is to maintain the SOFC system in proper operating condition so as to extend the lifetime of the SOFC stack as long as possible.

In this work, three algorithms have been developed: one aims at SOFC stack off-line diagnosis, working on polarization test data; the other two serve for on-line fault detection and identification, relying on SOFC voltage and/or current signal or actual measurements. For the on-board diagnosis, the importance of the state of health of the stack, as a specific sensor, was remarked. We proposed to firstly verify this point before performing any diagnosis for the system.

The three algorithms are based on k-means clustering, wavelet transformation and Bayesian network model, respectively. The selection of these data analysis techniques was made in the consideration of the given type of data and based on the corresponding goals. 5 databases originated from different SOFC stack tests were selected to validate these algorithms and their generalizability.

In off-line diagnosis, the analyzer always has to work on a massive process data. Analyzing it by manual selection of variables and extraction of features is time consuming and prone to bias due to the expectations of the analyzer (the data may be subjectively interpreted). Moreover, the data is usually a rich collection of full-scale experiments designed by process operators. For the analyzer who lacks of expertise knowledge/information about the design and the real procedure followed in the experiments, performing the segmentation on data for individual case analysis can be a difficult and heavy work. In the consideration of this situation, *k*-means clustering was selected in this work for organizational learning and pattern recognition from the data. We firstly used this technique to classify the SOFC operating

* Refer to the web page: http://www.real-sofc.org/

variables' data in order to know in what significant operating conditions the stacks had been tested. Then, the SOFC response variables' data were classified by the same means. As a result, not only the two different operating modes were correctly found out, the severe degradation of the stacks in each operating mode was also recognized in the data classification process. In order to determine effective indicators for stack degradation, feature ranking technique was applied to sort the response variables based on their determinant degree on the classification solution. It was found that in the first operating mode with a higher air flow rate to CPO[*], the stack's severe degradation could be indicated by the stack top temperature. However, in the other operating mode, this variable is not indicative to the state of health of the stack. The severe degradation of the stack in this mode can only be indicated by the ASR value. In addition, a meaningless variable was arranged into the operating variable set with the aim of checking the sensitivity of the clustering algorithm to the disturbance data. Finally, we found that the clustering solution was not influenced by this disturbing variable.

For on-line diagnosis, a 3-steps diagnostic method had been proposed beforehand: the former two steps for SOFC failure and system fault detection, the last for system fault identification. In this thesis, the system fault was represented by a kind of abnormal operating conditions where the SOFC delivers a low-level current density but is operated with high-level fuel utilization. Besides, the conditions with high fuel utilization and high stack temperature were considered harmful to the SOFC stack, as well.

The wavelet transform based algorithm serves for the fault detection phase. The wavelet transform is used to decompose steady-state voltage signal of SOFC. The basic diagnostic principle is to employ the fluctuating behaviors of the signal to indicate the actual state of health of the fuel cell. Three feature variables were extracted to characterize the fluctuating behaviors present in a signal. They are the relative wavelet energy (RWE), the total wavelet entropy (TWP) and the relative wavelet entropy (RWP), respectively. In the validation phase, we found that these variables were not only indicative to the state of health of SOFC, but also discriminative enough for distinguishing the SOFC failure from the system faults. In other words, the two steps pre-designed for the fault detection phase could be simultaneously accomplished by the wavelet-based algorithm. In addition, the RWE also showed the capability to reflect the progressive degradation process of the SOFC. The validation was carried out with the signals from two different SOFC test benches. The results demonstrate that this diagnostic algorithm is generic for different SOFC systems. The testing signals were in different lengths. For those sampled at 1Hz, the minimal length that allows fault indication is 1000, that is, about 17 minutes of diagnosis delay. For the signals sampled at 3 Hz, the minimal length for the signal decreases to 800, that is, less than 5 minutes of delay for diagnosis implementation. It is worth noting that this signal-based fault detection algorithm is an extension on the work of Nadia Steiner who developed a wavelet-packet-transform based algorithm for PEMFC diagnosis in her Ph.D study [Steiner'09]. Compared with this previous achievement, our algorithm reveals several advantages in the aspect of practical application:

[*] CPO: **C**atalytic **P**artial **O**xidation. The Hexis SOFC system includes a natural gas reformer.

1) The algorithm is relying on discrete wavelet transform which takes less computational time than the wavelet package transform;
2) It allows a lower requirement for the sampling rate of the signals under study.
3) The proposed feature variables are much effective for the faults indication so that the decision-making tool based on in-depth feature data analysis is not required.

Finally, the Bayesian network based algorithm supports system fault identification. It is based on a Bayesian model which is used to estimate the actual operating parameters of the SOFC given only the measurements of stack voltage and current. A Bayesian network was proposed as a meta-model to represent the causal relationships between the SOFC's operating and response variables. The structure of this model was set up by our expertise knowledge and validated according to the network structures learnt from two experimental databases from different test benches. The model was then trained (or parameterized) by two discretized datasets which involved polarization test data and the measurements in the transients during operating point changes. In this way, the information on the SOFC performance in different operating conditions could be learnt and represented by the Bayesian network. The model's estimation accuracy for each query variable was calculated and given in Chapter 5. Its capability for the system fault identification was also tested with the experimental data from the VTT system test. As a result, the Bayesian model could identify 67% of the 1449 samples measured in the faulty operating modes. Finally, a three-dimensional I-O map (a two-dimensional grid plane covered by coloured paves) was proposed to illustrate the mapping relation between the (I, U) pair and a single operating variable that was modelled by the Bayesian network. On this map, there is a zone covered by coloured paves, which represent the region where all the polarization data lie in. This map gives an insight into the problem of the Bayesian model in the estimation of two operating variables of interest, i.e. the fuel utilisation and the stack temperature. Based on this map, we found that when the (I, U) points are not discriminative for distinguishing different operating conditions, the model will give an incorrect estimation to the operating variables. Additionally, besides the estimation ability, the parameterized Bayesian model can also been viewed as a knowledge base used to verify the state of health of the SOFC stack. As the given (I, U) point lies outside and especially below the coloured region, the model would not be able to recognize it and thereby output null value for all query variables. Such an output implies that the SOFC stack is in a severely degraded state.

Both of these two algorithms have been validated for two different SOFC test benches (in VTT and FCLAB). The overall in-situ diagnosis process for SOFC system based on them is illustrated in the figure below.

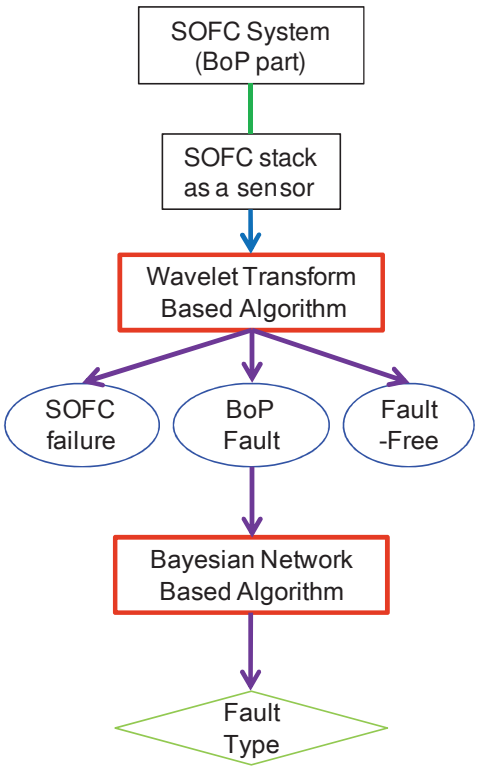

2. Recommendations for future work

In this thesis, the validities of the developed diagnostic algorithms were all tested off-line. The Bayesian network model was parameterized and validated by steady and transient experimental data whereas the wavelet transform based algorithm was tested with only the steady-state signals measured when the system regained the stability after the change of operating condition.

Consequently, in the future work, it is necessary to check the indicative capability of the proposed feature variables with transient signals. It is recommended that this validation could be carried out on-line on a real system with several stacks which will be a valuable test bench for the real usability of this signal-based diagnostic algorithm. For such a large-scale system, realistic errors and considerable noises will be present in the process signals, which is favourable to test the robustness of the indicators.

The Bayesian network-based modelling for SOFC could also be improved. In this work, we had carried out a “hard” discretization procedure in the data pre-processing phase in order to transform the quantitative variables to the qualitative ones. The definition of the intervals for the values of each variable was determined based on the expertise knowledge and the nature of the data. Thus, for a different SOFC system and/or database, the discretization rules must be re-defined. Furthermore, the boundary of single intervals and the transition between the intervals of a variable is abrupt rather than “smooth”, which may result in mistaken qualitative definition to an observation of an input variable and leads to a wrong estimation result. To automate the parameterization of the Bayesian model, it is required to develop a

generalizable and "soft" method for the data discretization (or variable transformation). The fuzzy logic method, which allows transforming variables with continuous numerical values into non-numeric linguistic variables (refer to the content in Chapter II.2.3.2.1), might be a solution.

Finally, we could also test the applicability of the *k*-means clustering algorithm to the impedance spectroscopy data of SOFC, for the purpose of determining the significant impedances discriminative and representative to the state of health of the fuel cell. Since the electrochemical impedance measurements could be performed in-situ, it is possible to develop this algorithm for the in-situ diagnosis application. In addition, the index "Silhouette" shows potential as an indicator for fuel cell prognostic application. This index may be useful for on-line fuel cell health assessment. For example, it is possible to prepare two groups of data: one represents the good state of health of fuel cell and the other for the degraded state. To implement the prognostic, the silhouette value of the fuel cell's observation relative to these two groups of data could be calculated and be used to indicate the actual state of health of the fuel cell.

Appendix-I.

		CONTROLLABLE PARAMETERS						MEASURED RESPONSES (RES.)				EXTRACTED RES.		Stack Operation Experience			
Stacks	test	NG flow (g/h)	2nd NG for 5 g/h Stack (g/h)	CPO Air flow (l/h)	Cathode air flow (g/h)	Preheat Air	Preheat CPO	T stack bottom (°C)	T stack Top (°C)	T CPO out (°C)	T CPO in (°C)	ASR (mΩ/cm^2)	OCV (mV)	Operation time (hours)	Total redox or/and thermal cycles	Redox cycles	Thermal cycles
HP060030	1	19,98	0,23	71,03	1001,41	24,83%	68,18%	949,33	962,62	730,77	761,05	59,17	4800,26	49	0	0	0
	2	19,97	0,24	70,98	1001,32	28,75%	67,58%	949,48	961,29	722,69	761,17	69,75	4875,03	2354	1	0	1
	3	19,98	0,26	71,03	999,66	28,48%	68,65%	949,51	959,93	724,08	760,85	72,29	4844,81	4865	1	0	1
	4	19,99	0,26	71,06	1000,28	29,36%	68,89%	948,44	959,90	732,87	760,43	77,55	4887,23	5471	1	0	1
HP060031	5	19,92	0,07	70,61	1000,73	34,22%	40,93%	949,30	953,28	727,86	770,67	57,82	4690,39	49	0	0	0
	6	19,92	0,10	70,61	999,45	31,68%	43,87%	949,53	933,78	726,39	780,71	72,10	4767,30	2354	1	0	1
	7	19,91	0,06	70,63	1000,22	33,74%	35,92%	949,61	851,47	721,93	780,13	72,97	4705,95	3690	1	0	1
HP060045	8	20,05	0,12	70,72	1000,31	30,36%	82,33%	949,26	956,31	722,42	730,55	55,04	4837,18	39	0	0	0
	9	20,08	0,18	70,79	999,74	25,89%	78,35%	949,67	922,68	702,25	730,62	65,48	4942,47	3297	0	0	0
	10	20,10	0,20	70,82	999,32	23,80%	84,57%	949,70	830,05	701,40	740,55	76,89	4914,70	6065	0	0	0
	11	20,09	0,20	70,79	1000,56	24,88%	88,97%	949,36	818,05	707,88	741,85	90,60	4921,11	6998	0	0	0
HP080025	12	19,98	0,13	65,59	999,45	37,76%	46,07%	849,26	857,51	720,05	774,88	92,53	4807,58	41	0	0	0
	13	19,96	0,15	65,61	999,48	39,46%	42,80%	849,44	858,11	720,45	763,36	87,62	4833,83	612	0	0	0
	14	19,96	0,16	65,58	999,71	39,71%	42,64%	849,28	858,20	719,54	760,51	86,40	4837,18	689	1	1	0
	15	19,96	0,13	65,59	999,99	39,17%	41,24%	849,47	858,40	720,76	761,88	88,08	4826,50	828	1	1	0
	16	19,95	0,15	65,58	999,92	39,72%	42,56%	849,46	858,45	719,68	761,04	85,98	4845,42	877	2	2	0
	17	19,97	0,15	65,59	1000,11	39,58%	41,36%	849,41	858,61	719,13	754,76	87,44	4828,64	952	2	2	0
	18	19,94	0,13	65,59	1000,67	39,32%	40,03%	849,38	858,58	719,54	754,26	89,59	4820,40	976	3	3	0
	19	19,97	0,15	65,58	999,32	39,41%	41,61%	849,42	858,51	720,11	758,81	90,52	4835,35	1000	4	4	0
	20	19,96	0,14	65,58	999,71	39,39%	42,24%	849,39	858,51	719,99	761,65	90,90	4858,24	1024	5	5	0
	21	19,97	0,15	65,58	999,91	39,52%	41,01%	849,48	858,74	719,97	758,62	93,57	4848,17	1048	6	6	0
	22	19,98	0,14	65,59	999,10	39,19%	40,84%	849,37	858,88	719,84	758,34	97,62	4841,15	1121	7	7	0
	23	19,97	0,13	65,59	1000,09	39,27%	39,67%	849,35	858,97	719,48	756,23	99,86	4843,29	1145	8	8	0
	24	19,96	0,13	65,59	1000,07	39,39%	40,61%	849,32	859,02	719,65	758,63	102,18	4853,36	1169	9	9	0
	25	19,97	0,15	65,57	1000,46	36,94%	43,94%	849,41	858,50	720,28	770,06	138,02	4891,20	1211	12	11	1
	26	19,98	0,13	65,59	999,92	36,81%	41,76%	850,59	859,12	722,37	776,47	226,77	4867,09	1283	12	11	1
	27	19,97	0,14	65,58	1000,31	39,15%	41,78%	850,35	859,18	721,04	770,97	167,86	4877,77	1313	13	12	1
	28	19,95	0,12	65,60	1000,28	39,15%	40,87%	850,17	858,74	721,08	772,05	195,72	4865,87	1337	14	13	1
	29	19,97	0,12	65,59	999,67	39,26%	40,33%	850,20	858,88	720,25	769,12	216,13	4862,82	1362	15	14	1
	30	19,98	0,16	65,57	999,86	39,09%	46,18%	850,40	858,94	719,62	775,35	216,88	4899,75	1381	15	14	1

Appendix-II.

An example is given below to illustrate the estimation process based on the established BN model. Inputting the numbers of the level in which the current and the voltage lie, the model will output a probability distribution over the values of each query variable. The value having the maximal probability will be picked up as the estimate of the variable. Finally, all estimates compose a signature to indicate the current system state. The solid arrows represent cause-to-effect inference while the dash ones imply effect-to-cause reasoning.

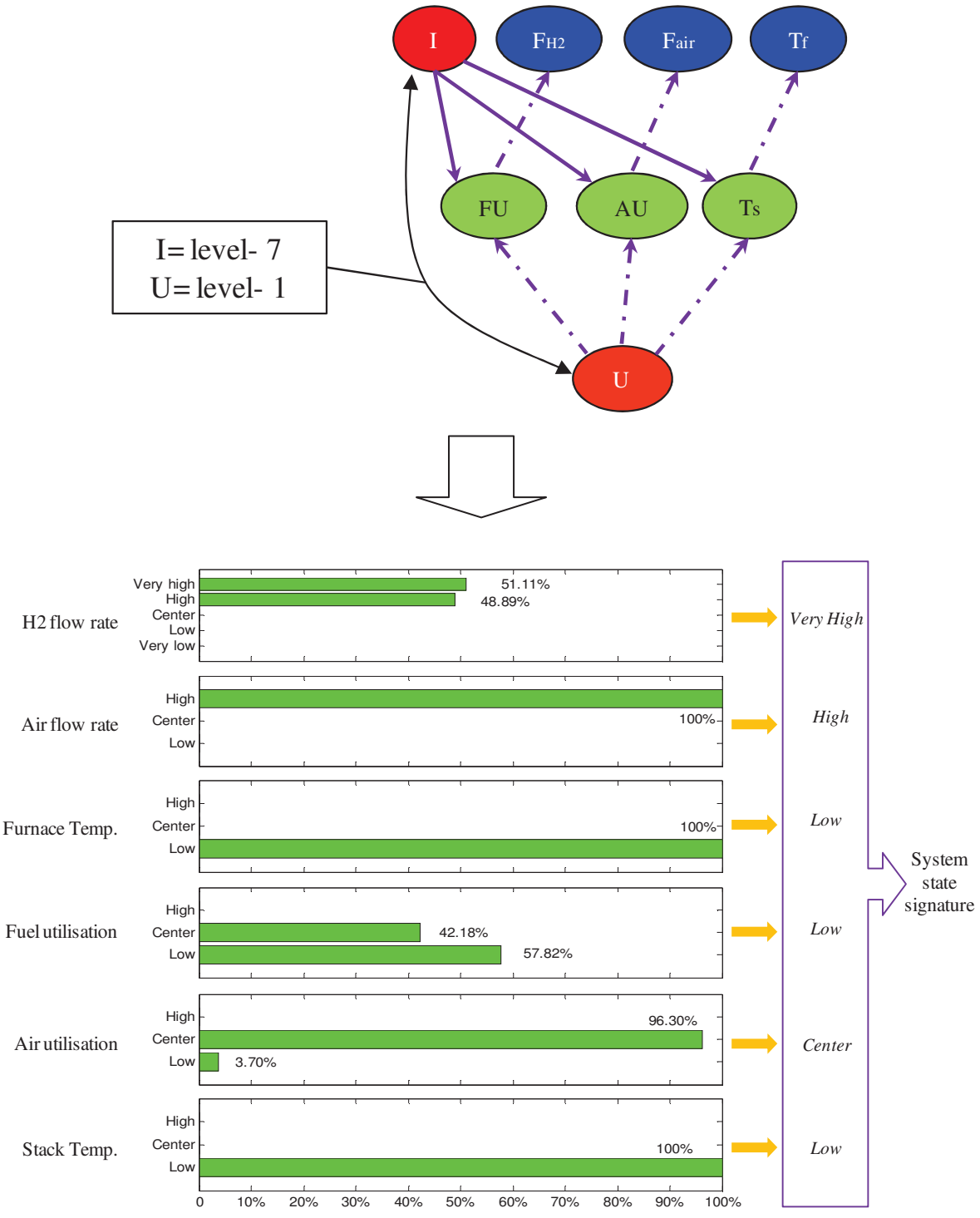

References

[Abdelghani'00] Abdelghani, M., Basseville, M., Benveniste, A., Hermans, L. & Auweraer, H.V.D. (2000). A Subspace-Based Fault Detection Algorithm with Application to In-Operation Monitoring and Diagnostics of Vibrating Structures. *Automatica, 36*, 101–109.

[Ahmad'12] Ahmad, R. & Kamaruddin, S. (2012). An overview of time-based and condition-based maintenance in industrial application. *Computers & Industrial Engineering, 63*, 135-149.

[Akaike'74] Akaike, H. (1974). A new look at the statistical model identification. *IEEE Transactions on Automatic Control, 19*, 716-723.

[Akorede'12] Akorede, M. F., Hizam, H., Ab Kadir, M. Z. A., Aris, I. & Buba, S. D. (2012). Mitigating the anthropogenic global warming in the electric power industry. *Renewable and Sustainable Energy Reviews, 16*, 2747-2761.

[Alzate-Restrepo'08] Alzate-Restrepo, V. & Hill, J. M. (2008). Effect of anodic polarization on carbon deposition on Ni/YSZ anodes exposed to methane. *Applied Catalysis A: General, 342*, 49-55.

[Anderson'06] Anderson, B. J., Gross, D. S., Musicant, D. R., Ritz, A. M. & Smith, T. G. (2006). Adapting K-Medians to Generate Normalized Cluster Centers. *In Proceedings of the Sixth SIAM International Conference on Data Mining.* Bethesda, Maryland.

[Angeli'10] Angeli, C. (2010). Diagnostic expert eystems: From expert's Knowledge to real-time systems. Book: *Advanced knowledge based systems: Model, Application & Research*, Sajjia & Akerkar (eds), pp. 50-73.

[Arriagada'02] Arriagada, J., Olausson, P. & Selimovic, A. (2002). Artificial neural network simulator for SOFC performance prediction. *Journal of Power Sources, 112*, 54-60.

[Arsie'10] Arsie, I., Di Filippi, A., Marra, D., Pianese, C. & Sorrentino, M. (2010). Fault Tree Analysis Aimed to Design and Implement On-Field Fault Detection and Isolation Schemes for SOFC Systems. *ASME Conference Proceedings, 2010*, 389-399.

[Åström'07] Åström, K., Fontell, E. & Virtanen, S. (2007). Reliability analysis and initial requirements for FC systems and stacks. *Journal of Power Sources, 171*, 46-54.

[Athamena'03] Athamena, B. & Abbassi, H. A. (2003). Fault Detection and Isolation Using Hybrid Parameter Estimation and Fuzzy Logic Residual Evaluation. *Informatica (Slovenia), 27*, 29-38.

[Badwal'00] Badwal, S. & Ciacchi, F. (2000). Oxygen-ion conducting electrolyte materials for solid oxide fuel cells. *Ionics, 6*, 1-21.

[Bagotsky'09] Bagotsky, V. S. (2009). *Fuel cells : problems and solutions,* Hoboken, N.J. (eds.), United States: John Wiley & Sons.

[Baker'75] Baker, R. T. K., Harris, P. S., Henderson, J. & Thomas, R. B. (1975). Formation of carbonaceous deposits from the reaction of methane over nickel. *Carbon, 13***,** 17-22.

[Bartelmus'09] Bartelmus, W. & Zimroz, R. (2009). A new feature for monitoring the condition of gearboxes in non-stationary operating conditions. *Mechanical Systems and Signal Processing, 23***,** 1528-1534.

[Bezdek'81] Bezdek, J. C. (1981). *Pattern Recognition with Fuzzy Objective Function Algorithms,* Norwell, M.A. (eds.), USA: Kluwer Academic Publishers.

[Bishop'06] Bishop, C. M. (2006). *Pattern Recognition and Machine Learning (Information Science and Statistics),* Secaucus, N.J. (eds.). USA: Springer-Verlag New York, Inc.

[Borgelt'06] Borgelt, C. & Kruse, R. (2006). Finding the Number of Fuzzy Clusters by Resampling. *2006 IEEE International Conference on Fuzzy Systems.* pp. 48-54. IEEE.

[Boutsidis'09] Boutsidis, C., Mahoney, M. W. & Drineas, P. (2009). Unsupervised Feature Selection for the k-means Clustering Problem. In *Adavances in neural information processing systems,* Bengio Y., Schuurmans D., Lafferty J., Williams C. & Culotta A. (eds.), pp. 153-161.

[Bradley'97] Bradley, P. S., Mangasarian, O. L. & Street, W. N. (1997). Clustering via Concave Minimization. *Advances in neural information procesing systems, 9***,** 368--374.

[Cable'07] Cable, T. L. & Sofie, S. W. (2007). A symmetrical, planar SOFC design for NASA's high specific power density requirements. *Journal of Power Sources, 174***,** 221-227.

[Cabouro'06] Cabouro, G., Caboche, G., Chevalier, S. & Piccardo, P. (2006). Opportunity of metallic interconnects for ITSOFC: Reactivity and electrical property. *Journal of Power Sources, 156***,** 39-44.

[Cadick. PE'99] Cadick. PE, J. (1999). Condition Based Maintenance: How to get started.

[Cassidy'96] Cassidy, M., Lindsay, G. & Kendall, K. (1996). The reduction of nickel/zirconia cermet anodes and the effects on supported thin electrolytes. *Journal of Power Sources, 61***,** 189-192.

[Cayan'08] Cayan, F. N., Zhi, M., Pakalapati, S. R., Celik, I., Wu, N. & Gemmen, R. (2008). Effects of coal syngas impurities on anodes of solid oxide fuel cells. *Journal of Power Sources, 185***,** 595-602.

[Chao'11] Chao, C.-C., Hsu, C.-M., Cui, Y. & Prinz, F. B. (2011). Improved Solid Oxide Fuel Cell Performance with Nanostructured Electrolytes. *ACS Nano, 5***,** 5692-5696.

[Charpentier'98] Charpentier, P., Fragnaud, P., Schleich, D., Denos, Y. & Gehain, E. (1998). Preparation of thin film SOFCs working at reduced temperature. *Ionics, 4***,** 118-123.

[Chebil'09] Chebil, J., Noel, G., Mesbah, M. & Deriche, M. (2009). Wavelet Decomposition for the Detection and Diagnosis of Faults in Rolling Element Bearings. *Jordan Journal of Mechanical and Industrial Engineering, 3***,** 260-267.

[Chnani'08] Chnani, M. (2008). Thesis: Modélisation Macroscopique de piles PEFC et SOFC pour l'étude de leur couplage. Belfort, France: University of Franche-Comté & Technology University of Belfort Montbéliard.

[Clement'02] Clement, A. & Vigouroux, B. (2002). Unsupervised classification of pixels in color images by hierarchical analysis of bi-dimensional histograms. *2002 IEEE International Conference on Systems, Man and Cybernetics.* pp. 85 -89.

[Comminges'12] Comminges, C., Fu, Q. X., Zahid, M., Steiner, N. Y. & Bucheli, O. (2012). Monitoring the degradation of a solid oxide fuel cell stack during 10,000 h via electrochemical impedance spectroscopy. *Electrochimica Acta, 59*, 367-375.

[Cooper'92] Cooper, G. F. & Dietterich, T. (1992). A Bayesian method for the induction of probabilistic networks from data. *MACHINE LEARNING, 9*, 309--347.

[Cornish'07] Cornish, R. (2007). Statistics: Cluster analysis. *http://mlsc.lboro.ac.uk/resources/statistics/Clusteranalysis.pdf*.

[Darwiche'09] Darwiche, A. (2009). *Book: Modeling and Reasoning With Bayesian Networks,* (Editor ed.). Cambridge University Press.

[Daubechies'92] Daubechies, I. (1992). *Ten Lectures on Wavelets,* (Editor ed.). SIAM: Society for Industrial and Applied Mathematics

[Deza'09] Deza, M. M. & Deza, E. (2009). *Encyclopedia of Diastances,* Springer.

[Dileo'99] Dileo, M., Manker, C. & Cadick, J. (1999). Condition Based Maintenance. *http://www.cadickcorp.com/download/cbm_tech8.pdf*

[Emre Cek'10] Emre Cek, M., Ozgoren, M. & Acar Savaci, F. (2010). Continuous time wavelet entropy of auditory evoked potentials. *Computers in Biology and Medicine, 40*, 90-96.

[Escobet'09] Escobet, T., Feroldi, D., de Lira, S., Puig, V., Quevedo, J., Riera, J. & Serra, M. (2009). Model-based fault diagnosis in PEM fuel cell systems. *Journal of Power Sources, 192*, 216-223

[Feng'94] Feng, M. & Goodenough, J. B. (1994). A superior oxide-ion electrolyte. *European journal of solid state and inorganic chemistry, 31*, 663-672.

[Fergus'05] Fergus, J. W. (2005). Metallic interconnects for solid oxide fuel cells. *Materials Science and Engineering: A, 397*, 271-283.

[Finnerty'98] Finnerty, C. M., Coe, N. J., Cunningham, R. H. & Ormerod, R. M. (1998). Carbon formation on and deactivation of nickel-based/zirconia anodes in solid oxide fuel cells running on methane. *Catalysis Today, 46*, 137-145.

[Fontana'09] Fontana, S., Chevalier, S. & Caboche, G. (2009). Metallic interconnects for solid oxide fuel cell: Effect of water vapour on oxidation resistance of differently coated alloys. *Journal of Power Sources, 193*, 136-145.

[Fouquet'03] Fouquet, D., Müller, A. C., Weber, A. & Ivers-Tiffée, E. (2003). Kinetics of oxidation and reduction of Ni/YSZ cermets. *Ionics, 9*, 103-108.

[Fouquet'06] Fouquet, N., Doulet, C., Nouillant, C., Dauphin-Tanguy, G. & Ould-Bouamama, B. (2006). Model based PEM fuel cell state-of-health

monitoring via ac impedance measurements. *Journal of Power Sources*, *159*, 905-913.

[Gannon'09] Gannon, P., Sofie, S., Deibert, M., Smith, R. & Gorokhovsky, V. (2009). Thin film YSZ coatings on functionally graded freeze cast NiO/YSZ SOFC anode supports. *Journal of Applied Electrochemistry, 39***,** 497-502.

[Gay'12] Gay, C. (2012). Thesis: Amélioration de l'efficacité énergétique des systèmes de micro-cogénération : association pile à combustible SOFC /Moteur Stirling. Belfort, France: Université de Franche-Comté.

[Gazzarri'08] Gazzarri, J. I. & Kesler, O. (2008). Short-stack modeling of degradation in solid oxide fuel cells: Part I. Contact degradation. *Journal of Power Sources, 176***,** 138-154.

[Ghahramani'03] Ghahramani, Z. (2003). Graphical Models: Parameter Learning. *In Handbook of brain theory and neural networks***,** 486--490.

[Girona'12] Girona, K., Laurencin, J., Fouletier, J. & Lefebvre-Joud, F. (2012). Carbon deposition in CH4/CO2 operated SOFC: Simulation and experimentation studies. *Journal of Power Sources, 210***,** 381-391.

[Giudici'09] Giudici, P. & Figini, S. (2009). *Applied Data Mining for Business and Industry,* (Editor ed.). John Wiley & Sons.

[Gong'07] Gong, M., Liu, X., Trembly, J. & Johnson, C. (2007). Sulfur-tolerant anode materials for solid oxide fuel cell application. *Journal of Power Sources, 168***,** 289-298.

[Gong'11] Gong, Y., Ji, W., Xie, B. & Wang, H. (2011). Effect of YSZ electrolyte surface modification on the performance of LSM/YSZ composite cathode. *Solid State Ionics, 192***,** 505-509.

[Gorte'03] Gorte, R. J. & Vohs, J. M. (2003). Novel SOFC anodes for the direct electrochemical oxidation of hydrocarbons. *Journal of Catalysis, 216***,** 477-486.

[Grossman'01] Grossman, R., Kamath, C. & Kumar, V. (2001). *Data Mining for Scientific and Engineering Applications,* Raju R. Namburu. (eds.), Springer.

[Hagen'06] Hagen, A., Barfod, R., Hendriksen, P. V., Liu, Y.-L. & Ramousse, S. (2006). Degradation of anode supported SOFCs as a function of temperature and current Load. *Journal of The Electrochemical Society, 153***,** A1165.

[Hagen'09] Hagen, A., Chen, M., Neufeld, K. & Liu, Y.-L. (2009). Effect of Humidity in Air on Performance and Long-Term Durability of SOFCs. pp. 439-446. ECS.

[Harmelen'08] Harmelen, F., Lifschitz, V. & Porter, B. (2008). *Handbook of Knowledge Representation,* Elsevier Science.

[Hartigan'79] Hartigan, J. A. & Wong, M. A. (1979). A K-Means Clustering Algorithm. *Applied Statistics, 28***,** 100–108.

[He'07] He, H. & Hill, J. M. (2007). Carbon deposition on Ni/YSZ composites exposed to humidified methane. *Applied Catalysis A: General, 317***,** 284-292.

[Heckerman'96] Heckerman, D. (1996). A Tutorial on Learning With Bayesian Networks. Learning in Graphical Models. *ftp://ftp.research.microsoft.com/pub/tr/tr-95-06.pdf*

[Hernandez'06] Hernandez, A., Hissel, D. & Outbib, R. (2006). Fuel cell fault diagnosis: A stochastic approach. *2006 IEEE International Symposium on Industrial Electronics.* pp. 1984 -1989.

[Hissel'07] Hissel, D., Candusso, D. & Harel, F. (2007). Fuzzy-Clustering Durability Diagnosis of Polymer Electrolyte Fuel Cells Dedicated to Transportation Applications. *Vehicular Technology, IEEE Transactions on, 56***,** 2414-2420.

[Hissel'04] Hissel, D., Péra, M. C. & Kauffmann, J. M. (2004). Diagnosis of automotive fuel cell power generators. *Journal of Power Sources, 128***,** 239-246.

[Hu'09] Hu, Y. & Zhao, C.-x. (2009). Unsupervised Texture Classification by Combining Multi-Scale Features and K-Means Classifier. *Chinese Conference on Pattern Recognition, 2009. CCPR 2009.* pp. 1-5). IEEE.

[Huang'00] Huang, K., Hou, P. Y. & Goodenough, J. B. (2000). Characterization of iron-based alloy interconnects for reduced temperature solid oxide fuel cells. *Solid State Ionics, 129***,** 237-250.

[Huang'98] Huang, K., Tichy, R. S. & Goodenough, J. B. (1998). Superior Perovskite Oxide-Ion Conductor; Strontium- and Magnesium-Doped LaGaO3: I, Phase Relationships and Electrical Properties. *Journal of the American Ceramic Society, 81***,** 2565-2575.

[Hung'04] Hung, S.-S., Kuo, T.-C. & Liu, D. S.-M. (2004). An Efficient Mining and Clustering Algorithm for Interactive Walk-Through Traversal Patterns. *IEEE/WIC/ACM International Conference on Web Intelligence, 2004. WI 2004. Proceedings.* pp. 356- 362. IEEE.

[Huo'08] Huo, H.-B., Zhu, X.-J., Hu, W.-Q., Tu, H.-Y., Li, J. & Yang, J. (2008). Nonlinear model predictive control of SOFC based on a Hammerstein model. *Journal of Power Sources, 185***,** 338-344.

[Hwang'11] Hwang, J.-W., Lee, Y.-S. & Cho, S.-B. (2011). Structure evolution of dynamic Bayesian network for traffic accident detection. *2011 IEEE Congress on Evolutionary Computation (CEC).* pp. 1655 -1671.

[Isermann'06] Isermann, R. (2006). *Fault-diagnosis systems, an introduction from fault detection to fault tolerance,* (Editor ed.). Springer Verlag.

[Ishihara'94] Ishihara, T., Matsuda, H. & Takita, Y. (1994). Doped LaGaO3 Perovskite Type Oxide as a New Oxide Ionic Conductor. *J. Am. Chem. Soc., 116***,** 3801-3803.

[Ivers-Tiffée'01] Ivers-Tiffée, E., Weber, A. & Herbstritt, D. (2001). Materials and technologies for SOFC-components. *Journal of the European Ceramic Society, 21***,** 1805-1811.

[Iwata'96] Iwata, T. (1996). Characterization of Ni-YSZ anode degradation for substrate-type solid oxide fuel cells. *Journal of The Electrochemical Society, 143***,** 1521.

[Jang'93] Jang, J. S. R. (1993). ANFIS: adaptive-network-based fuzzy inference system. *Systems, Man and Cybernetics, IEEE Transactions on, 23*, 665-685.

[Jeong'06] Jeong, I.-J., Leon, V. J. & Villalobos, J. R. (2006). Integrated decision-support system for diagnosis, maintenance planning, and scheduling of manufacturing systems. *International Journal of Production Research, 45*, 267-285.

[Joshi'04] Joshi, A. V., Steppan, J. J., Taylor, D. M. & Elangovan, S. (2004). Solid Electrolyte Materials, Devices, and Applications. *Journal of Electroceramics, 13*, 619-625.

[Keep'77] Keep, C. W., Baker, R. T. K. & France, J. A. (1977). Origin of filamentous carbon formation from the reaction of propane over nickel
. *Journal of Catalysis, 47*, 232-238.

[Kim'06] Kim, T., Liu, G., Boaro, M., Lee, S.-I., Vohs, J. M., Gorte, R. J., Al-Madhi, O. H. & Dabbousi, B. O. (2006). A study of carbon formation and prevention in hydrocarbon-fueled SOFC. *Journal of Power Sources, 155*, 231-238.

[Lang'08] Lang, M., Auer, C., Eismann, A., Szabo, P. & Wagner, N. (2008). Investigation of solid oxide fuel cell short stacks for mobile applications by electrochemical impedance spectroscopy. *Electrochimica Acta, 53*, 7509-7513.

[Laosiripojana'07] Laosiripojana, N. & Assabumrungrat, S. (2007). Catalytic steam reforming of methane, methanol, and ethanol over Ni/YSZ: The possible use of these fuels in internal reforming SOFC. *Journal of Power Sources, 163*, 943-951.

[Larminie'03] Larminie, J. & Dicks, A. (2003). *Fuel Cell Systems Explained (2nd Edition),* (Editor ed.). John Wiley & Sons.

[Larrain'06] Larrain, D., Van herle, J. & Favrat, D. (2006). Simulation of SOFC stack and repeat elements including interconnect degradation and anode reoxidation risk. *Journal of Power Sources, 161*, 392-403.

[Lauritzen'88] Lauritzen, S. & Spiegelhalter, D. (1988). Local Computations with Probabilities on Graphical Structures and Their Application to Expert Systems. *Journal of the Royal Statistical Society. Series B (Methodological), 50*.

[Lewis'97] Lewis, S. A. & Edwards, T. G. (1997). Smart sensors and system health management tools for avionics and mechanical systems. *Digital Avionics Systems Conference, 1997. 16th DASC., AIAA/IEEE.* pp. 8.5-1-8.5-7 vol.2.

[Li'08] Li, M. J., Ng, M. K., Cheung, Y.-m. & Huang, J. Z. (2008). Agglomerative Fuzzy K-Means Clustering Algorithm with Selection of Number of Clusters. *IEEE Transactions on Knowledge and Data Engineering, 20*, 1519-1534.

[Li'10] Li, T. S., Wang, W. G., Chen, T., Miao, H. & Xu, C. (2010). Hydrogen sulfide poisoning in solid oxide fuel cells under accelerated testing conditions. *Journal of Power Sources, 195*, 7025-7032.

[Litzelman'08] Litzelman, S. J., Hertz, J. L., Jung, W. & Tuller, H. L. (2008). Opportunities and Challenges in Materials Development for Thin Film Solid Oxide Fuel Cells. *Fuel Cells, 8***,** 294-302.

[Liu'11] Liu, R. R., Kim, S. H., Taniguchi, S., Oshima, T., Shiratori, Y., Ito, K. & Sasaki, K. (2011). Influence of water vapor on long-term performance and accelerated degradation of solid oxide fuel cell cathodes. *Journal of Power Sources, 196***,** 7090-7096.

[Liu'09] Liu, Y. L., Hagen, A., Barfod, R., Chen, M., Wang, H. J., Poulsen, F. W. & Hendriksen, P. V. (2009). Microstructural studies on degradation of interface between LSM–YSZ cathode and YSZ electrolyte in SOFCs. *Solid State Ionics, 180***,** 1298-1304.

[Lorente'12] Lorente, E., Millan, M. & Brandon, N. P. (2012). Use of gasification syngas in SOFC: Impact of real tar on anode materials. *International Journal of Hydrogen Energy, 37***,** 7271-7278.

[Lu'04] Lu, C., An, S., Worrell, W. L., Vohs, J. M. & Gorte, R. J. (2004). Development of intermediate-temperature solid oxide fuel cells for direct utilization of hydrocarbon fuels. *Solid State Ionics, 175***,** 47-50.

[Lunze'02] Lunze, J. (2002). Qualitative methods for fault diagnosis. In H. Unbehauen (Ed.) *Control systems, Robotics and Automation.* Oxford, UK: Encyclopedia of Life Support Systems (EOLSS) Publishers.

[Lussier'08] Lussier, A., Sofie, S., Dvorak, J. & Idzerda, Y. U. (2008). Mechanism for SOFC anode degradation from hydrogen sulfide exposure. *International Journal of Hydrogen Energy, 33***,** 3945-3951.

[Ma'10] Ma, Q., Tietz, F., Leonide, A. & Ivers-Tiffée, E. (2010). Anode-supported planar SOFC with high performance and redox stability. *Electrochemistry Communications, 12***,** 1326-1328.

[MacQueen'67] MacQueen, J. B. (1967). Some Methods for Classification and Analysis of MultiVariate Observations. In L. M. L. Cam & J. Neyman (Eds.) *Proc. of the fifth Berkeley Symposium on Mathematical Statistics and Probability.* pp. 281-297). University of California Press.

[Mai'11] Mai, A., Iwanschitz, B., Weissen, U., Denzler, R., Haberstock, D., Nerlich, V. & Schuler, A. (2011). Status of Hexis' SOFC Stack Development and the Galileo 1000 N Micro-CHP System. *ECS Transactions, 35***,** 87-95.

[Mathworks'96] Mathworks (1996). Matlab toolbox: Statistics toolbox for use with Matlab. The Matheworks Inc.

[Matsuzaki'01] Matsuzaki, Y. & Yasuda, I. (2001). Dependence of SOFC cathode degradation by chromium-containing alloy on compositions of electrodes and electrolytes. *Journal of The Electrochemical Society, 148***,** A126-A131.

[Mench'08] Mench, M. M. (2008). *Fuel cell engines,* (Editor ed.). Wiley Online Library.

[Mermelstein'10] Mermelstein, J., Millan, M. & Brandon, N. (2010). The impact of steam and current density on carbon formation from biomass gasification tar on Ni/YSZ, and Ni/CGO solid oxide fuel cell anodes. *Journal of Power Sources, 195***,** 1657-1666.

[Milewski'09] Milewski, J. & Świrski, K. (2009). Modelling the SOFC behaviours by artificial neural network. *International Journal of Hydrogen Energy, 34*, 5546-5553.

[Misiti'09] Misiti, M., Misiti, Y., Oppenheim, G. & Poggi, J.-M. (2009). Wavelet Toolbox 4, User's Guide for Matlab.

[Mizusaki'91] Mizusaki, J., Tagawa, H., Tsuneyoshi, K. & Sawata, A. (1991). Reaction kinetics and microstructure of the solid oxide fuel cells air electrode La0.6Ca0.4MnO3/YSZ. *Journal of The Electrochemical Society, 138*, 1867-1873.

[Mooi'11] Mooi, E. & Sarstedt, M. (2011). Chapter 9: Cluster analysis. *A Concise Guide to Market Research: The process, Data, and Methods Using IBM SPSS statistics.* (p. 308). Springer.

[Murphy'07] Murphy, K. (2007). Bayes Net toold box for Matlab. http://code.google.com/p/bnt/.

[Nasser'06] Nasser, S., Alkhaldi, R. & Vert, G. (2006). A Modified Fuzzy K-means Clustering using Expectation Maximization. *2006 IEEE International Conference on Fuzzy Systems.* pp. 231-235). IEEE.

[Neapolitan'03] Neapolitan, R. E. (2003). *Learning Bayesian networks,* (Editor ed.). Prentice Hall.

[Nerlich'10] Nerlich, V., Schuler, A., Mai, A. & Doerk, T. (2010). Cogeneration in single family homes with fuel cell heating appliances. *Proceedings of the 18th WHEC 2010, Essen, 78-6*.

[Nesaraj'10] Nesaraj, A. S. (2010). Recent developments in solid oxide fuel cell technology – a review. *Industrial Research, 13*, 117-131.

[Nielsen'10] Nielsen, J., Hagen, A. & Liu, Y. L. (2010). Effect of cathode gas humidification on performance and durability of Solid Oxide Fuel Cells. *Solid State Ionics, 181*, 517-524. http://www.sciencedirect.com/science/article/pii/S0167273810000937.

[Norušis'03] Norušis, M. J. (2003). Chapter 16: Cluster Analysis. *SPSS 12.0 statistical procedures companion.* pp. 361-391). Prentice Hall.

[Novosel'08] Novosel, Avsec, M. & Macek, J. (2008). The interaction of SOFC anode materials with carbon monoxide. *Materiali in Tehnologije, 42*, 51-57.

[Onanena'10] Onanena, R., Oukhellou, L., Candusso, D., Same, A., Hissel, D. & Aknin, P. (2010). Estimation of fuel cell operating time for predictive maintenance strategies. *The 10th Chinese Hydrogen Energy Conference, 35*, 8022-8029.

[Onanena'11] Onanena, R., Oukhellou, L., Candusso, D., Harel, F., Hissel, D. & Aknin, P. (2011). Fuel cells static and dynamic characterizations as tools for the estimation of their ageing time. *The 3rd Annual Korea-USA Joint Symposium on Hydrogen & Fuel Cell Technologies, 36*, 1730-1739.

[Park'09] Park, E.-W., Moon, H., Park, M.-s. & Hyun, S. H. (2009). Fabrication and characterization of Cu–Ni–YSZ SOFC anodes for direct use of methane via Cu-electroplating. *International Journal of Hydrogen Energy, 34*, 5537-5545.

[Patan'08] Patan, K. (2008). *Artificial Neural Networks for the Modelling and Fault Diagnosis of Technical Processes*. Springer Berlin Heidelberg.

[Paya'97] Paya, B. A., Esat, I. I. & Badi, M. N. M. (1997). Artificial neural network based fualt diagnostics of rotating machinery using wavelet transforms as a preprocessor. *Mechanical Systems and Signal Processing, 11*, 751-765.

[Pearl'00] Pearl, J. (2000). *Causality: Models, Reasoning, and Inference,* Cambridge University Press.

[Peng'04] Peng, Z. K. & Chu, F. L. (2004). Application of the wavelet transform in machine condition monitoring and fault diagnostics: a review with bibliography. *Mechanical Systems and Signal Processing, 18*, 199-221.

[Piccardo'09] Piccardo, P. & Amendola, R. (2009). SOFC's interconnects materials development. *Proc. Internat. Workshop "Advances and inonvations in SOFCs"*. Katarino, Bulgaria.

[Piccardo'06] Piccardo, P., Chevalier, S., Molins, R., Viviani, M., Caboche, G., Barbucci, A., Sennour, M. & Amendola, R. (2006). Metallic interconnects for SOFC: Characterization of their corrosion resistance in hydrogen/water atmosphere and at the operating temperatures of differently coated metallic alloys. *Surface and Coatings Technology, 201*, 4471-4475.

[Pihlatie'10] Pihlatie, M. (2010). Stability of Ni-YSZ composites for solid oxide fuel cells during reduction and re-oxidation. Helsinki, Finland.

[Pihlatie'09] Pihlatie, M., Kaiser, A. & Mogensen, M. (2009). Redox stability of SOFC: Thermal analysis of Ni–YSZ composites. *Solid State Ionics, 180*, 1100-1112.

[Polikar'96a] Polikar, R. (1996a). The Wavelet Tutorial Part II: Fundamentals: The fourier transform and the short term fourier transform. http://www.public.iastate.edu/~rpolikar/WAVELETS/WTpart2.html.

[Polikar'96b] Polikar, R. (1996b). The Wavelet Tutorial Part III: Multiresolution Analysis and the Continuous Wavelet Transform. http://www.public.iastate.edu/~rpolikar/WAVELETS/WTpart3.html.

[Polikar'96c] Polikar, R. (1996c). The Wavelet Tutorial Part IV: Multiresolution Analysis: The Discrete Wavelet Transform. http://www.public.iastate.edu/~rpolikar/WAVELETS/WTpart4.html.

[Qian'04] Qian, G., Sural, S., Gu, Y. & Pramanik, S. (2004). Similarity between Euclidean and cosine angle distance for nearest neighbor queries. *Proceedings of the 2004 ACM symposium on Applied computing SAC 04, 2*, 1232.

[Ramesohl'11] Ramesohl, S. (2011). Oral presentation: The German NIP lighthouse project callux Field Test of Residential Fuel Cells. Tokyo.

[Riascos'07] Riascos, L. A. M., Simoes, M. G. & Miyagi, P. E. (2007). A Bayesian network fault diagnostic system for proton exchange membrane fuel cells. *Journal of Power Sources, 165*, 267-278.

[Rodionov'96] Rodionov, S. & Martin, J. H. (1996). A Knowledge-Based System for the Diagnosis and Prediction of Short-Term Climatic Changes in the North Atlantic. *Journal of Climate, 9*, 1816-1823.

[Rosso'01] Rosso, O. A., Blanco, S., Yordanova, J., Kolev, V., Figliola, A., Schormann, M. & Basar, E. (2001). Wavelet entropy: a new tool for analysis of short duration brain electrical signals. *Journal of Neuroscience Methods, 105*, 65-75.

[Rousseeuw'87] Rousseeuw, P. J. (1987). Silhouettes: A graphical aid to the interpretation and validation of cluster analysis. *Journal of Computational and Applied Mathematics, 20*, 53-65.

[Sajja'10] Sajja, P. S. & Akerkar, R. (2010). Knowledge-based systems for development. *Advanced knowledge based systems: Model, Application & Research,* Sajja & Akerkar (eds), pp. 1-11.

[Sakai'06] Sakai, N., Horita, T., Yamaji, K., Xiong, Y. P., Kishimoto, H., Brito, M. E. & Yokokawa, H. (2006). Material transport and degradation behavior of SOFC interconnects. *Solid State Ionics, 177*, 1933-1939.

[Sarantaridis'07] Sarantaridis, D. & Atkinson, A. (2007). Redox Cycling of Ni-Based Solid Oxide Fuel Cell Anodes: A Review. *Fuel Cells, 7*, 246–258.

[Sasaki'11] Sasaki, K., Haga, K., Yoshizumi, T., Minematsu, D., Yuki, E., Liu, R., Uryu, C., Oshima, T., Ogura, T., Shiratori, Y., Ito, K., Koyama, M. & Yokomoto, K. (2011). Chemical durability of Solid Oxide Fuel Cells: Influence of impurities on long-term performance. *Journal of Power Sources, 196*, 9130-9140.

[Schwarz'78] Schwarz, G. (1978). Estimating the Dimension of a Model. *The Annals of Statistics, 6*, 461-464.

[Shannon'48] Shannon, C. (1948). A mathematical theory of communication. *Bell system technical journal, 27*.

[Singhal'00] Singhal, S. C. (2000). Advances in solid oxide fuel cell technology. *Solid State Ionics, 135*, 305-313.

[Singhal'03] Singhal, S. C. & Kendall, K. (2003). *High-temperature Solid Oxide Fuel Cells: Fundamentals, Design and Applications,* Elsevier Science.

[Souza'97] Souza, S., Visco, S. J. & De Jonghe, L. C. (1997). Thin-film solid oxide fuel cell with high performance at low-temperature. *Solid State Ionics, 98*, 57-61.

[SRI'09] SRI (2009). Condition-Based Maintenance (CBM). *Southwest Research Institute.*

[Stambouli'02] Stambouli, A. B. & Traversa, E. (2002). Solid oxide fuel cells (SOFCs): a review of an environmentally clean and efficient source of energy. *Renewable and Sustainable Energy Reviews, 6*, 433-455.

[Steele'01] Steele, B. C. H. & Heinzel, A. (2001). Materials for fuel-cell technologies. *Nature, 414*, 345-352.

[Steiner'09] Steiner, N. Y. (2009). Diagnostic non intrusif de groupes électrogènes à Piles à Combustible de type PEMFC. Belfort, France: University of Franche-Comté.

[Steiner'10] Steiner, N. Y., Candusso, D., Hissel, D. & Mocoteguy, P. (2010). Model-based diagnosis for proton exchange membrane fuel cells. *Mathematics and Computers in Simulation, 81*, 158-170.

[Steiner'11a] Steiner, N. Y., Hissel, D., Mocoteguy, P. & Candusso, D. (2011a). Non intrusive diagnosis of polymer electrolyte fuel cells by wavelet packet transform. *International Journal of Hydrogen Energy, 36***,** 740-746.

[Steiner'11b] Steiner, Y. N., Hissel, D., Moçotéguy, P. & Candusso, D. (2011b). Diagnosis of polymer electrolyte fuel cells failure modes (flooding & drying out) by neural networks modeling. *International Journal of Hydrogen Energy, 36***,** 3067-3075

[Tietz'02] Tietz, F., Buchkremer, H.-P. & Stöver, D. (2002). Components manufacturing for solid oxide fuel cells. *Solid State Ionics, 152–153***,** 373-381.

[Tu'04] Tu, H. & Stimming, U. (2004). Advances, aging mechanisms and lifetime in solid-oxide fuel cells. *Journal of Power Sources, 127***,** 284-293.

[VijayaVenkataRaman'12] VijayaVenkataRaman, S., Iniyan, S. & Goic, R. (2012). A review of climate change, mitigation and adaptation. *Renewable and Sustainable Energy Reviews, 16***,** 878-897.

[Virkar'10] Virkar, A. V. (2010). Mechanism of oxygen electrode delamination in solid oxide electrolyzer cells. *International Journal of Hydrogen Energy, 35***,** 9527-9543.

[Walker'08] Walker, J. S. (2008). *A primer on wavelets and teir scientific applicaitons, second edition,* University of Wisconsin, Eau Claire, Wisconsin, U.S.A: Chapman & Hall/CRC, Taylor & Francis Groups, LLC.

[Wang'11a] Wang, K., Hissel, D., Péra, M.-C. & Steiner, Y.-N. (2011a). Developing a generic tool for in-situ diagnosis on solid oxide fuel cell (SOFC). In: *Fundamentals and Developments of Fuel Cells (FDFC) Conference*, 19-21 January 2011, Grenoble, France.

[Wang'11b] Wang, K., Hissel, D., Péra, M. C., Steiner, N., Marra, D., Sorrentino, M., Pianese, C., Monteverde, M., Cardone, P. & Saarinen, J. (2011b). A Review on solid oxide fuel cell models. *International Journal of Hydrogen Energy, 36***,** 7212-7228.

[Wang'12] Wang, K., Péra, M.-C., Hissel, D., Steiner, N., Pohjoranta, A. & Pofahl, S. (2012). SOFC modelling based on discrete Bayesian network for system diagnosis use. (Oral presentation). *The 8th Power Plant & Power System Control Symposium (PPPSC)*, 2-5 September, Toulouse, France.

[Wasterlain'10] Wasterlain, S. (2010). Approches expérimentales et analyse probabiliste pour le diagnsotic de piles à combustible de type PEM. Belfort, France: Université de Franche-Comté.

[Will'00] Will, J., Mitterdorfer, A., Kleinlogel, C., Perednis, D. & Gauckler, L. J. (2000). Fabrication of thin electrolytes for second-generation solid oxide fuel cells. *Solid State Ionics, 131***,** 79-96.

[Wu'10] Wu, J. & Liu, X. (2010). Recent Development of SOFC Metallic Interconnect. *Journal of Materials Science & Technology, 26***,** 293-305.

[Wu'07] Wu, X. J., Zhu, X. J., Cao, G. Y. & Tu, H. Y. (2007). Modeling a SOFC stack based on GA-RBF neural networks identification. *Journal of Power Sources, 167***,** 145-150.

[Yang'10] Yang, L. & Deng, M. (2010). Based on k-Means and Fuzzy k-Means Algorithm Classification of Precipitation. *2010 International Symposium on Computational Intelligence and Design (ISCID).* pp. 218-221. IEEE.

[Yokokawa'12] Yokokawa, H., Horita, T., Yamaji, K., Kishimoto, H. & Brito, M. E. (2012). Degradation of SOFC Cell/Stack Performance in Relation to Materials Deterioration. *Journal of the Korean Ceramic Society.* pp. 11-18.

[Yokokawa'03] Yokokawa, H. & Sakai, N. (2003). Fuel cell principle, systems and applications. *Handbook of Fuel Cells Fundamentals Technology and Application.* pp. 219-266). John Wiley & Sons.

[Yokokawa'08] Yokokawa, H., Tu, H., Iwanschitz, B. & Mai, A. (2008). Fundamental mechanisms limiting solid oxide fuel cell durability. *Journal of Power Sources, 182***,** 400-412.

[Zheng'09] Zheng, N. & Xue, J. (2009). Statistical Learning and Pattern Analysis for Image and Video Processing. *Advances***,** 319-341.

[Zhu'01] Zhu, B., Liu, X., Zhou, P., Zhu, Z., Zhu, W. & Zhou, S. (2001). Cost-effective yttrium doped ceria-based composite ceramic materials for intermediate temperature solid oxide fuel cell applications. *Journal of Materials Science Letters, 20***,** 591-594.

[Zhu'03] Zhu, W. Z. & Deevi, S. C. (2003). Opportunity of metallic interconnects for solid oxide fuel cells: a status on contact resistance. *Materials Research Bulletin, 38***,** 957-972.

[Zou'08] Zou, B.-j. & Umugwaneza, M. P. (2008). Shape-Based Trademark Retrieval Using Cosine Distance Method. *Eighth International Conference on Intelligent Systems Design and Applications, 2008. ISDA '08.* pp. 498-504. IEEE.

Résumé :

Le projet Européen « GENIUS » ambitionne de développer les méthodologies génériques pour le diagnostic de systèmes piles à combustible à haute température de type oxyde solide (SOFC). Le travail de cette thèse s'intègre dans ce projet ; il a pour objectif la mise en œuvre d'un outil de diagnostic en utilisant le stack comme capteur spécial pour détecter et identifier les défaillances dans les sous-systèmes du stack SOFC. Trois algorithmes de diagnostic ont été développés, se basant respectivement sur la méthode de classification k-means, la technique de décomposition du signal en ondelettes ainsi que la modélisation par réseau Bayésien. Le premier algorithme sert au diagnostic ex-situ et est appliqué pour traiter les donnés issues des essais de polarisation. Il permet de déterminer les variables de réponse significatives qui indiquent l'état de santé du stack. L'indice Silhouette a été calculé comme mesure de qualité de classification afin de trouver le nombre optimal de classes dans la base de données. La détection de défaut en temps réel peut se réaliser par le deuxième algorithme. Puisque le stack est employé en tant que capteur, son état de santé doit être vérifié préalablement. La transformée des ondelettes a été utilisée pour décomposer les signaux de tension de la pile SOFC dans le but de chercher les variables caractéristiques permettant d'indiquer l'état de santé de la pile et également assez discriminatives pour différentier les conditions d'opération normales et anormales. Afin d'identifier le défaut du système lorsqu'une condition d'opération anormale s'est détectée, les paramètres opérationnelles réelles du stack doivent être estimés. Un réseau Bayésien a donc été développé pour accomplir ce travail. Enfin, tous les algorithmes ont été validés avec les bases de données expérimentales provenant de systèmes SOFC variés, afin de tester leur généricité.

Abstract:

The EU-project "GENIUS" is targeted at the investigation of generic diagnosis methodologies for different Solid Oxide Fuel Cell (SOFC) systems. The Ph.D study presented in this thesis was integrated into this project; it aims to develop a diagnostic tool for SOFC system fault detection and identification based on validated diagnostic algorithms, through applying the SOFC stack as a sensor. In this context, three algorithms, based on the k-means clustering technique, the wavelet transform and the Bayesian method, respectively, have been developed. The first algorithm serves for ex-situ diagnosis. It works on the classification of the polarization measurements of the stack, aiming to figure out the significant response variables that are able to indicate the state of health of the stack. The parameter "Silhouette" has been used to evaluate the classification solutions in order to determine the optimal number of classes/patterns to retain from the studied database. The second algorithm allows the on-line fault detection. The wavelet transform has been used to decompose the SOFC's voltage signals for the purpose of finding out the effective feature variables that are discriminative for distinguishing the normal and abnormal operating conditions of the system. Considering the SOFC as a sensor, its reliability must be verified beforehand. Thus, the feature variables are also required to be indicative to the state of health of the stack. When the stack is found being operated improperly, the actual operating parameters should be estimated so as to identify the system fault. To achieve this goal, a Bayesian network has been proposed serving as a meta-model of the stack to accomplish the estimation. At the end, the databases originated from different SOFC systems have been used to validate these three algorithms and assess their generalizability.

■ École doctorale SPIM 16 route de Gray F - 25030 Besançon cedex

■ tél. +33 (0)3 81 66 66 02 ■ ed-spim@univ-fcomte.fr ■ www.ed-spim.univ-fcomte.fr